3 THERMAL EVALUATION

This chapter identifies and describes the principal thermal design features of the MIDUS packaging that are important to safety. In addition, the thermal evaluations of the package under NCT (§71.71) and HAC (§71.73) that demonstrate compliance with the applicable performance requirements of 10 CFR 71 are discussed. The thermal evaluation presented in the body of this chapter is for the liquid payload (i.e., Content #01) described in Section 1.2.2.1. For clarity, the body of this chapter is not revised extensively for additional contents. Instead, the thermal evaluation of each additional payload is presented in SAR addenda, starting in Chapter 9.

The thermal evaluations demonstrate that the maximum temperatures of all components of the package remain below their respective temperature limits under both NCT and HAC. Further, the package is designed, constructed, and prepared for transport such that, in still air at 38°C and in the shade, no accessible surface of the package has a temperature exceeding 50°C. These results assure that the thermal performance of the package will not cause any loss or dispersal of radioactive contents, no significant increase in external surface radiation levels, and no substantial reduction in the effectiveness of the packaging, in accordance with the requirements of §71.43(f) and §71.51(a)(1).

The thermal evaluation of the package is performed by analysis using the Thermal Desktop® and SINDA/FLUINT computer programs. These computer programs are used together to create the thermal models, calculate the solution, and post-process the analysis results. Thermal Desktop® is an application module of AutoCAD™ that provides graphical input and output display functions and computes thermal mass, conduction, and radiation exchange conductors based on the model geometry and thermal/optical properties. SINDA/FLUINT is a general-purpose computer program that is used to solve steady-state and transient finite difference and/or finite element problems. The Thermal Desktop® and SINDA/FLUINT computer programs are tested, installed, operated, and maintained in accordance with the requirements of the Energy*Solutions* QA program. These computer programs have been validated in accordance with the requirements of the Energy*Solutions* QA program and shown to correctly solve the general class of problems that they are used to solve.

The analytical methodology used for the HAC thermal evaluation has been determined to be acceptable based upon the results of the confirmatory tests discussed in Section 2.12.4. A full-scale test package was subjected to sequential HAC free drop, HAC puncture, and HAC thermal tests in accordance with the requirements of §71.73. Prior to performing the confirmatory tests, the package thermal response to the thermal test conditions was predicted using the same analytical methodology used for the HAC thermal analysis. The thermal model was adjusted to reflect the package deformation expected to result from the HAC free drop and HAC puncture drop tests, as well as the differences between the anticipated environment of the furnace test and the regulatory HAC thermal test. The results of the confirmatory test demonstrate that the analytical methodology used for the thermal evaluation provides an accurate representation of the peak package temperatures reached during the 30-minute fire and the

transient temperature response of the package. A detailed discussion of the confirmatory test results is provided in Section 2.12.4.

3.1 Description of Thermal Design

The MIDUS package is designed as a totally passive thermal system for transporting up to 4,400 Ci of ^{99}Mo plus daughters. Full details of the package design are described in Section 1.2. The following sections summarize the design features affecting the thermal performance of the package, including the package geometry, materials of construction, and the decay heat loading.

3.1.1 Design Features

Figure 3-1 illustrates the package's key thermal design features. The package is constructed primarily from stainless steel, depleted uranium, and polyurethane foam.

The polyurethane foam provides significant impact and thermal protection during the HAC free drop and thermal tests. However, the same thermal protection afforded by the foam significantly restricts the transfer of heat from the payload to the overpack exterior surfaces under NCT. To counter this effect, the overpack base assembly design has a thermal spider, which is a 3 mm thick ring of copper with eight arched legs that bridge the space between the overpack base inner and outer shells. The thermal spider is brazed to the bottom surface of the overpack base inner shell and to the outer shell, providing good mechanical connections for effective heat transfer. The spider is sized to enhance the transfer of the payload's decay heat load from the interior of the package during NCT conditions, while limiting the transfer of heat into the package under HAC conditions.

The incorporation of an offset in the design of interface between the overpack's base and lid flanges, plus the robust design of the flanges, ensures that the drop events that are assumed to precede the HAC fire event will not significantly deform or "spring" the flanges. Therefore, neither radiative nor convective heat transfer from the HAC fire is able to penetrate to the interior of the package. This design feature, the additional offsets designed into the overpack's base and lid interior closure surfaces, and the relatively thin overpack inner shell effectively isolate the cask from conductive heat transfer from the exterior of the package during the fire event.

The polyurethane foam provides significant impact and thermal protection during the HAC fire event through a combination of low thermal conductivity and thermal decomposition. Since the thermal decomposition of the foam is accompanied by gas generation, the overpack lid and base assemblies have four nylon threaded screws that function as pressure-relief devices during the HAC fire event. During normal operations they remain in place, protecting the foam by means of elastomeric weather seal O-rings During the fire, they quickly melt, allowing the hot gases produced by the thermal decomposition of the foam to escape the overpack shells. This prevents catastrophic failure (splitting) of the overpack shells due to internal pressure. In addition, the vents aid in heat dissipation by allowing mass transfer of hot gases out of the overpack shells.

The package design does not rely on mechanical cooling systems to meet containment requirements.

3.1.2 Content's Decay Heat

The maximum activity of the payload is limited to 4,400 Ci of ^{99}Mo plus daughters at full transient equilibrium. However, the initial thermal power of the payload is conservatively calculated for a bounding activity of 4,500 Ci of ^{99}Mo plus daughters at full transient equilibrium using ORIGEN [3.1]. The package payload produces an initial thermal power of 17.8W. This is the same basis as used to derive the radiation source terms, further described in Section 5.2.

^{99}Mo is the predominate thermal source, contributing 81% of the thermal power. ^{99m}Tc contributes the remainder. The payload's initial thermal power decays rapidly due to the short half-lives of these two contributors. The half-lives of ^{99}Mo and ^{99m}Tc are approximately 66 hours and 6 hours, respectively. To account for this rapid decay, the thermal source power is modeled as a transient with the following magnitude:

$$Q(t) = Q_o e^{-0.0105t}$$

where Q_o is the initial decay heat (W) and t is time (hours). The time-dependent heat load by this equation was compared to the ORIGEN decay calculations and matched well with ORIGEN's predicted power at several decay times ranging from 0–192 hours.

About 81% of the decay heat energy is deposited in the product, product bottle, and secondary container. The remaining 19% is deposited into the cask cavity shell and depleted uranium (DU) gamma shielding.

3.1.3 Summary Tables of Temperatures

Table 3-1 summarizes the maximum package temperatures resulting from NCT heat that affect structural integrity, containment, and shielding. Because a transient thermal analysis is used for the evaluation of NCT heat, the table also reports the time that the peak temperatures are reached. The package has considerable thermal margin for NCT heat. The smallest thermal margins for NCT heat are 82°C for the cask containment O-ring seal and 60°C for the overpack lid foam. The minimum package temperatures are limited only by the minimum ambient temperature due to the rapid decay of the thermal power. Therefore, the minimum temperature for all package components is -40°C.

The peak temperatures of the package resulting from the HAC fire, along with the pre-fire damage condition from which they result and times at which they occur after fire initiation, are summarized in Table 3-2. As seen from the table, significant thermal margin exists for all package components, with the smallest margin of 67°C for the cask containment O-ring seal. The package temperatures under post-fire steady-state conditions will be significantly lower than the peak temperatures for NCT heat. This is due to the rapid decay of the thermal power of the cask payload and the lower thermal resistance of the package following the fire.

3.1.4 Summary Tables of Maximum Pressures

Table 3-3 summarizes the maximum normal operating pressure (MNOP) and maximum pressure under HAC.

Table 3-1 – Summary of Package Temperatures for NCT

Package Component/ Location	NCT Heat[1]		Temperature Limit (°C)
	Max. Temp. (°C)	Time After Loading (Hr)	
Cask Cavity Fill Gas (Bulk Avg.)	78	34.25	N/A
Cask Containment O-ring Seal	68	34.25	150
Cask Closure Bolt	67	34.25	427
Cask Closure Lid	67	34.25	427
Cask Inner Shell, Maximum	71	34.25	427
Cask Inner Shell, Average[2]	70	[2]	427
Cask Outer Shell	67	34.25	427
Cask DU Shield	67	34.25	1,130
Shield Plug DU	72	34.50	1,130
Overpack Base Outer Shell	71	53.00	427
Overpack Base Inner Shell	66	33.00	427
Overpack Base Foam, Maximum	71	53.00	149
Overpack Base Foam, Bulk Avg.	65	55.25	149
Overpack Closure Flanges	69	53.50	427
Overpack Lid Outer Shell	89	52.75	427
Overpack Lid Flange/Inner Shell	68	53.75	427
Overpack Lid Foam, Maximum	89	52.75	149
Overpack Lid Foam, Bulk Avg.	70	54.25	149

Notes:
1. Initial conditions for NCT heat thermal evaluation are maximum decay heat, 38°C ambient air temperature, and insolation. Package is assumed to be at room temperature at time of loading.
2. Average nodal temperature when the cask inner shell maximum temperature is reached.

Table 3-2 – Summary of Package Temperatures for HAC Thermal Test

Package Component/ Location	Controlling Damage Condition	Max. Temp. (°C)	Time After Fire Initiation (hr)	Temp. Limit (°C)
Cask Cavity Fill Gas (Bulk Avg.)	Side	146	3.13	---
Cask Containment O-Ring Seal	Side	145	2.00	204[1]
Cask Closure Bolt	Side	147	1.88	427
Cask Closure Lid	Top	150	1.13	427
Cask Inner Shell, Maximum	Side	142	2.63	427
Cask Inner Shell, Average[2]	Side	141	[2]	427
Cask Outer Shell	Bottom	221	0.55	427
Cask DU Shield	Bottom	162	0.67	1,130
Shield Plug DU	Side	143	3.13	1,130
Overpack Base Outer Shell	Top	780	0.50	1,427
Overpack Base Inner Shell	Top	465	0.53	1,427
Overpack Closure Flanges	Bottom	766	0.50	1,427
Overpack Lid Outer Shell	Bottom/Side	782	0.50	1,427

Notes:
1. Temperature limit for exposure for up to 2 hours.
2. Estimated by averaging all component nodal temperatures when the maximum temperature is achieved.

Table 3-3 – Summary Table of Maximum Pressures in the Containment System

Case	Max. Pressure (bar)
MNOP	6.9
HAC	12.6

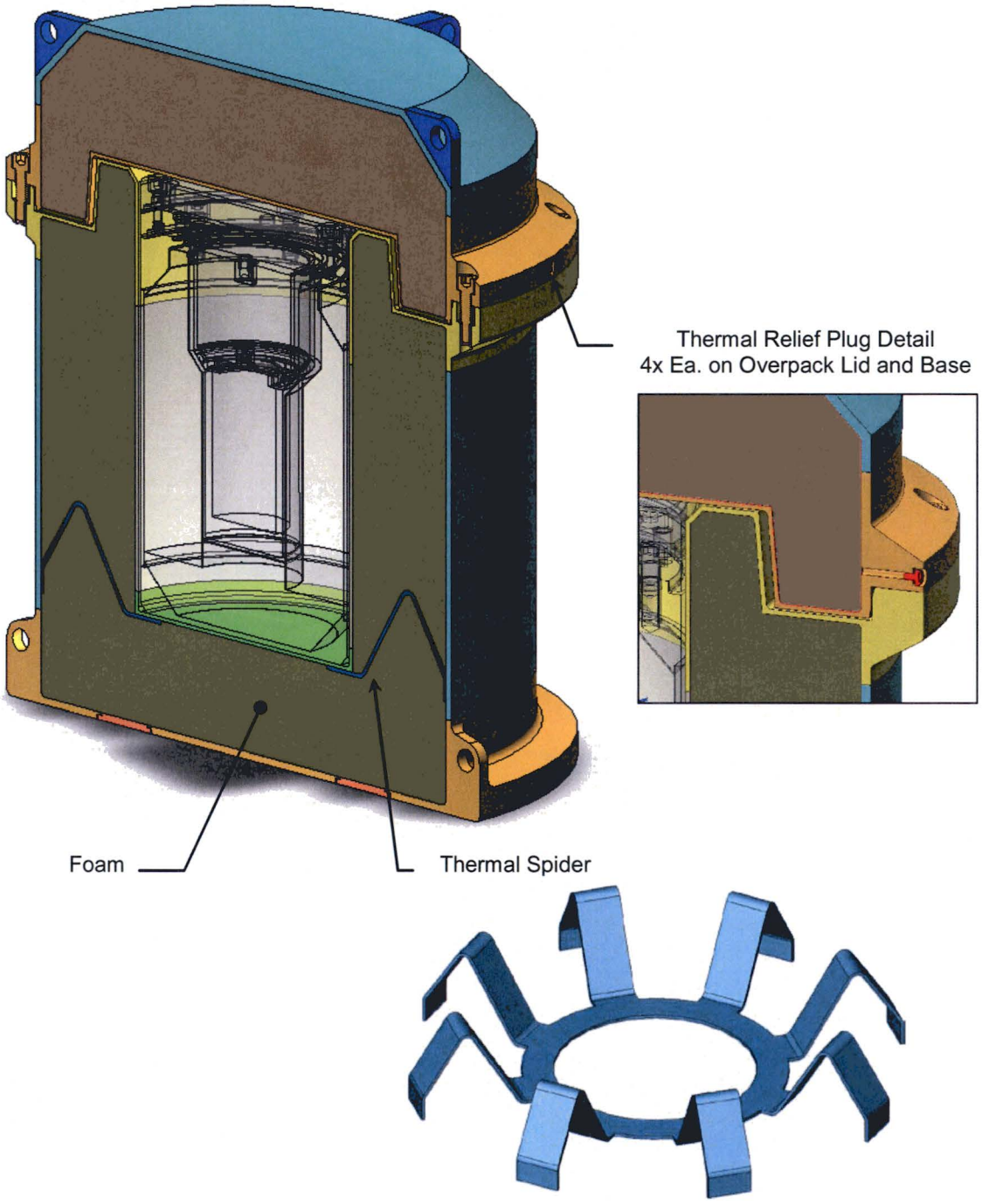

Figure 3-1 – Package Thermal Design Features

3.2 Material Properties and Component Specifications

3.2.1 Material Properties

The package is fabricated primarily from Type 304 and/or Type 316 stainless steel, SA-320/A320, Grade L43 alloy bolting steel, DU alloy, copper, and polyurethane foam materials. The temperature-dependent thermal conductivity and specific heat properties of these materials used for the thermal evaluation are summarized in Table 3-4.

The thermal properties of stainless steel given in Table 3-4 are those for Type 304 stainless steel. As shown in the ASME Code, Section II, Part D [3.2], Table TCD, the temperature-dependent values of thermal conductivity and thermal diffusivity for Type 316 stainless steel (Material Group K) are approximately 5% to 8% lower than those for Type 304 stainless steel (Material Group J) in the temperature range of interest. The use of the Type 304 stainless steel properties for the thermal evaluation does not significantly affect the package temperatures under NCT conditions, but its use conservatively bounds the potential for heat transfer into the package under HAC.

The thermal properties of the air used for the thermal evaluation are summarized in Table 3-5. The mass density of air is calculated based on the ideal gas law using a molecular weight of 28.966 g/mole. The heat transfer correlations for air used in the thermal evaluation are described in Section 3.5.3.

The package surface emissivities and absorptivities used in the thermal evaluation are summarized in Table 3-6. The emissivity of stainless steel varies with surface finish and ranges from 0.25 to 0.28 for as-received finish, 0.40 for commercial sand blast finish, and 0.54 for white metal blast finish [3.3]. The emissivity for weathered stainless steel is in the range of 0.48 to 0.50 ([3.4], Appendix A-1). The surface condition of the overpack exterior is assumed to be weathered and oxidized, since it is exposed directly to the environment and the effects of normal handling. The assumed condition of the different package surfaces, which reflect the anticipated conditions of use and maintenance of the package, and the corresponding emissivities used in the thermal analysis are summarized in Table 3-6.

3.2.2 Component Specifications

The technical specifications of the components that are important to the thermal performance of the package include the allowable service temperatures and pressures for NCT and HAC. The allowable service temperatures for all components encompass the maximum and minimum temperatures anticipated during NCT and HAC. The minimum service temperature for all package components is less than or equal to -40°C. The maximum service temperatures of the package components are based on the component's functional requirements for the service conditions. The maximum service temperature for structural components is limited to the maximum temperature limit given in Section II, Part D [3.2] of the ASME Code for the components' material specification(s). The maximum service temperature for components that

are not relied upon for structural support are typically established to prevent gross thermal failure (e.g., melting).

The temperature limit for all steel components of the package that are relied upon for structural support is equal to the maximum temperature limit of 427°C specified in Section II, Part D [3.2] of the ASME Code. The only exception is the temperature limit of the overpack shells for the HAC thermal test. During the HAC thermal test, the overpack shells do not provide structural support, but are relied upon to shield the overpack foam from direct exposure to the fire. Therefore, the temperature limit for the overpack shells under HAC thermal loading is limited to the melting point of stainless steel, which is approximately 1,427°C.

Since neither the copper nor the DU materials of the package are used for any structural components, the maximum operating temperature of these materials is limited by their melting points. Copper has a melting point of approximately 1,080°C, while the DU has a melting point of 1,130°C. There is no limit on the minimum allowable operating temperature for either material.

The polyurethane foam material that fills the overpack base and lid shell assemblies has a continuous service temperature range of -40°C to 149°C. The material properties of foam do not undergo any irreversible changes within this temperature range. The peak temperature of the polyurethane foam is limited to 149°C for all NCT and HAC, except for the HAC thermal test. The foam properties used for the structural evaluation of the package for NCT and HAC free drop conditions are based on a maximum bulk average foam temperature of 82°C. Therefore, the bulk average temperature of the overpack base and lid foam cores should not exceed 82°C. No temperature limits are imposed on the polyurethane foam for the HAC thermal test since the thermal decomposition of the foam material plays a significant role in the level of thermal protection provided by the package.

The cask containment, leak-test, and cleanliness O-rings are fabricated from an ethylene propylene compound material. This material has a continuous service temperature range of -40°C to 150°C [3.5] when exposed to non-aggressive media. The continuous service range is used for the O-ring temperature limits for NCT. During the HAC thermal test, the O-rings are subjected to elevated temperatures for a short period of time. The cask O-ring temperatures typically remain at or near the peak values for only a short period of time: typically one to two hours. The ethylene propylene O-ring compound is capable of withstanding a temperature of 204°C for up to 2 hours [3.5]. Therefore, the maximum temperature of the O-rings is limited to 204°C for the HAC thermal test.

Table 3-4 – Thermal Properties of Packaging Materials (2 Pages)

Material	Temperature (°C)	Thermal Conductivity (W/m-°C)[1]	Specific Heat[2] (J/g-°C)
Stainless Steel[3]	-40	*14.25*	*0.4688*
	21.1	14.88	0.4775
	37.8	15.06	0.4799
	93.3	16.10	0.4998
	148.9	16.96	0.5135
	204.4	18.00	0.5284
	260.0	18.87	0.5375
	315.6	19.56	0.5445
	371.1	20.42	0.5527
	426.7	21.11	0.5559
	537.8	22.85	0.5704
	648.9	24.23	0.5782
	760.0	25.79	0.5892
	815.6	26.48	0.5939
SA-320/A320, Grade L43 Alloy Bolting Steel[4]	-40	*30.86*	*0.3918*
	21.1	33.40	0.4383
	37.8	34.10	0.4510
	93.3	35.65	0.4899
	148.9	36.69	0.5231
	204.4	37.04	0.5502
	260.0	37.04	0.5743
	315.6	36.69	0.5971
	371.1	36.17	0.6213
	426.7	35.48	0.6500
	537.8	33.58	0.7159
	648.9	31.15	0.8375
	760.0	25.96	0.7215
	815.6	25.96	0.6326
Polyurethane Foam[5]	---	0.038	1.478

Table 3-4 – Thermal Properties of Packaging Materials (2 Pages)

Material	Temperature (°C)	Thermal Conductivity (W/m-°C)[1]	Specific Heat[2] (J/g-°C)
Copper[6]	-73	413.0	0.356
	127	393.0	0.397
	327	379.0	0.417
	527	366.0	0.433
	727	352.0	0.451
	927	339.0	0.480
Depleted Uranium[7]	20	25.3	0.116
	60	26.0	0.117
	225	30.3	0.129
	440	33.4	0.160

Notes:
1. Thermal conductivity values given in units of Btu/hr-ft-°F are multiplied by 1.7295 to convert to SI units.
2. Specific heat is calculated as TC/(TD x density).
3. Based on thermal conductivity (TC) and thermal diffusivity (TD) from ASME Code, Section II, Part D [3.2], Table TCD, Material Group J (18Cr-8Ni). The density of this material is 8.0 g/cm^3.
4. Thermal properties for SA-320, Grade L43 steel from ASME Code, Section II, Part D, 1999 Edition, Table TCD, Material 2Ni-3/4Cr-1/3Mo. The density of this material is 7.84 g/cm^3.
5. Data from foam manufacturer's on-line product literature [www.generalplastics.com]. Density of material is 0.216 g/cm^3.
6. Thermal properties of pure copper [3.6]. Density of copper is 8.933 g/cm^3.
7. Thermal properties of depleted uranium [3.7]. Density of DU is 19.06 g/cm^3.
8. Values shown in *italics* are calculated by linear interpolation or linear extrapolation.

Table 3-5 – Thermal Properties of Air

Temperature (°C)	Thermal Conductivity (W/m-K)	Specific Heat (J/g-K)	Dynamic Viscosity (N-s/m^2 x 10^6)
-40.0	0.0209	1.0042	15.184
-17.8	0.0227	1.0045	16.341
10.0	0.0248	1.0055	17.724
37.8	0.0269	1.0071	19.044
93.3	0.0308	1.0121	21.525
148.9	0.0345	1.0191	23.827
204.4	0.0381	1.0278	25.985
260.0	0.0415	1.0378	28.019
315.6	0.0449	1.0488	29.934
371.1	0.0482	1.0606	31.744
426.7	0.0514	1.0730	33.473
482.2	0.0545	1.0857	35.135
537.8	0.0576	1.0986	36.735
648.9	0.0634	1.1242	39.766
760.0	0.0688	1.1487	42.601
815.6	0.0713	1.1603	43.953

Notes:
1. Properties based on curve fits in [3.8].

Table 3-6 – Package Surface Emissivity and Absorptivity Properties

Package Surface	Surface Material	Surface Condition	Emissivity, ε	Solar Absorptivity, α
Overpack Exterior	Type 304/316 stainless steel	Weathered, oxidized	0.45	0.52[1]
Overpack Interior	Type 304/316 stainless steel	Slightly oxidized[2]	0.40	N/A
Cask Surfaces	Type 304/316 stainless steel	Un-oxidized, as-received[3]	0.28	N/A
Gamma Shields	DU	Oxidized[4]	0.60	N/A
Product Container/Hardware	Stainless steel	Satin finish[5]	0.30	N/A
Ambient Environment	---	---	1.00	N/A

Notes:
1. Per Reference [3.9].
2. Properties assumed between those for weathered and as-received properties.
3. Assumes some dulling of surface finish from machining.
4. Based on lower-bound value for oxidized finish.
5. Similar to as-received stainless steel.

3.3 Thermal Evaluation under Normal Conditions of Transport

This section describes the thermal evaluation of the package under normal conditions of transport (NCT). The evaluation is conducted using analytical methods in accordance with 10 CFR 71 and Regulatory Guide 7.8 for the applicable NCT thermal loads. The results are compared with the allowable limits of temperature and pressure for the package components.

Analytical Approach

The thermal analysis of the package is conducted using the SINDA/FLUINT and Thermal Desktop® computer programs. SINDA/FLUINT is a general-purpose code used for both finite difference (i.e., lumped parameter) and finite element solutions under steady-state and transient conditions. Thermal Desktop® is a computer program that provides graphical input and output display functions, as well as computing the thermal mass, conduction, and radiation exchange conductors for the defined geometry and thermal/optical properties. These programs are well benchmarked and widely used for thermal analysis.

For this application, the SINDA/FLUINT and Thermal Desktop® computer programs are used to develop a solids model representation of the package. The geometric and material information contained in this solids model is used to develop and execute thermal models that simulate the steady-state and transient temperatures arising from the evaluated NCT and HAC. The thermal models incorporate temperature-dependent material properties and heat transfer via conduction, convection, and radiation. Algorithms are also programmed into the solution process for the purposes of computing the convective heat transfer coefficients as a function of the local geometry and the gas thermal properties which, in turn, are based on the local species content of the gas and the local temperature and pressure.

Thermal Model Description

The three-dimensional half-symmetry finite element model of the package shown in Figure 3-2 is used for NCT thermal evaluation. The package thermal model is constructed from sub-models that represent the overpack base and lid, cask, shield lid, and payload. The thermal model accurately captures the geometry of the package design features, including the lifting/tie down lugs, the base and closure flanges, the circular, sloped, and flat surfaces of the overpack lid, and the multi-facets of the base and lid flanges. A total of approximately 16,200 thermal nodes, 7,950 planar elements, and 9,800 solids are used to provide geometric and thermal resolution within the model.

The thermal sub-models of the overpack base and lid consist of approximately 10,700 nodes, 7,100 solids, and 5,300 planar elements that capture the multi-faceted surfaces of the base and lid flanges. The volume between the inner and outer surfaces of the overpack are filled rigid polyurethane foam that is installed in-situ, providing intimate contact between the foam and the surrounding overpack shells. As such, the heat transfer between the foam and the overpack shells is modeled using a low-contact resistance (i.e., 0.0016 $^{o}C\text{-}m^2/W$).

The shield lid is simulated using approximately 310 nodes to represent the 17 mm thick by 214 mm diameter DU shield and its 3 mm thick stainless steel casing.

The cask is simulated using approximately 5,100 nodes, 2,750 solids, and 2,400 planar elements. The modeling includes elements to simulate the closure bolts, the closure seals, and the shield plug. A separate model is used for the cask lid, the inner and outer shells of the cask, the shield plug casing, and the radial, bottom, and shield plug segments of the DU.

The package payload is modeled as a stepped, right cylinder using 159 thermal nodes. The thermal mass of the payload is determined as the average of 150 ml (150 g) of water and 850 g of stainless steel to represent the combination of the product, the product bottle, the secondary container, the snap ring, and the optional stainless steel cavity dunnage. This level of modeling is adequate since the peak temperature within the payload is not required for the purposes of this calculation. The decay heat load is simulated as a uniform surface heat flux on the exterior of the payload model. As discussed in Section 3.1.2, approximately 81% of the total decay heat is deposited on the surface of the payload container, while the remaining 19% is deposited as a surface heat flux on the inner surface of the cask's inner shell. Heat transfer from the payload to the cask is computed as conduction and radiation across the air space between the payload and the cask's inner shell and as conduction and radiation into the cask's shield plug.

Heat transfer within each component is modeled using temperature-dependent thermal properties for the associated materials from Section 3.2.1. Heat transfer between the separate components of the thermal models is simulated as a combination of radiation and conduction links. The radiation links are computed based on calculated view factors between the various model surfaces and the assigned optical properties for the associated surfaces. The conduction links are computed as conduction across nominal air gaps existing between the components or as a contact resistance for surfaces in direct contact with one another. The size of the gaps is set by the nominal clearance dimensions between the various components as obtained from the design drawings. The thermal conductivity of the air in the gaps is computed as a function of the local temperature.

Heat transfer from the exterior of the overpack to the ambient is computed as a combination of convection and radiation. The convection coefficient for each surface is computed as a function of the temperature difference between the surface and the ambient and the thermo-physical properties of air. The semi-empirical relationships used to predict the applicable convection coefficients are described in Section 3.5.3.

For the purposes of the NCT evaluations, the bottom surfaces of the package are assumed to be an adiabatic boundary. This modeling approach provides a conservative estimate of the package temperatures.

3.3.1 Heat and Cold

The thermal evaluations of the package under NCT load conditions are conducted using a transient analysis methodology to capture the temperature response within the package during a typical transportation cycle. This methodology is appropriate given the relatively rapid reduction in the decay heat source, as defined in Section 3.1.2. The transportation cycle is assumed to begin with a sequence of events that include the source being loaded within an empty cask, the cask being sealed and placed within its overpack, and finally the overpack lid being installed and secured. For the purposes of this safety evaluation, all of these operations are assumed to occur instantaneously at time = 0. In practice, some time will be required to accomplish these functions and during this time the payload's thermal source will continue to decay below the initial load limit of 17.8 W.

For the NCT heat evaluation, the package is assumed to be moved outdoors at time = 0 and subjected to a constant ambient temperature of 38°C and a diurnal insolation cycle. To capture the peak of the insolation cycle during the initial portion of the transportation cycle, the transient analysis assumes a start time of 8 AM. As shown by the results of the structural analysis presented in Section 2.6, no thermally significant damage will occur as result of the NCT drop events. As such, the thermal model described above is used without modification for the evaluations of the thermal performance under NCT.

Figure 3-3 illustrates the predicted transient thermal response of the package for NCT heat. The effect of the diurnal insolation cycle can be seen in the temperature response of the overpack base and lid shells. The initial portion of the temperature response for the cask seals and the gas in the cask cavity is dominated by the initial heat-up of the cask, while the later portion of the response reflects the influence of the diurnal insolation cycling. The transient demonstrates that slightly more than 34 hours is required before the peak cask temperature is achieved. After that time point, the decreasing source decay heat load (also illustrated in the figure) results in ever lower package temperatures. As seen from the figure, the decay heat load is reduced by 50% after approximately 66 hours.

The transient response of the package to NCT heat is also illustrated by the color contour temperature plots presented in Figure 3-5 and Figure 3-6. The temperature distribution at 28.5 hours after loading, when the overpack lid outer shell is near its peak temperature under the diurnal insolation cycle, is shown in Figure 3-5. However, the maximum payload and gas cavity temperature within the cask is not achieved until approximately 34.25 hours after the start of the transient. Figure 3-6 depicts the temperature within the package at the time when the peak payload and gas cavity temperatures are achieved.

The peak package temperatures occurring during the NCT heat transient are summarized in Table 3-1. As seen from the table, a significant thermal margin exists for all components, with the smallest being 82°C for the cask containment O-ring seal and 60°C for the overpack lid foam. The peak bulk average temperature within the gas cavity is predicted to be approximately 78°C which, as seen from Figure 3-3, occurs only for a short time period before reducing under the diurnal heating cycle of the insolation. The subsequent peak in the gas cavity temperature is approximately 3°C cooler due to the continued decrease in the source decay heat level.

A thermal evaluation of the package is also performed for NCT heat with zero insolation to establish the pre-fire package temperatures used in the HAC thermal evaluation and to demonstrate compliance with the requirements of §71.43(g). Without insolation heating, the temperature of the overpack outer shell rises initially due to convective heat transfer with the 38°C ambient air and then continues to rise slowly as the decay heat from the payload makes its way through the cask components. At 36 hours into the transient, the temperature of the overpack outer shell reaches a maximum of 44°C and then slowly decreases as the thermal power of the payload continues to decay. This evaluation confirms that the maximum temperature of the accessible surfaces of the package will be less than 50°C, in accordance with §71.43(g).

For the NCT cold evaluation, the package is assumed to be moved outdoors at time = 0 and subjected to a constant ambient temperature of -29°C and zero insolation. A transient thermal analysis is performed for NCT cold to account for the rapid decay of the payload thermal power. Figure 3-4 illustrates the predicted transient thermal response of the package for NCT cold. The figure shows that the peak temperatures within the package occur at or shortly after the time of loading. As seen, the overpack shell temperatures decrease rapidly, but do not reach steady-state conditions by the end of the transient. Given the continuous decrease in the decay heat source term, the package temperatures will eventually reach equilibrium with the ambient environment. Therefore, the minimum package temperature of -29°C that may be achieved under this condition is within the allowable limit for all components.

3.3.2 Maximum Normal Operating Pressure

The maximum normal operating pressure (MNOP) of the package is calculated for NCT heat, considering the highest bulk average temperature of the gases within the containment system, the minimum free volume of the cask cavity, and all possible sources of gases generated over a period of one-year. These sources include gases present in the containment system at the time of loading and radiolytic decomposition of the product and packaging materials.

The highest bulk average temperature of the gases within the cask cavity is 78°C for NCT heat. As shown in Figure 3-3, the maximum gas temperature is reached at approximately 34 hours after loading and decreases quickly beyond this time due to the rapid decay of the payload's thermal power. However, the maximum bulk average temperature of the gases in the cask cavity is conservatively assumed to exist at any time over a one-year period.

The minimum free volume of the cask cavity is 661 ml. This corresponds to the total cavity volume minus the volumes of the shield plug, payload internals, and product. The maximum volume of the product bottle, secondary container, secondary container O-ring, snap ring, and dunnage (user-supplied payload internals) is 125 ml [Section 1.2.2]. This is the volume of the materials of construction, not counting enclosed spaces. The product volume may vary from 0 to 150 ml.

The payload generates hydrogen due to radiolysis. As a result, the cask cavity will become pressurized during the shipment period. The producer of the ^{99}Mo has performed extensive

experimental testing to quantify the pressure rise on the identical product. This experimental data is used as the basis for calculating the cask internal pressure. Because the radiolytic properties of the product are highly dependent on its chemical formulation, these results are only valid for the same ^{99}Mo solution.

Section 3.5.5 shows the experimental test results. The data represent specific gas formation, Q, in gauge bar·cm^3/ml versus the specific activity in Ci/ml. All data used to prepare the numerical fit have been extrapolated to $t=\infty$; therefore, the results conservatively include 100% decay of the ^{99}Mo and daughter product (66 hour and 6 hour half-lives). In addition, a 2σ uncertainty has been added to the experimental data for further conservatism.

There are three independent seals that must fail before the containment seal becomes significantly pressurized (the product bottle, secondary container, and cask cleanliness seals). The volume used for the pressure calculations is, therefore, the total free volume of the containment cavity, and not the volume of the product bottle. The product bottle is designed for internal pressures well beyond the range expected to develop during NCT or HAC service. But the product bottle and other payload internals are user-supplied items and not a part of the certified packaging. A failure of the product bottle would result in the full calculated MNOP against the containment seal.

Using an initial temperature of 20°C, a peak temperature of 80°C, and the maximum specific gas formation, Q, from Section 3.5.5, the calculated MNOP as a function of activity and dispensed product volume are shown in Table 3-7. Inspection of Table 3-7 confirms the intuitive conclusion that greater activities result in greater MNOP. Greater dispensed volumes, however, tend to reduce MNOP because the specific gas generation is a linear function of the specific activity of the product. Higher dispensed volumes dilute the specific activity, thus decreasing the specific gas formation. This effect outweighs the effect of the additional fluid displacing free volume in the cask cavity.

The package is designed for Type B(U) service, so the maximum MNOP is 7 bar. Table 3-7 shows that at a bounding payload activity of 4,500 Ci, the calculated pressure is 7.0 bar for most of the range of dispensed volume. However, at 4,400 Ci, the pressure is 6.8 bar along most of the dispensed volume range. For conservatism, therefore, the maximum payload activity is specified as 4,400 Ci. The activity specification for this package design is governed by radiolytic gas pressure generation.

The producer of the ^{99}Mo has performed mass spectrometer measurements of the gas samples obtained during the pressure tests. Two samples were tested. The test results show that the composition of the pure evolved gas is determined to be 1.8% and 0.8% hydrogen by volume. The average is 1.3%, with a 2σ uncertainty of 1.4%. So the concentration of hydrogen in the pure evolved radiolysis product is conservatively estimated to be 1.3% + 1.4% = 2.7% by volume. Concentrations in the package will be lower due to dilution from the initial air in the package cavity.

The maximum hydrogen concentration is well below 5% by volume, and, therefore, does not constitute a risk for flammability or ignition.

Table 3-7 – Calculated MNOP as a Function of Activity and Dispensed Volume

Activity Ci	Pressure (bar) vs. Dispensed Product Volume (ml)									
	60	70	80	90	100	110	120	130	140	150
3000	4.4	4.4	4.3	4.3	4.2	4.2	4.1	4.0	4.0	3.9
3100	4.6	4.6	4.5	4.5	4.4	4.3	4.3	4.2	4.2	4.1
3200	4.8	4.7	4.7	4.6	4.6	4.5	4.5	4.4	4.4	4.3
3300	5.0	4.9	4.9	4.8	4.8	4.7	4.7	4.6	4.6	4.5
3400	5.1	5.1	5.1	5.0	5.0	4.9	4.9	4.8	4.8	4.7
3500	5.3	5.3	5.2	5.2	5.1	5.1	5.1	5.0	5.0	4.9
3600	5.5	5.5	5.4	5.4	5.3	5.3	5.2	5.2	5.2	5.1
3700		5.6	5.6	5.6	5.5	5.5	5.4	5.4	5.4	5.3
3800		5.8	5.8	5.7	5.7	5.7	5.6	5.6	5.6	5.5
3900		6.0	6.0	5.9	5.9	5.9	5.8	5.8	5.8	5.7
4000		6.2	6.1	6.1	6.1	6.0	6.0	6.0	6.0	5.9
4100		6.3	6.3	6.3	6.3	6.2	6.2	6.2	6.2	6.1
4200		6.5	6.5	6.5	6.4	6.4	6.4	6.4	6.4	6.3
4300			6.7	6.7	6.6	6.6	6.6	6.6	6.6	6.5
4400			6.9	6.8	6.8	6.8	6.8	6.8	6.8	6.7
4500			7.0	7.0	7.0	7.0	7.0	7.0	7.0	6.9

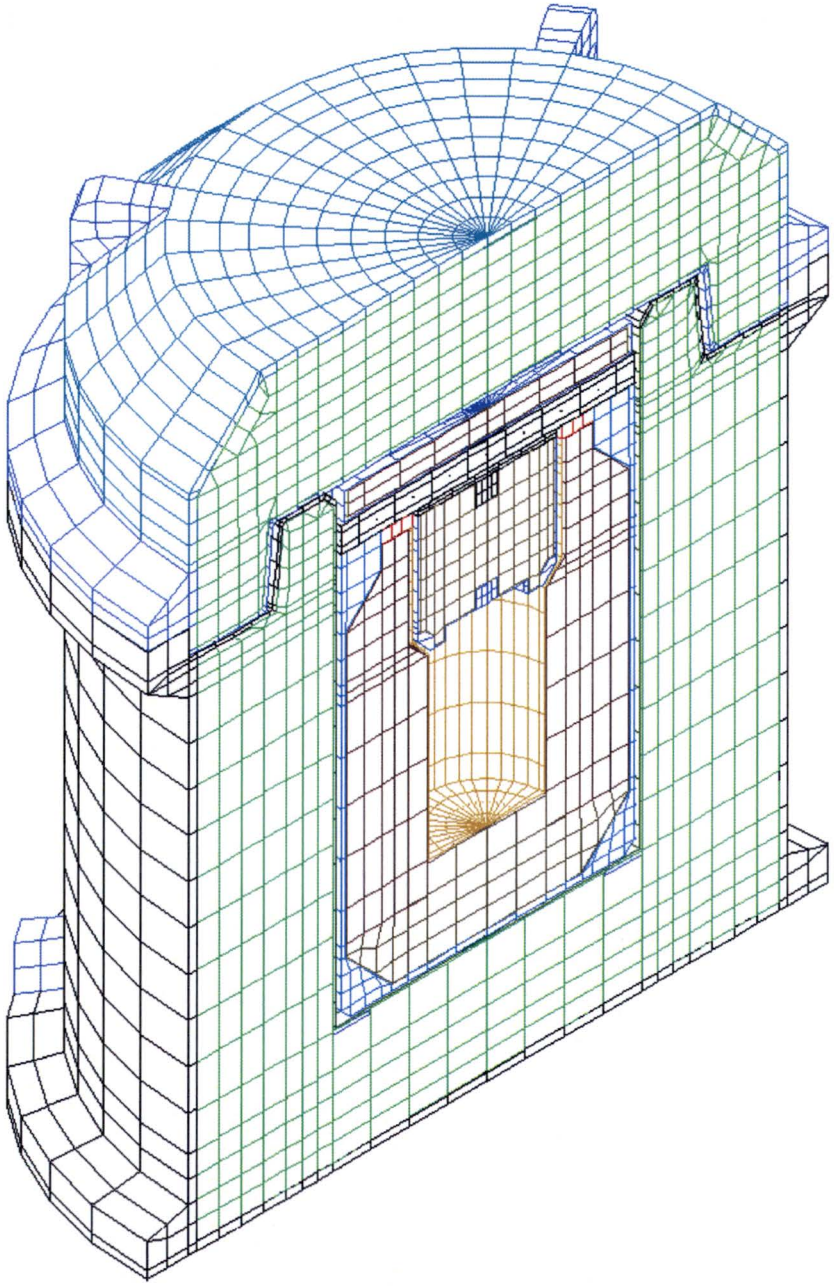

(Note: Payload sub-model not shown)

Figure 3-2 – MIDUS Package Thermal Model for NCT

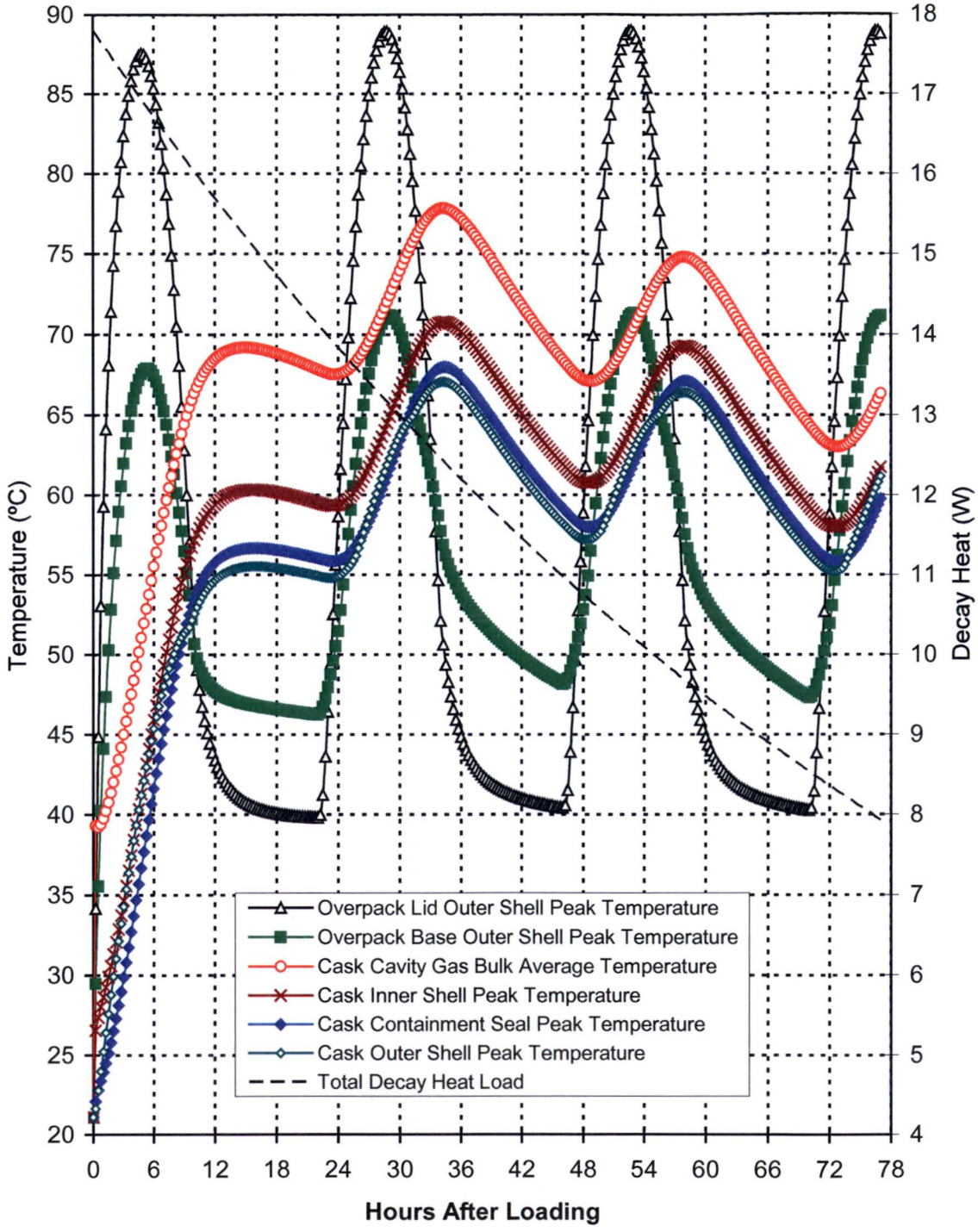

Figure 3-3 – NCT Heat Temperature Transient Results

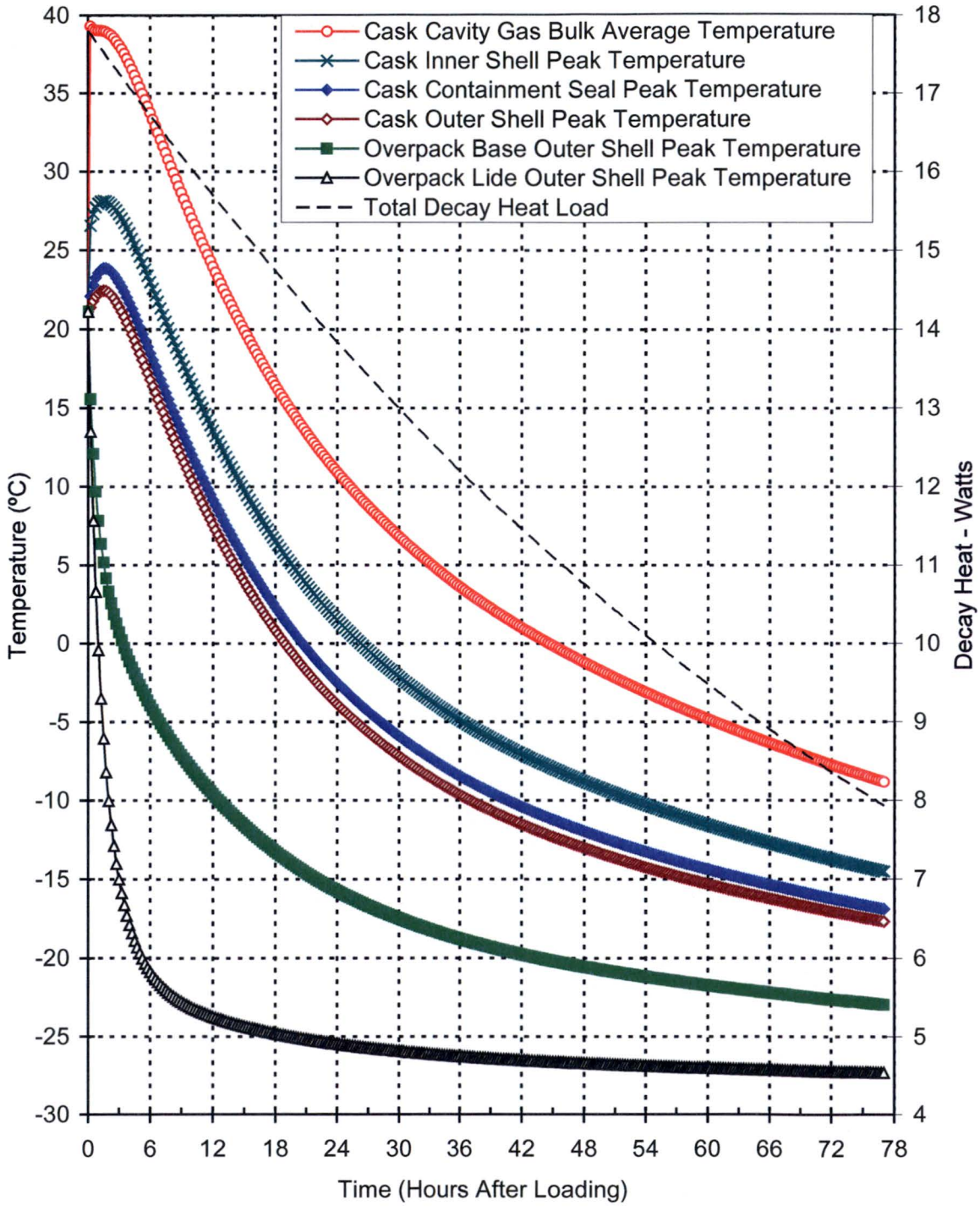

Figure 3-4 – NCT Cold Temperature Transient Results

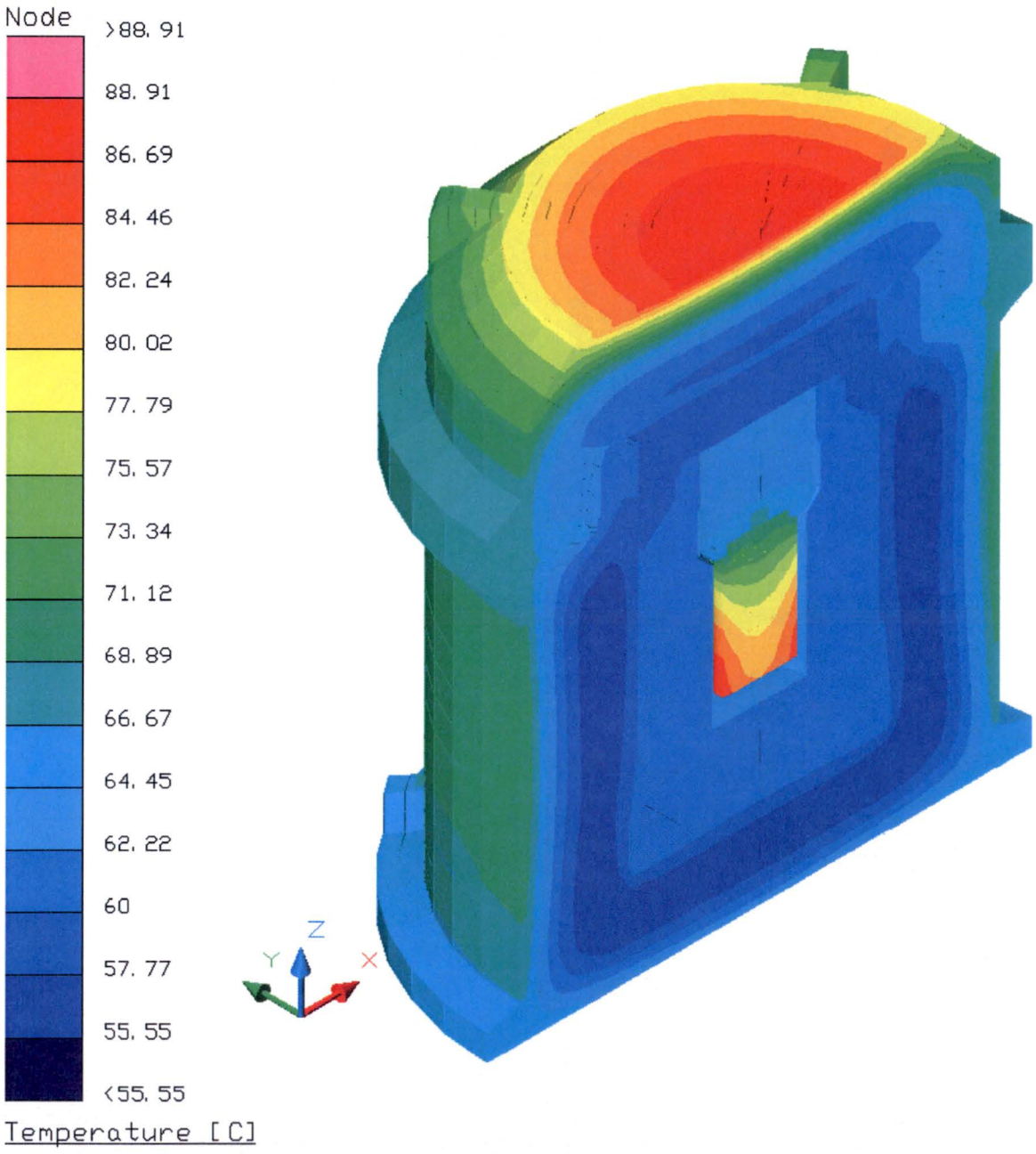

Figure 3-5 – Package NCT Heat Temperature Distribution at Time of Peak Overpack Shell Temperature (28.5 Hours After Loading)

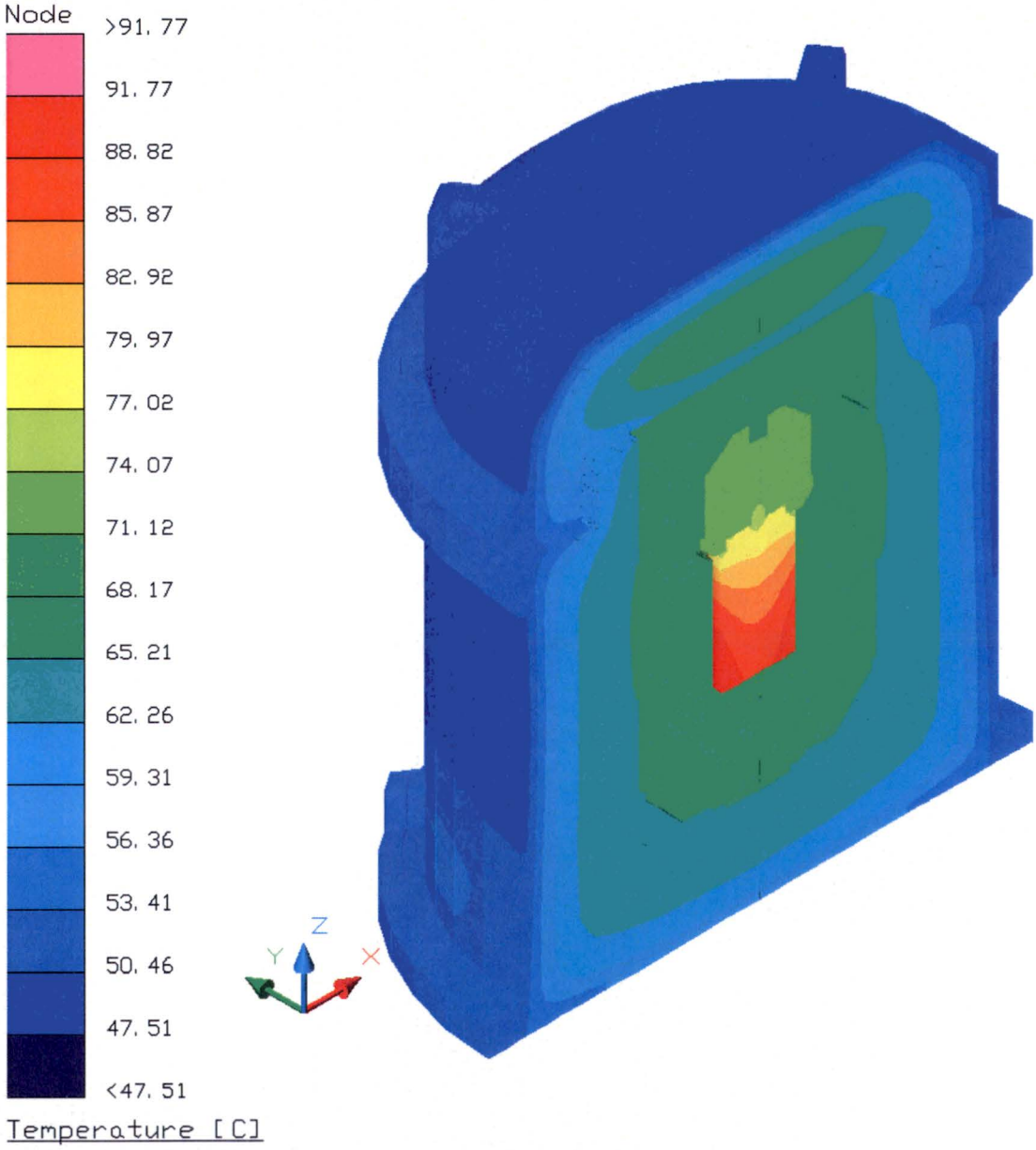

Figure 3-6 – Package NCT Heat Temperature Distribution at Time of Peak Payload/Cavity Gas Temperature (34.25 Hours After Loading)

3.4 Thermal Evaluation under Hypothetical Accident Conditions

This section presents the predicted system temperatures and pressures for the package under the hypothetical accident condition (HAC) thermal test specified in §71.73(c)(4). Because the solar loading is applied as a diurnal cycle, the starting point for the fire is assumed to be 11:30 a.m. to maximize the solar loading on the package after the fire.

The HAC transient analysis is continued for a sufficient time after the end of the fire to ensure that all package components have reached their peak temperatures. A post-fire, steady-state analysis is not conducted because it would not provide meaningful results. This conclusion is based on a combination of the following facts: 1) the thermal resistance of the damaged package is lower than the undamaged package due to the loss of foam, increased surface emissivity, etc., and 2) the short-term source decay heat load will continue to decrease until it reaches essentially zero. For these reasons, a transient evaluation of the package temperatures after the fire will continue to show a decrease in temperature levels until the source heat load has reached zero. Therefore, the maximum post-fire, steady-state temperatures that can occur will be bounded by those presented for NCT.

3.4.1 Initial Conditions

The initial temperature distribution for the HAC evaluation is taken from the NCT heat condition without insolation (see Section 3.3.1). Since that analysis is transient, the time point selected for the extraction of the initial temperatures is when the cask seals and the payload temperature reach their predicted maximums, which occurs at the 34.25 hour point into the transient. For additional conservatism, the temperature of each individual component is set equal to the maximum temperature occurring anywhere within that component.

3.4.2 Fire Test Conditions

The thermal evaluation of the package for the HAC thermal test is performed by analysis. The analytical model used for the HAC thermal evaluation is similar to the NCT thermal model described in Section 3.3. The differences between the HAC thermal model and NCT thermal model are described in the following paragraphs.

The emissivities of the package surfaces are increased for the HAC thermal evaluation to reflect the expected surface conditions during the fire. The emissivity of the interior and exterior surfaces of the overpack outer shell is increased from 0.45 to 0.9 for the HAC thermal evaluation to account for a combination of oxidization and/or accumulation of foam char on these surfaces. The emissivity of the overpack bolting flange surfaces is increased from 0.40 to 0.75 near the outer circumference and to 0.60 near the inner circumference to capture the effects of the expected heating and oxidization of these surfaces during the fire. Since the temperatures of the overpack inner shell and the cask surfaces are not expected to increase significantly during the fire, their emissivities are the same as those used for the NCT thermal evaluation.

For the HAC thermal evaluation, all exterior surfaces of the package, including the bottom end of the overpack base, are exposed to simulate a fully engulfing fire. Further, the convective

coefficients used during the 30-minute fire are computed assuming forced convection, assuming a conservatively high gas velocity of 15 m/s, as discussed in Section 3.5.3. The convective heat transfer coefficients following the 30-minute fire are based on natural convection in still air.

The thermal decomposition of the overpack foam is accounted for in the HAC thermal models. When exposed to fire, the overpack foam produces an intumescent char that seals any large voids caused by impact damage and provides a secondary thermal barrier that insulates and protects the underlying materials. The thermal decomposition of the foam produces gases, which are vented through the thermal relief ports in the overpack base and lid. The relatively low thermal conductivity of the remaining undamaged foam also provides significant thermal protection of the cask.

As explained in Section 3.5.4, the depth of foam char during the 30-minute HAC fire event is a strong function of foam density. Since the char depth is higher for lower density foam, the char depth considered in the HAC thermal evaluation is based on a lower-bound foam density. The average density of the foam used in the overpack is required to be within ±10% of 0.216 g/cm^3 (13.5 pcf). A lower-bound foam density of 0.187 g/cm^3 (11.7 pcf), which is 15% lower than the nominal foam density, is conservatively assumed for the HAC thermal evaluation. As discussed in Section 3.5.4, the predicted char depth of 0.187 g/cm^3 foam for a 30-minute fire event is 60 mm. To conservatively bound the thermal effects of foam recession, the outer 60 mm of foam is removed from all exterior regions of the overpack that are not damaged from the HAC free drop. Heat transfer between the exterior shell of the package and the outer surface of the foam is computed assuming radiation and convection across the void space previously occupied by the removed foam segments. A surface emissivity of 0.9 is assumed for both the foam and shell surfaces, while the convection is based on an air-filled space. Since this modeling approach assumes that the foam is immediately decomposed at the start of the fire instead of gradually over a 30-minute time period, and it ignores the thermal protection afforded by the generated foam char, the predicted heat transfer into the package during the fire is conservatively high. The char depth of the foam in the regions of the overpack damaged from the HAC free drop impact is handled in a similar manner, accounting for the increased density of the crushed foam, as discussed below.

The HAC thermal models account for the cumulative damage to the package that is expected to result from the HAC free drop and HAC puncture tests prior to the HAC thermal test. Section 2.7.8 summarizes the cumulative damage sustained by the package from the HAC free drop and HAC puncture tests. The twenty-six HAC free drops and seven HAC puncture tests considered in the structural evaluation are examined for their potential impact on the thermal performance of the package. A qualitative evaluation of the predicted package damage associated with each scenario concludes that the cask does not sustain any significant damage from any of the HAC free drop or HAC puncture tests. The maximum overpack damage results from the drop evaluations performed for the hot thermal condition with the upper-bound cask mass properties and the lower-bound material strength properties. Furthermore, the overpack damage resulting from the HAC top end drop, HAC bottom end drop, and HAC side drop orientations is considered to be the most significant for the thermal evaluation. Although the HAC top and bottom corner drops result in slightly larger foam crush values, the associated foam crush is highly localized and not considered to be thermally significant. Finally, the overpack damage sustained during the HAC puncture tests is localized

and too moderate to warrant separate evaluation. Instead, the overpack damage resulting from the HAC puncture tests is bounded by the conservatisms applied to the evaluated scenarios.

The nature of the overpack damage resulting from the HAC bottom end drop, HAC top end drop, and HAC side drop orientations is sufficiently different in each orientation to warrant three separate evaluations. The three HAC thermal evaluations are summarized as follows:

Bottom End Drop Damage

The results of the structural evaluation show that the HAC bottom end drop permanently crushes the foam on the bottom end of the overpack base by approximately 45 mm, reducing the overall foam thickness from 86 mm to 41 mm. A bounding foam crush depth of 60 mm is conservatively assumed for the bottom end drop damage, leaving 26 mm of foam with a compressed density of 0.623 g/cm^3. While the reduced foam thickness and higher density yields a lower thermal protection from a thermal conductivity point of view, the higher foam density also yields a significantly higher resistance to thermal decomposition. Based on the same approach used to predict the char depth of the undamaged foam, 12 mm of char depth is predicted in the region of the crushed foam. Thus, the modeled thickness of the foam underneath the bottom end of the overpack cavity, accounting for both the foam crush resulting from the HAC bottom end drop and the foam recession during the 30-minute fire, is 14 mm.

The model used to perform the HAC thermal analysis for the bottom end drop damage is shown in Figure 3-7. The positions of the overpack inner shell and cask are moved downward by 49 mm to bound the permanent damage predicted in the structural evaluation. As shown in Figure 3-7, the entire downward shift is assumed to be accommodated by permanent deformation of the overpack base flange region. The crushed foam directly underneath the bottom end of the overpack cavity, which has an increased density of 0.623 g/cm^3, is modeled with the corresponding thermal conductivity of 0.087 W/m-K. The outer regions of the foam that will be charred during the 30-minute fire are removed from the model at the beginning of the HAC thermal transient.

The cask is modeled in the same manner as that described for the NCT thermal evaluation. The package is assumed to remain upright during the HAC thermal test, with the cask resting on the bottom of the overpack cavity. The heat transfer between the shield lid and the inside surface of overpack lid is simulated as conduction across a 54 mm thick air-filled space. The radiation exchange between the exterior of the cask and the interior of the overpack is calculated to account for the shift in the cask and overpack geometry.

Top End Drop Damage

The results of the structural evaluation show that the HAC top end drop permanently crushes the foam directly over the overpack cavity by approximately 56 mm, reducing the overall thickness of the foam from 95 mm to 39 mm. A bounding foam crush depth of 62 mm is conservatively assumed for the top end drop damage, leaving 33 mm of foam with a compressed density of 0.534 g/cm^3. Based on the same approach used to predict the char depth of the undamaged foam, 17 mm of char depth is predicted in the region of the crushed foam. Thus, the modeled thickness

of the foam above the top end of the overpack cavity, accounting for both the foam crush resulting from the HAC top end drop and the foam recession during the 30-minute fire, is 16 mm.

The model used to perform the HAC thermal analysis for the top end drop damage is shown in Figure 3-8. The positions of the overpack lid inner shell and cask are moved upward by 48 mm to bound the permanent damage predicted in the structural evaluation. The crushed foam directly above the top end of the overpack cavity, which has an increased density of 0.534 g/cm^3, is modeled with the corresponding thermal conductivity of 0.074 W/m-K. The outer regions of the foam that will be charred during the 30-minute fire are removed from the model at the beginning of the HAC thermal transient.

The cask is modeled in the same manner as that described for the NCT thermal evaluation. The package is assumed to remain upside down during the HAC thermal test, with the cask resting on the top end of the overpack cavity. The heat transfer from the shield lid to the underside of the overpack lid is simulated as a contact resistance, while the heat transfer between the shield lid and the bottom surface of the overpack cavity is simulated as conduction across a 48 mm thick air-filled space. The radiation exchange between the exterior of the cask and the interior of the overpack is calculated to account for the shift in the cask and overpack geometry.

Side Drop Damage

The results of the structural evaluation show that the side drop will cause non-uniform crushing of the foam along the impacted side of the package. At the side of impact, the foam crush depth ranges from 58 mm at the bottom end of the overpack cavity to 35 mm at the top of the overpack cavity. Rather than modeling this variation in form crush depth, a uniform foam crush depth of 49 mm is modeled over the entire length of the overpack cavity. The modeled crush depth bounds the predicted foam crush over the top 60% of the overpack cavity. Since the heat transfer into the bottom end of the overpack cavity is dominated by conductance through the thermal spider, the fact that the predicted crush over the bottom region of the cavity is not bounded by the modeled crush depth is not thermally significant. Also, the separation of the inner shell from the foam along the segment of the package opposite of the drop damage is not modeled since the presence of this layer of air tends to increase the thermal resistance between the inner and outer shell.

As a result of the 49 mm crush depth, the density of the crushed foam is increased by a factor of approximately 1.89. Based on the same approach used to predict the char depth of the undamaged foam, 30 mm of char depth is predicted in the region of the crushed foam. Thus, the modeled thickness of the foam on the impacted side of the overpack cavity, accounting for both the foam crush resulting from the HAC top end drop and the foam recession during the 30-minute fire, is 25 mm.

The model used to perform the HAC thermal analysis for the side drop damage is shown in Figure 3-9. The model incorporates the general modifications for HAC conditions, including conservatively removing those foam segments that are not expected to survive the 30-minute exposure to the HAC fire environment, and compressing the foam along a 60° subtended angle of

the impacted side of the overpack cavity to a density of 0.353 g/cm^3 with the associated increase in the local foam conductivity from 0.038 W/m-K to 0.054 W/m-K. Radiation conductors are added to simulate the potential increase in the local heat transfer due to the collapse of the offset segments in the base flange.

The thermal modeling of the cask and payload remains the same as that used for the NCT model. The package is assumed to remain on its side during the HAC thermal test. As such, the cask is modeled as having line contact with the impacted side of the overpack cavity. For conservatism, the heat transfer between the cask bottom end and the overpack cavity is simulated using the same level of contact resistance used in the NCT model for an upright package. The radiation exchange between the exterior of the cask and the interior of the overpack is calculated to account for the shift in the overpack geometry.

For all three HAC thermal analysis, the ambient temperature is raised to 800°C at time = 0 to simulate the presence of a fully engulfing fire and maintained for 30 minutes. After 30 minutes, the ambient temperature is lowered to 38°C. The transient analysis is continued for an additional 9.5 hours to capture the peak temperatures within each of the package components. Solar heating is applied to the exterior of the package in the form of a diurnal cycle, with the peak insolation occurring at the end of the 30-minute fire. The results of the HAC thermal evaluation are discussed in Section 3.4.3.

3.4.3 Maximum Temperatures and Pressure

The maximum temperatures of the package components for the HAC thermal test are summarized in Table 3-2. The results show that the maximum temperatures of the package components are all considerably lower than the maximum allowable temperatures. The smallest temperature margin for the HAC thermal test occurs in the cask containment O-ring seal, which reaches a maximum temperature of 145°C versus an HAC temperature limit of 204°C.

The temperature transients of the key components of the package for the three different HAC free drop damage scenarios considered in the HAC thermal evaluation are shown in Figure 3-10 through Figure 3-12. These figures show that the package thermal response is similar for all three HAC free drop damage scenarios. In all cases, the overpack outer shell temperature rises quickly to approximately 780°C, as expected given its relatively low thermal mass. The thermal response of the overpack closure flange lags a bit due to its higher thermal mass, but approaches the flame temperature by the end of the 30-minute fire. In contrast, the overpack inner shell is largely isolated from the high fire temperatures by the shielding effect of the outer shell, the undamaged foam that surrounds it, and the relatively thin metal of the base flange that connects the inner and outer shells. The principal means of heat transfer to the overpack inner shell is conduction through the thermal spider at the base of the overpack cavity. The peak temperatures of the cask components are reached between 1 and 4 hours after the start of the HAC fire test. After the peak temperatures are reached, they continued to fall until equilibrium is eventually reached with the ambient temperature. This is due to the rapid decay of the payload thermal power. The HAC thermal evaluation for the side drop damage results in the highest temperatures for most cask components.

The maximum pressure within the cask cavity under the evaluated damage scenarios is estimated by conservatively assuming that the regulatory NCT pressure limit of 7 bar exists within the cask cavity at the start of the fire event. Assuming that pressurization of the cask cavity under HAC conditions is due to a combination of real gas expansion of the constituents in the cavity at the start of the HAC event and steam vapor generation, the maximum pressure that will be achieved within the cavity during the HAC thermal test (P_{HAC}) can be computed from:

$$P_{HAC} = P_{NCT} \times \left(\frac{T_{HAC}}{T_{NCT}} \right) + P_{Saturation}$$

Where P_{NCT} is the maximum pressure at NCT conditions (7 bar), T_{HAC} is the absolute temperature of cask cavity gas at HAC conditions, T_{NCT} is the absolute temperature of cask cavity gas at NCT conditions, and $P_{Saturation}$ is the saturation pressure of steam at HAC temperature.

From Table 3-1 and Table 3-2, the highest bulk average temperatures of gases in the cask cavity for NCT and HAC are 78°C and 146°C, respectively. The saturation pressure of steam at 146°C is approximately 4.2 bar. Therefore, the peak pressure reached within the cask containment system under HAC thermal loading is conservatively estimated to be 12.6 bar. This estimate conservatively assumes that the pressurization under NCT conditions does not involve any steam vapor since any vapor existing in the cavity prior to the HAC event will serve to reduce any further amount of vapor that can accumulate within the cavity.

3.4.4 Maximum Thermal Stresses

As discussed in Section 2.7.4.3, the only significant thermal stresses in the cask assembly due to the HAC thermal test occur in the cask closure bolts. The closure bolt stresses arise from differential thermal expansion between the dissimilar materials of the closure lid and closure bolts and from increased internal pressure due to the elevated temperature of the gases in the cask cavity. The results of the structural evaluation show that the maximum stresses in the cask closure bolts due to the HAC thermal test satisfy the applicable allowable stress design criteria. Furthermore, since the closure bolt stresses do not exceed the material yield strength, no inelastic deformation of the cask closure bolts will result from the HAC thermal test.

3.4.5 Accident Conditions for Fissile Material Packages for Air Transport

Not applicable.

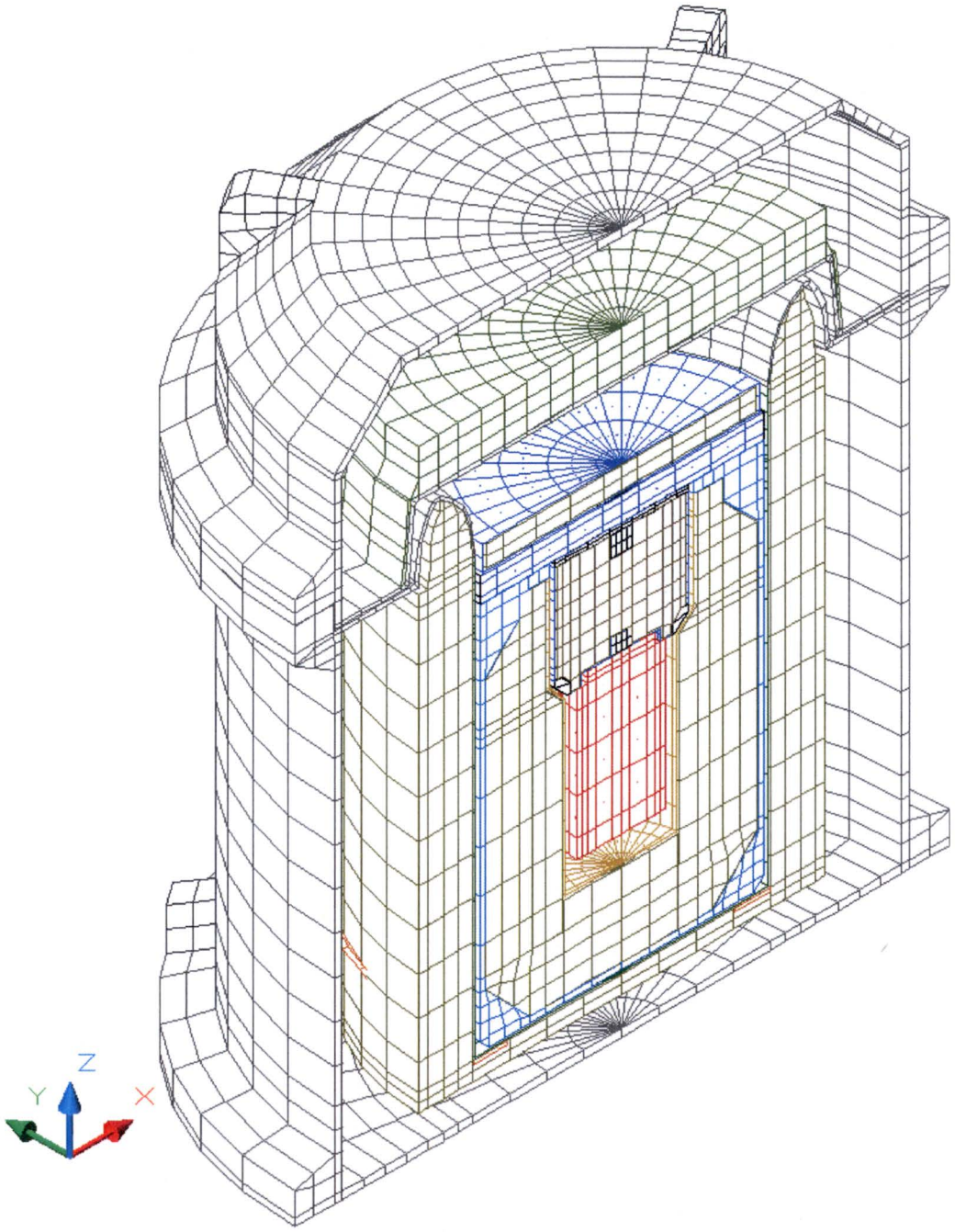

Figure 3-7 – MIDUS Package HAC Thermal Model, Bottom End Drop Damage Configuration

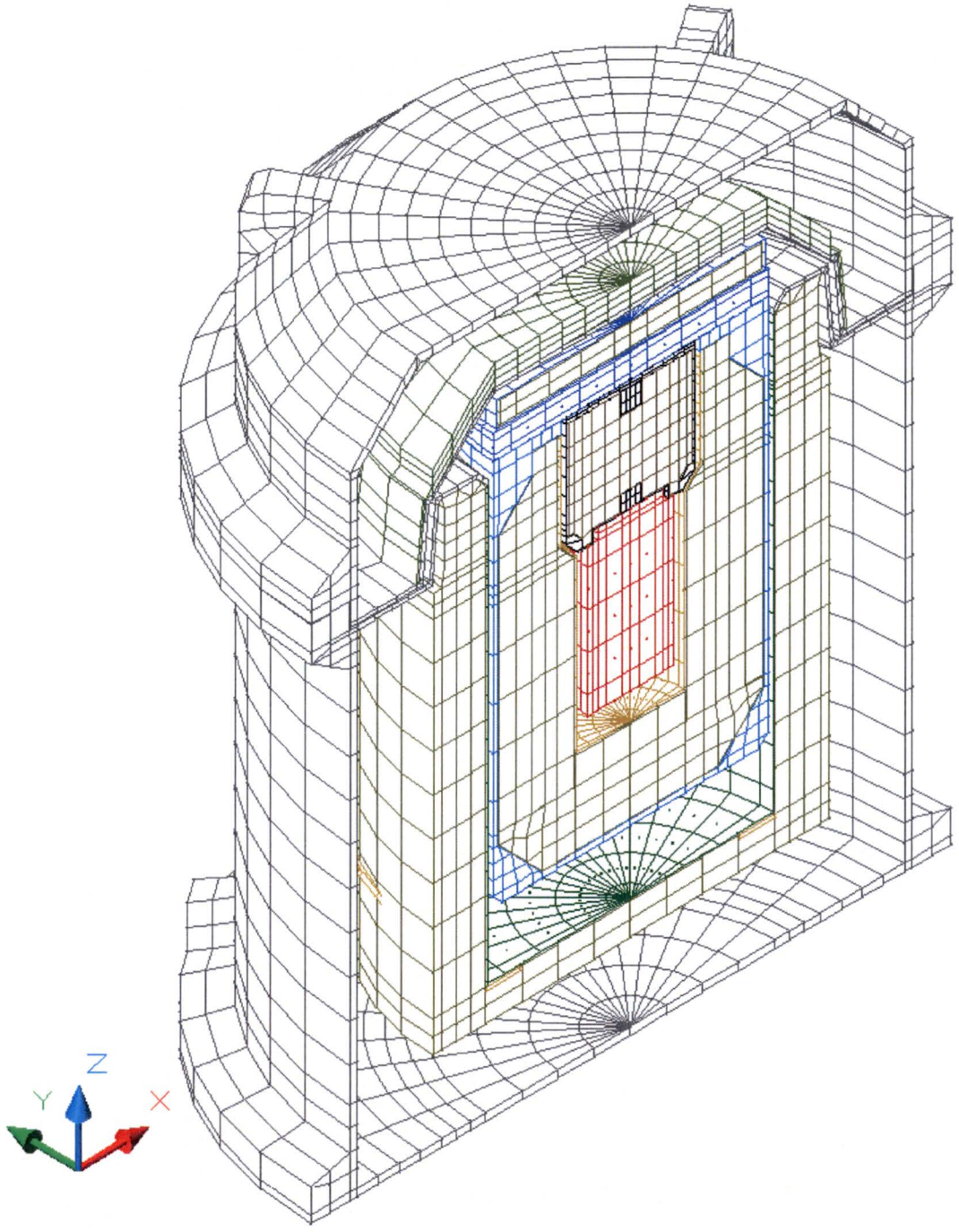

Figure 3-8 – MIDUS Package HAC Thermal Model, Top End Drop Damage Configuration

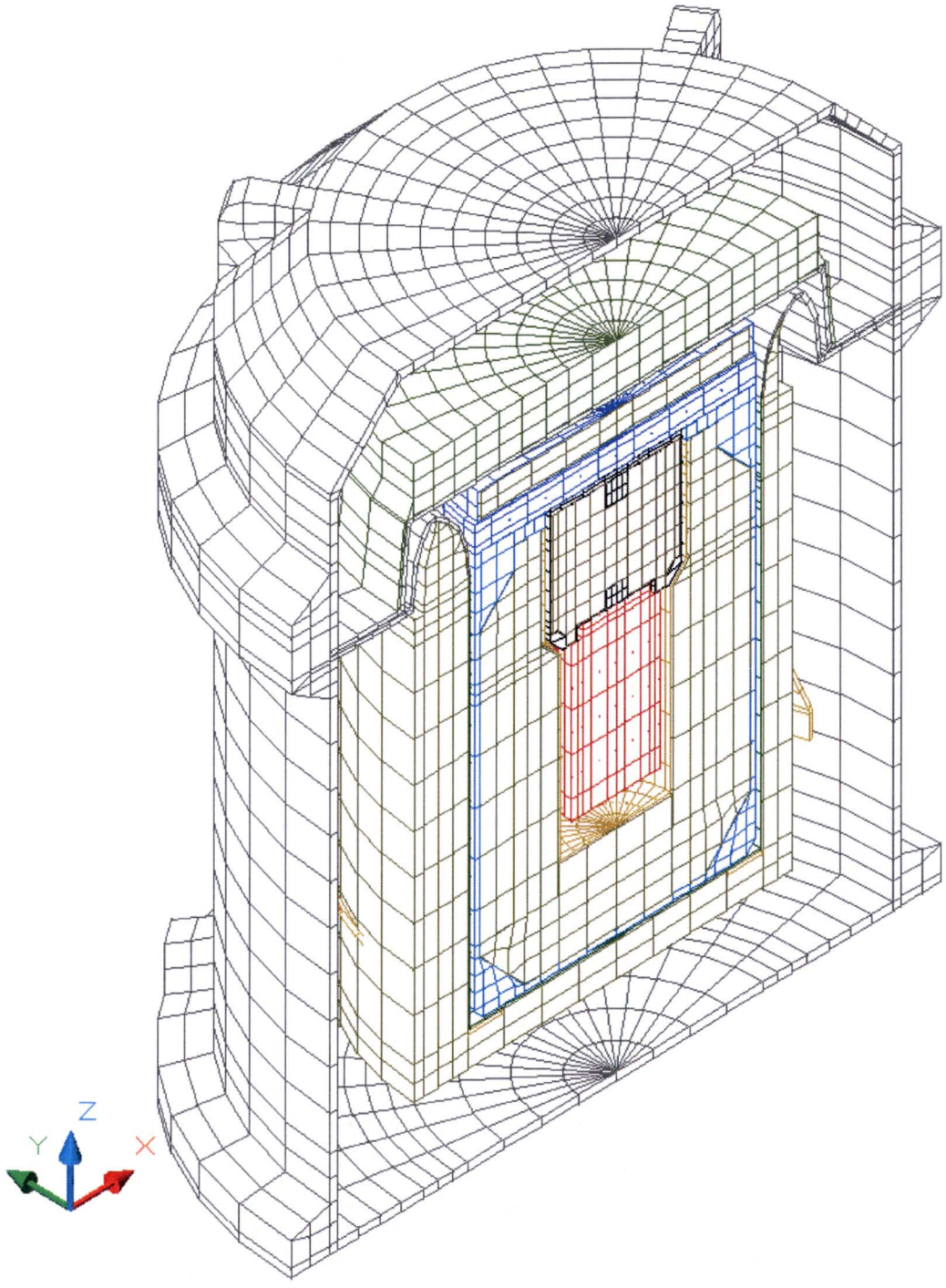

Figure 3-9 – MIDUS Package HAC Thermal Model, Side Drop Damage Configuration

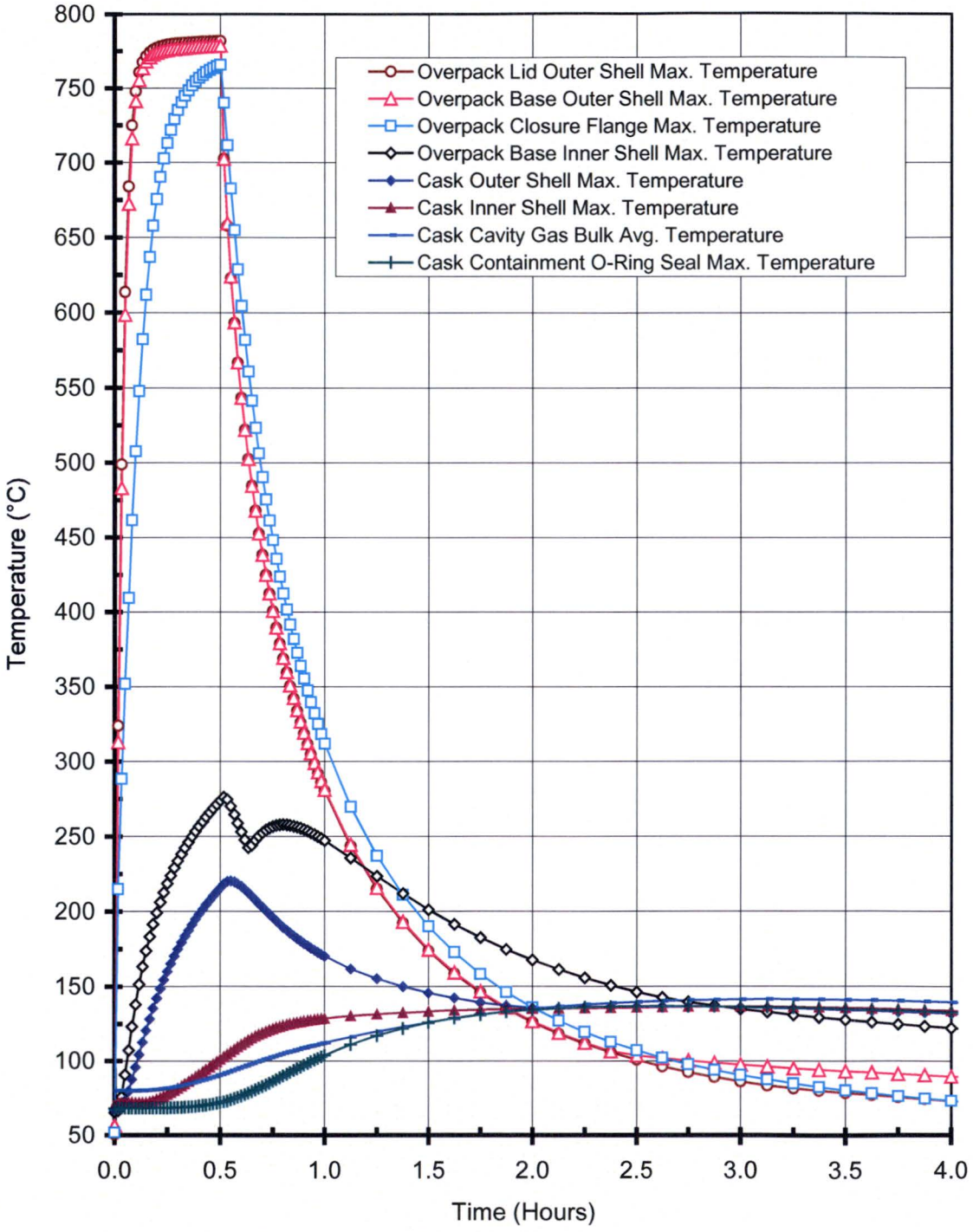

Figure 3-10 – Package Temperatures for HAC Thermal Test with Bottom End Damage

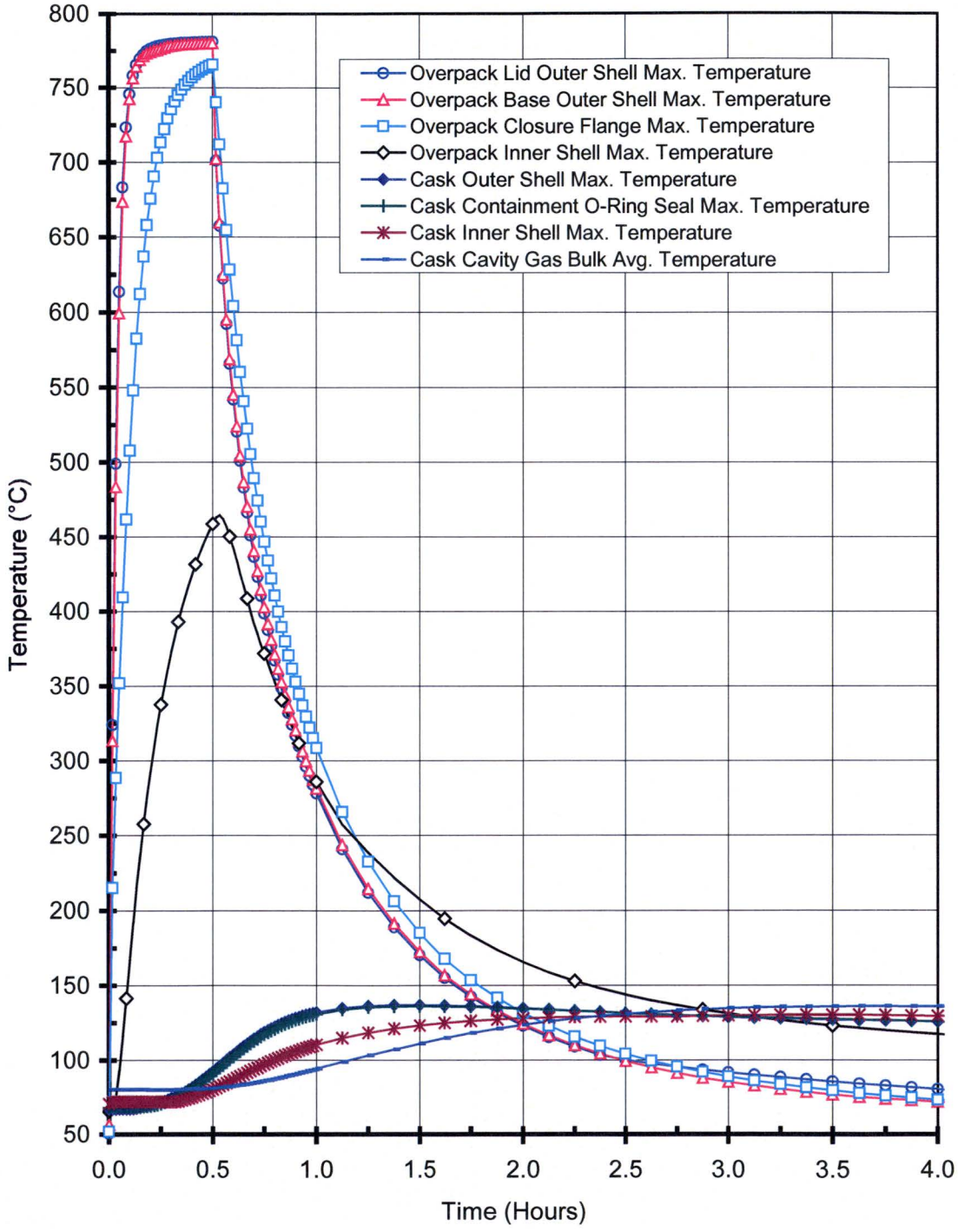

Figure 3-11 – Package Temperatures for HAC Thermal Test with Top End Damage

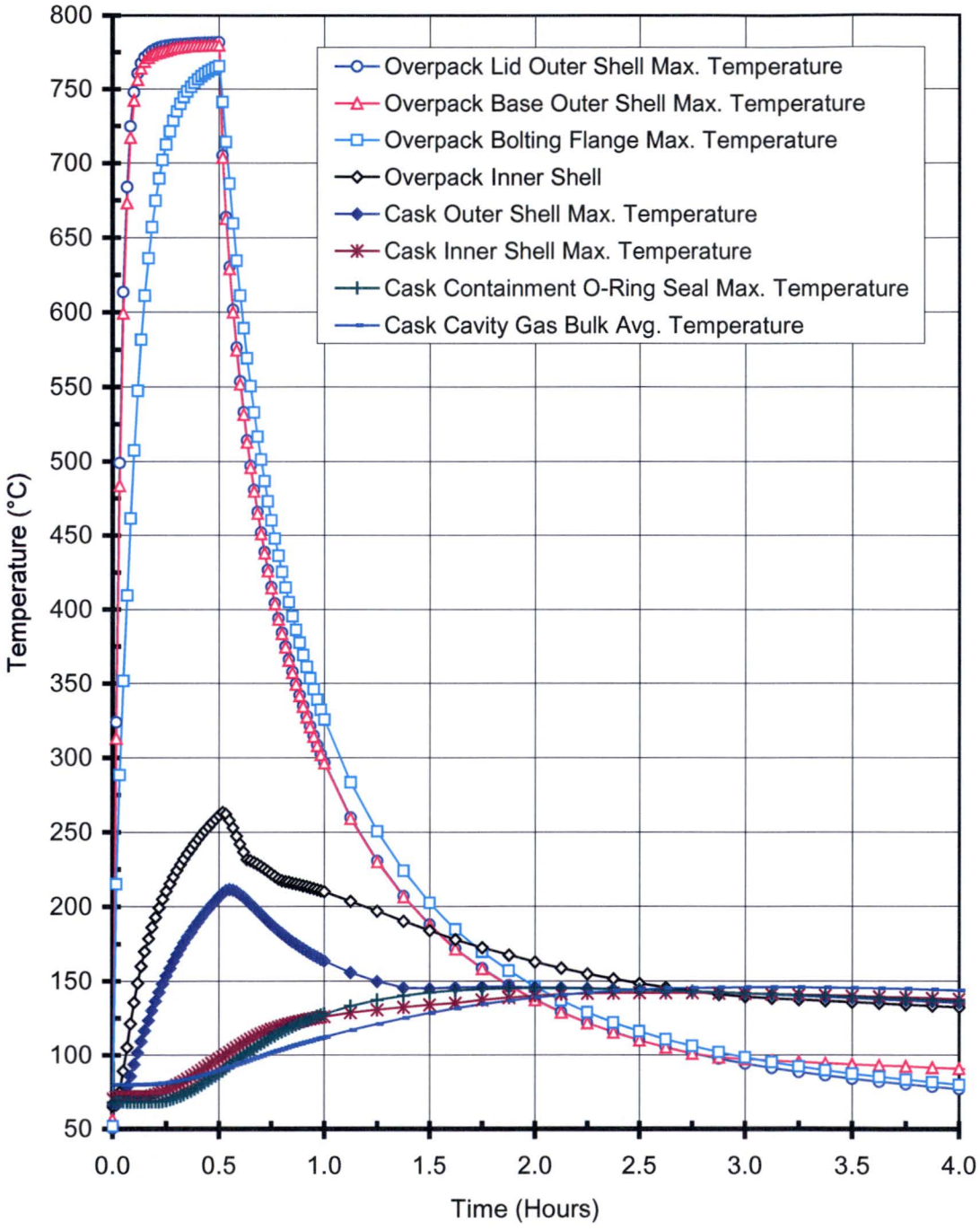

Figure 3-12 – Package Temperatures for HAC Thermal Test with Side Damage

3.5 Appendix

3.5.1 References

[3.1] "ORIGEN 2.1 - Isotope Generation and Depletion Code, Matrix Exponential Method," RSICC Computer Code Collection CCC-371, Oak Ridge National Laboratory, February 1996.

[3.2] American Society of Mechanical Engineers (ASME) Boiler and Pressure Vessel Code, Section II, Part D, *Materials*, 2001 Edition with Addenda through July 1, 2003.

[3.3] Frank, R. C., and W. L. Plagemann, *Emissivity Testing of Metal Specimens.* Boeing Analytical Engineering coordination sheet No. 2-3623-2-RF-C86-349, August 21, 1986. Testing accomplished in support of the TRUPACT-II design program.

[3.4] Surface Optics Corporation, *Surface Optical Property Measurements on Sierra Nuclear Corp. Supplied Sample Materials*, Report #SOC-R6001-030-002-0698, June 1998.

[3.5] Parker Hannifin Corporation, *Parker O-Ring Handbook*, ORD 5700/USA, 2001.

[3.6] Incropera and DeWitt, *Fundamentals of Heat and Mass Transfer*, 5th Edition, John Wiley & Sons Publishers, 2002.

[3.7] General Electric, *Properties of Solids, Thermal Conductivity, Metallic Materials, Heat Transfer Division*, July 1974.

[3.8] Rohsenow, Hartnett, and Choi, *Handbook of Heat Transfer*, 3rd Edition, McGraw-Hill Publishers, 1998.

[3.9] G. G. Gubareff, J. E. Janssen, and R. H. Torborg, *Thermal Radiation Properties Survey*, 2nd Edition, Honeywell Research Center, 1960.

[3.10] Guyer, E.C., *Handbook of Applied Thermal Design*, McGraw-Hill, Inc., 1989.

[3.11] Rohsenow, Hartnett, and Ganic, *Handbook of Heat Transfer Fundamentals*, 2nd Edition, McGraw-Hill Publishers, 1985.

[3.12] Kreith, Frank, *Principles of Heat Transfer*, 3rd Edition, Harper & Row, 1973.

[3.13] C.L. Williamson, Z.L. Iams, "Thermal Assault and Polyurethane Foam Evaluating Protective Mechanisms for Transport Containers." General Plastics Manufacturing Company, Tacoma, WA, presented at Waste Management '05 Symposium, Tucson, AZ, 2005.

[3.14] C.L. Williamson, Z.L. Iams, "Thermal Assault and Polyurethane Foam - Evaluating Protective Mechanisms." General Plastics Manufacturing Company, Tacoma, WA, presented at PATRAM International Symposium, Berlin, Germany, 2004.

3.5.2 Computer Analysis Results

Due to the extent of the computer output associated with each design load case, a sample input and output file are not provided.

3.5.3 Heat Transfer Correlations

The evaluation of the thermal performance of the package over the wide range of potential operating conditions encountered during NCT and HAC conditions is based on semi-empirical relationships for convection heat transfer. The convective heat transfer coefficient, h_c, has a form of:

$$h_c = Nu\frac{k}{L}$$

where k is the thermal conductivity of the gas at the mean film temperature and L is the characteristic length of the vertical or horizontal surface. These semi-empirical relationships are chosen to account for the variation in convection heat transfer rates between laminar and turbulent operating conditions, the orientation of the package, and the shape and orientation of the specific surface experiencing convective heat transfer.

The natural convective heat transfer coefficient, h, for the sidewall surfaces of a vertically oriented package is calculated from the correlation for a vertical cylinder [3.10]. This correlation relates the heat transfer coefficient, h, to the Nusselt number, a non-dimensional parameter. The Nusselt number, in turn, is computed as follows:

$$Nu = \left[\left(Nu_{l,cyl} \right)^6 + \left(Nut \right)^6 \right]^{1/6}, \quad 1 < Ra < 10^{12},$$

$$Nu_{l,cyl} = Cf\, Nu_l,$$

$$Nu_l = \frac{2.8}{\ln\left[1 + \frac{2.8}{\left(Cl\, Ra^{1/4} \right)} \right]},$$

$$Cl = \frac{0.671}{\left[1+\left(\frac{0.492}{Pr}\right)^{\frac{9}{16}}\right]^{\frac{4}{9}}},$$

$$Cf = \frac{1.8\phi}{\ln[1+1.8\phi]},$$

$$\phi = \frac{\frac{Lc}{D}}{Cl\,Ra^{1/4}},$$

$$Nu_t = C_v Ra^{\frac{1}{3}},$$

$$Cv = \frac{0.13\left(Pr^{0.22}\right)}{\left(1+0.61\,Pr^{0.81}\right)^{0.42}},$$

$$Ra = \frac{\beta g \Delta T Lc^3}{\nu \alpha},$$

$$Pr = \frac{\mu Cp}{k},$$

where,

h = heat transfer coefficient
k = thermal conductivity of air
α = thermal diffusivity
Cp = specific heat at constant pressure
ν = kinematic viscosity
β = coefficient of thermal expansion
g = acceleration due to gravity,
Lc = length of cylinder
D = diameter of cylinder,
ΔT = temperature difference between surface and surroundings

Once the Nusselt number, Nu, is determined, the convection coefficient used in the thermal model is computed via:

$$h_c = Nu\frac{k}{L}$$

In a similar manner, the natural convection from vertical surfaces, such as the ends of a horizontal package, is computed using Equations 6-39 to 6-42 of [3.11], where the characteristic length is the height of the surface. These equations, which are applicable over the range of Rayleigh number (Ra) between 1 and 10^{12}, are as follows:

$$Nu^T = \overline{C}_L Ra^{1/4}$$

$$\overline{C}_l = \frac{4}{3}\left[\frac{0.503}{\left(1+(0.492/Pr)^{9/16}\right)^{4/9}}\right]$$

$$Nu_L = \frac{2.8}{\ln\left(1+2.8/Nu^T\right)}$$

$$Nu_t = C_t^V Ra^{1/3}$$

$$C_t^V = \frac{0.13\,Pr^{0.22}}{\left(1+0.61\,Pr^{0.81}\right)^{0.42}}$$

$$Nu = \frac{h_c L}{k} = \left[(Nu_L)^6 + (Nu_t)^6\right]^{1/6}$$

where

$$Ra_L = \frac{\rho^2 g_c \beta L^3 \Delta T}{\mu^2} \times Pr$$

h_c = convection coefficient
Nu = Nusselt number
g_c = gravitational acceleration
β = coefficient of thermal expansion
ΔT = temperature difference
ρ = density of air at the film temperature
μ = dynamic viscosity
Pr = Prandtl number
L = characteristic length
k = thermal conductivity of air at the mean film temperature
Ra = Rayleigh number
h_c = convection coefficient

Note that k, c_p, and μ are each computed as a function of air temperature, as taken from Table 3-5. Values for ρ are computed using the ideal gas law, β for an ideal gas is simply the inverse of the absolute temperature of the gas, and Pr is computed using the values for k, c_p, and μ. Unit conversion factors are used as required to reconcile the units for the various properties used.

Calculation of the convection coefficient between the overpack shell and the ambient environment when the package is horizontal is computed using a correlation for horizontal cylinders [Equation 3-43, Chapter 1, [3.9]]. The characteristic length, D, is the outer diameter of the cylinder. This equation, applicable for $10^{-5} < Ra < 10^{12}$, is as follows:

$$Nu = \frac{h_c D}{k} = \left\{ 0.60 + \frac{0.387 Ra_D^{1/6}}{\left[1 + (0.559/Pr)^{9/16}\right]^{8/27}} \right\}^2$$

Natural convection from horizontal surfaces is computed from Equations 4.39 and 4.40 of [3.8] where the characteristic dimension (L) is equal to the plate surface area divided by the plate perimeter. For a heated surface facing upwards or a cooled surface facing downwards and $Ra > 1$:

$$Nu = \frac{h_c L}{k} = \left[(Nu_L)^{10} + (Nu_t)^{10} \right]^{1/10}$$

$$Nu_L = \frac{1.4}{\ln\left(1 + 1.677/\left(\overline{C_L} Ra^{1/4}\right)\right)}$$

$$\overline{C_L} = \frac{0.671}{\left[1 + (0.492/Pr)^{9/16}\right]^{4/9}}$$

$$Nu_t = 0.14 Ra^{1/3}$$

For a heated surface facing downwards or a cooled surface facing upwards and $10^3 < Ra < 10^{10}$, the correlation is as follows:

$$Nu = Nu_L = \frac{2.5}{\ln\left(1 + 2.5/Nu^T\right)}$$

$$Nu^T = \frac{0.527}{\left(1 + (1.9/Pr)^{9/10}\right)^{2/9}} Ra^{1/5}$$

For forced convection encountered during the HAC fire event, the convective heat transfer coefficient, h_c, is computed from correlations for flat surfaces [Table 6-5, [3.12]] where the characteristic dimension (L) is equal to the length along the surface. For conservatism, a gas velocity of 15 m/s and a characteristic length of 38 mm are used when computing the forced convection coefficient for all surfaces.

For Reynolds number (Re) < 5×10^5 and Prandtl number (Pr) > 0.1, the forced convection coefficient is computed via:

$$Nu = 0.664 Re_L^{0.5} Pr^{0.33}$$

For Reynolds number (Re) > $5x10^5$ and Prandtl number (Pr) > 0.5, the forced convection coefficient is computed via:

$$Nu = 0.036 Pr^{0.33} [Re_L^{0.8} - 23{,}200]$$

Radiation Heat Transfer

Radiation heat transfer is computed using the standard gray-body relationship as expressed by equation 1-8 of [3.12]:

$$q = \sigma A_1 \mathbf{F}_{1-2} \left(T_1^4 - T_2^4\right)$$

where σ is the Stefan-Boltzmann constant, and values of (A_1 $\mathbf{F}_{1-2}$) are calculated within the Thermal Desktop computer program using a Monte Carlo ray tracing algorithm. The SINDA/FLUINT program automatically computes the T^4 values using the absolute temperature and adds the Stefan-Boltzmann constant σ.

3.5.4 Foam Response to Fire

The General Plastics LAST-A-FOAM® FR-3700 rigid polyurethane foam [www.generalplastics.com] has been used in numerous radioactive materials (RAM) packages. The FR-3700 formulation is specially designed to allow predictable impact-absorption performance under dynamic loading, while also providing an intumescent char layer that insulates and protects the underlying materials, even when exposed to pool-fire conditions. Upon exposure to fire temperatures, this proprietary foam decomposes into an intumescent char that swells and tends to fill voids or gaps created by free drop or puncture bar damage. The thermal decomposition absorbs a significant amount of the heat transferred into the foam, which is then expelled from the package as a high-temperature gas. At the same time, the resultant char layer shields the underlying undamaged foam from further direct exposure to the external high temperatures. This behavior has been observed in numerous fire tests of other RAM packages.

Since the decomposition of the foam under elevated temperatures is an endothermic process, the foam is self-extinguishing and will not support a flame once the external fire is removed. However, the gases generated by the decomposition process are combustible and will burn under piloted conditions. Further, a portion of these generated gases could remain trapped within the charred layer of the foam for a period of time after the cessation of the HAC fire event and could support further combustion, although at a much reduced level, until a sufficient time has passed for their depletion from the cell structure.

The mechanisms behind the observed variations in the thermal properties and behavior of the FR-3700 foam at elevated temperatures are varied and complex and only limited research has been conducted in this area. No definitive analytical model of the foam properties under HAC conditions currently exists. Instead, a combination of empirical data and modeling conservatism is used to simulate the thermal performance of the LAST-A-FOAM® FR-3700 polyurethane foam for this application.

The [3.13] and [3.14] references describe the setup and results of a series of fire tests conducted on 5-gallon cans filled with FR-3700 foam at densities from 0.107 to 0.412 g/cm^3 (6.7 to 25.8 pounds per cubic foot (pcf)). Under the fire tests, one end of the test articles (i.e., the hot face surface) was subjected to an open diesel fueled burner flame at temperatures of 980 to 1,200°C (1,800 to 2,200°F) for 30+ minutes. A thermal shield prevented direct exposure to the burner flame on any surface of the test article other than the hot face. Each test article was instrumented with thermocouples located at various depths in the foam. In addition, samples of the foam were subjected to thermogravimetric analysis (TGA) to determine the thermal decomposition vs. temperature. The exposure temperatures for the tests varied from 21 to 820°C (70 to 1,500°F) and were conducted in both air and nitrogen atmospheres. Since the results for the nitrogen environment (see Figure 3-13) are more representative of the low oxygen environment existing for the encased foam, it is used for the basis of this evaluation. These test results indicate that the following steps occur in the thermal breakdown of the foam under the level of elevated temperatures reached during the HAC fire event:

- Below 120°C (250°F), the variations in foam thermal properties with temperature are slight and reversible. Thus, fixed values for specific heat and thermal conductivity are appropriate.
- Between 120 and 260°C (250 and 500°F), small variations in foam thermal properties occur as water vapor and non-condensable gases are driven out of the foam. Thus, fixed values for specific heat and thermal conductivity are appropriate.
- Irreversible thermal decomposition of the foam begins as the temperature rises above 260°C (500°F) and increases non-linearly with temperature. Based on the TGA testing (see Figure 3-13), approximately two-thirds of this decomposition occurs over a narrow temperature range centered about 354°C (670°F).
- The decomposition is accompanied by vigorous outgassing from the foam and an indeterminate amount of internal heat generation. The internal heat generation arises from the gases generated by the decomposition process that are combustible under piloted conditions. However, since the decomposition process is exothermic, the foam will not support combustion indefinitely and further, the outgassing process removes a significant amount of heat itself via mass transport.
- The weight loss due to outgassing not only has a direct effect on the heat flux into the remaining virgin foam, but changes the composition of the resulting foam char, since the foam constituents are lost at different rates. This change in composition affects both the specific heat and the thermal conductivity of the foam char layer.
- As temperature continues to rise, the developing char layer begins to take on the characteristics of a gas-filled cellular structure where radiative interchange from one cell surface to another becomes a significant portion of the overall heat transfer mechanism. This change in the dominant heat transfer mechanism causes the apparent heat conductivity to take on a highly non-linear relationship with temperature.
- Finally, at temperatures above 675°C (1,250) °F, the thermal breakdown of the foam is essentially completed and only about 5 to 10% of the original mass is left. In the absence

of direct exposure to a flame or erosion by the channeling of the outgas products through the foam, the char layer will be the same or slightly thicker than the original foam depth. This char layer will continue to provide radiative shielding to the underlying foam material.

The sharp transition in the state of the foam noted in Figure 3-13 at or about 354°C (670°F) can be used to correlate the depth of the foam char and the occurrence of this temperature level within the foam. Figure 3-14 illustrates the relationship between foam recession (i.e., char depth) and foam density following exposure to a 30-minute fire as compiled from a series of tests. The correlation between the foam recession depth and the foam density is expressed by the relation:

$$y = -0.94681 - 11.64 \times \log_{10}(x)$$

where, y = the recession depth, cm
x = foam density (g/cm^3)

Based on this correlation, the recession depth expected for nominal 0.216 g/cm^3 (13.5 pcf) density foam is estimated to be 6.8 cm (2.7 inches). The fabrication tolerance for the foam density is $\pm$15%. Therefore, the actual foam density that may exist within the packaging ranges from 0.187 to 0.248 g/cm3 (11.7 to 15.5 pcf). The recession depth associated with the lower bound on the foam density is 7.5 cm (3 inches).

An additional correction to the expected recession is required to account for the fact that the thermal testing upon which the correlation is based used a flame temperature 980 to 1,200°C (1,800 to 2,200°F), whereas the regulatory fire flame temperature is specified as 800°C (1,475°F). Instrumented fire test results for 0.128, 0.256, and 0.384 g/cm3 (8, 16, and 24 pcf) density foam are used to estimate the correction to the predicted foam recession depth. Figure 3-15 illustrates the predicted foam temperature vs. depth and foam density at the end of a 30-minute fire event with a flame temperature of 800°C (1,475°F). Interpolating the figure data for a foam density of 0.187 g/cm3 (11.7 pcf) and foam temperature of 354°C (670°F) indicates that this temperature would be reached at a depth of approximately 4.5 cm (1.8 inches) after 30 minutes. This compares with the predicted recession depth of 7.5 cm (3 inches) at the higher flame temperature. For conservatism, the average of these two values is assumed for the predicted recession depth, or 6 cm (2.4 inches). The portions of the foam at depths greater than this from the exterior surfaces of the package are predicted to remain essentially unaffected by the HAC fire event.

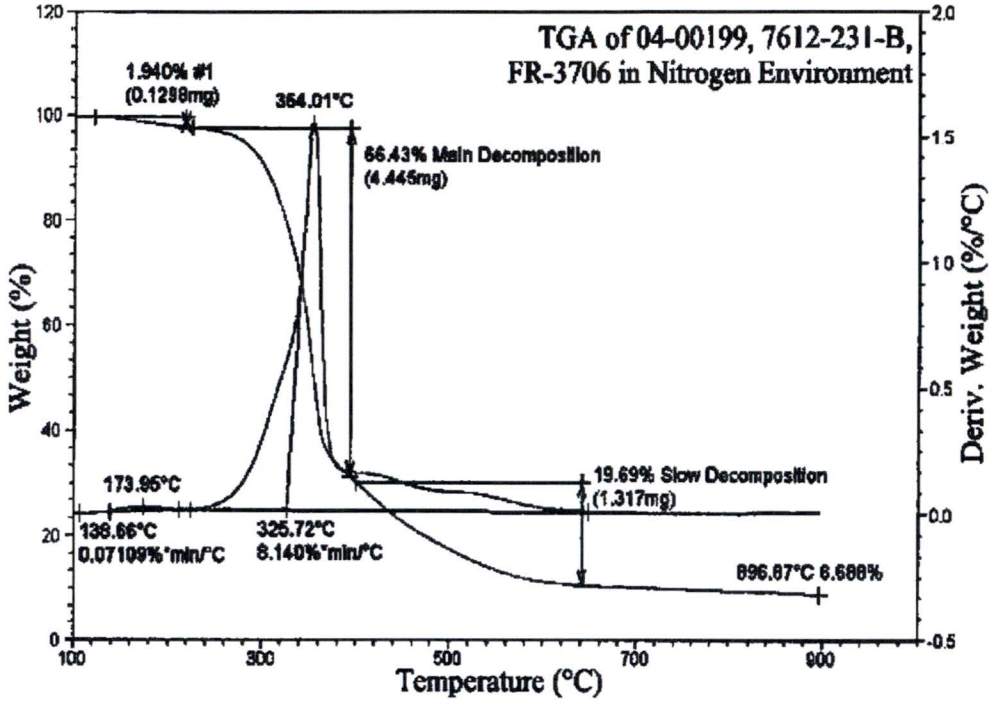

Figure 3-13 – TGA Analysis of Foam Decomposition in Nitrogen

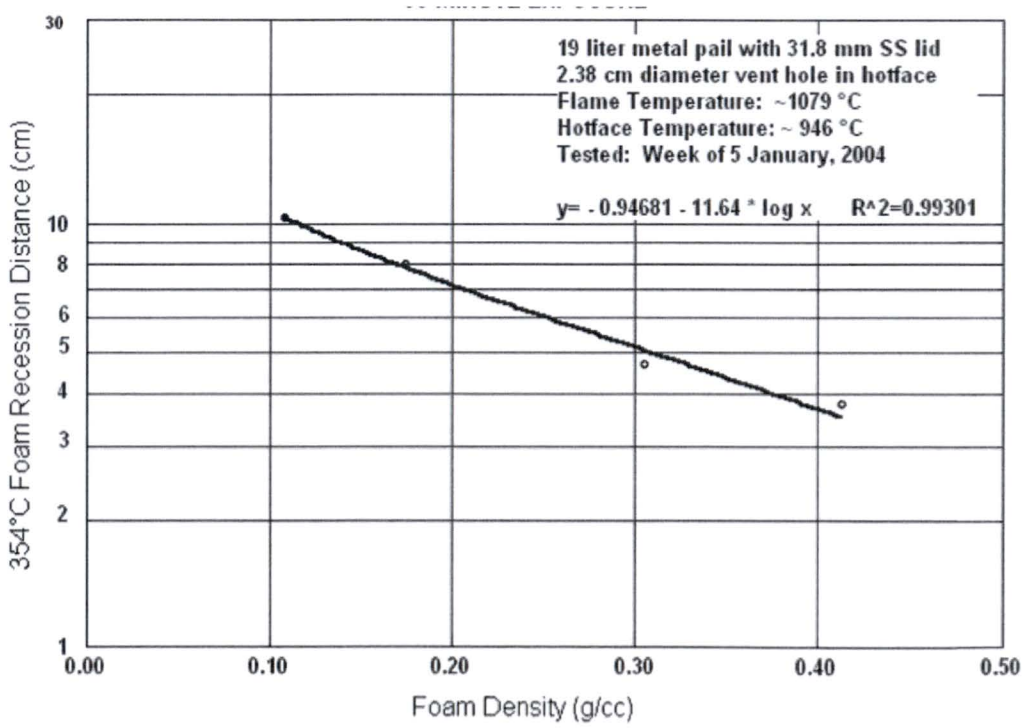

Figure 3-14 – Foam Recession vs. Density for 30-Minute Fire

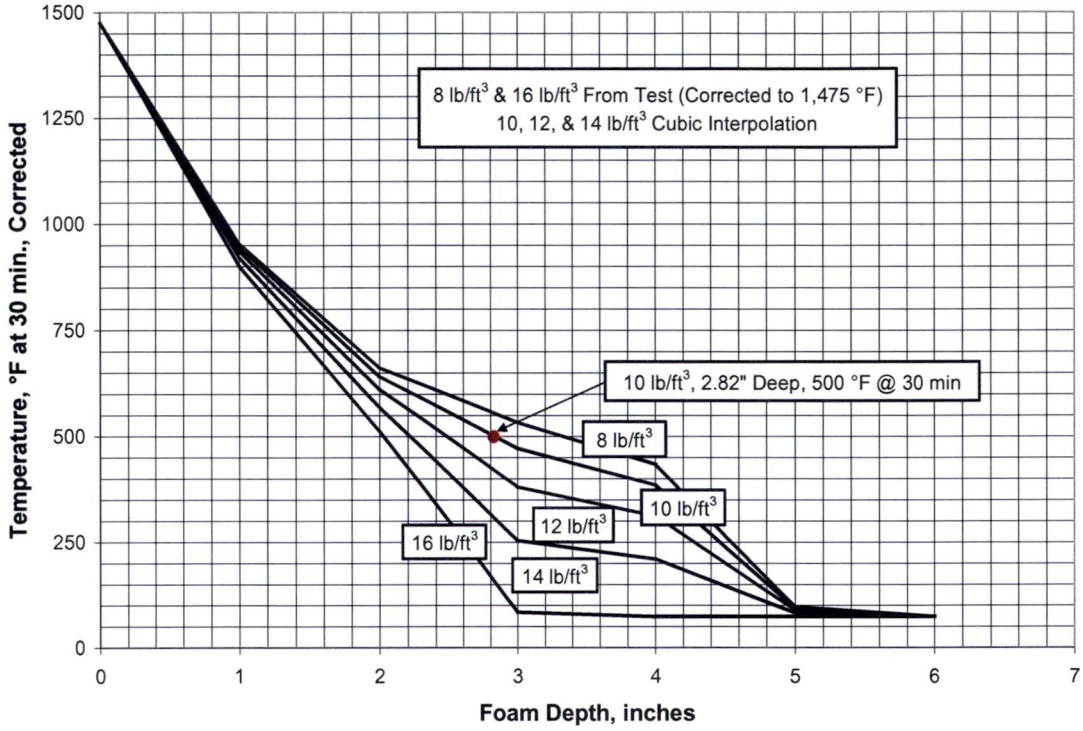

Figure 3-15 – Foam HAC Performance, Corrected for 1,475°F Flame Temperature

3.5.5 Radiolytic Gas Generation in Mallinckrodt Produced ^{99}Mo Solutions

(Proprietary Attachment)

Proprietary Attachment Withheld (g)

3.5.6 Hydrogen Generation in Mallinckrodt Produced ^{99}Mo Solutions

(Proprietary Attachment)

Proprietary Attachment Withheld (g)

4 CONTAINMENT

The MIDUS package containment boundary is designed, constructed, operated, and maintained to assure no loss or dispersal of radioactive contents under the tests specified in 10 CFR 71, §71.71 and §71.73. This chapter describes the package's containment system design and how it meets the containment requirements under NCT and HAC tests, and defines the criteria for leak-rate testing during package fabrication, use, maintenance, and repair.

4.1 Description of the Containment System

The package has a simple, robust containment system design. There are no welds within the containment boundary. Other than the main closure, there are no penetrations to the containment system, and no valves or pressure relief devices of any kind. The package does not rely on any filter or mechanical cooling system to meet containment requirements.

The containment system materials of construction are evaluated in Section 2.2.2 and selected to avoid chemical, galvanic, or other reactions. The materials of construction are compatible with each other and the chemical form of the payload.

The containment system is designed, fabricated, examined, tested, and inspected in accordance with the ASME B&PV Code, Section III, Division 3, Subsections WA and WB with certain exceptions. Section 2.1.4 and Table 2-9 and Table 2-10 of this SAR discuss the exceptions and their bases.

Figure 4-1 shows an overview of the package containment design. The package is securely closed using eight steel closure bolts (figure item 1). The containment system consists of a stainless-steel closure lid (item 2), an elastomeric containment O-ring (item 3), and a monolithic stainless-steel inner containment shell (item 4), which is integral with the cask flange. Figure 4-2 illustrates the package containment boundary.

There are two other seals indicated in Figure 4-1: a test O-ring (item 6) located outside the containment seal, and a cleanliness O-ring (item 8) located on the shield plug (item 7). The test port (item 5) is a tapped hole that communicates with the small space between the containment and test O-rings. It provides a means for performing a pre-shipment pressure-rise leak test. The cleanliness O-ring performs a housekeeping function, and it indirectly provides a post-accident shielding function as discussed in Sections 5.1.1.1 and 5.3.1.2. A third seal, not shown in the figure, is the metal-to-metal seal on the product bottle cap. Although none of these seals are relied upon for containment, each is capable of providing containment-quality sealing and thus provides a substantial safety margin to the package design.

The complete specifications for the containment system, including the materials of construction, testing requirements, required material thicknesses, O-ring seal specifications, and bolt torques, are listed in Drawings TYC01-1604 and -1605, in Section 1.3.2.

The cask closure bolts are physically protected from damage by the closure lid's recessed bolt-hole design. The closure lid also has a shear lip feature that protects the bolts from shear failure due to transverse impact loads. The closure bolts are positive fasteners that securely close the package. They cannot be opened unintentionally, or by any pressure that may arise within the package (Section 2.4.3). In addition, a tamper-indicating seal applied to the package prior to shipment further assures that the package cannot be opened unintentionally.

Ethylene-propylene is the specified containment O-ring material. It offers good resistance to sodium hydroxide and sodium nitrate [4.1], the two components of the payload solution. The manufacturer's recommended temperature range for continuous service of ethylene-propylene O-rings is -40°C to 150°C. For short exposures, the material can withstand a temperature 204°C for 2 hours or less [4.1]. Sections 3.3.1 and 3.4.3 show that the containment O-ring temperatures are below these recommended values for the NCT and HAC conditions, respectively. A Sandia National Laboratories test program compared several elastomeric O-ring compounds for performance under transportation package conditions [4.2]. It found that ethylene-propylene O-rings perform well at both cold and high temperatures, independently confirming the manufacturer's ratings.

Radiation can affect the properties of O-ring materials, reducing their resistance to compression set. Ethylene propylene elastomers have good radiation-resistance properties and, like many O-ring compounds, provide adequate performance into the 10^6–10^7 rads exposure range [4.1]. For conservatism, the radiation-resistance for the containment O-ring is specified as 10^6 rads.

Radiation exposure to the containment seal during shipping is very low. The package is designed for contact maintenance at the cask flange area. At those exposure rates, the service life for an elastomeric seal would be many hundreds of thousands of use-cycles. Thus, exposure of the containment O-ring during package shipment is not a controlling factor for O-ring replacement.

During package loading, the payload is lowered into the cask cavity. It travels past the containment seal for a few seconds per loading cycle, shielded only by the product and the steel in the payload internals. Calculations show that the maximum instantaneous energy deposition in the containment seal is on the order of 2×10^5 rads/hr. At this peak exposure rate, it would take five continuous hours, or about 900 load/unload cycles at 10 seconds' effective exposure per insertion or removal, to reach 10^6 rads. Since no significant increase in compression setting would occur until 1 to 1000 times this exposure, replacement of the containment seal is controlled by general wear and damage considerations, and not radiation exposure.

Flammable gas is generated by the payload due to radiolysis during shipment. Experiments using the identical product show that these gases do not accumulate beyond 5% (by volume) of the free gas volume in any confined region of the package. No credit is taken for getters, catalysts, or other recombination devices. Therefore the package-cavity gas does not constitute a flammability hazard. The flammable gas generation is discussed further in Section 3.3.2.

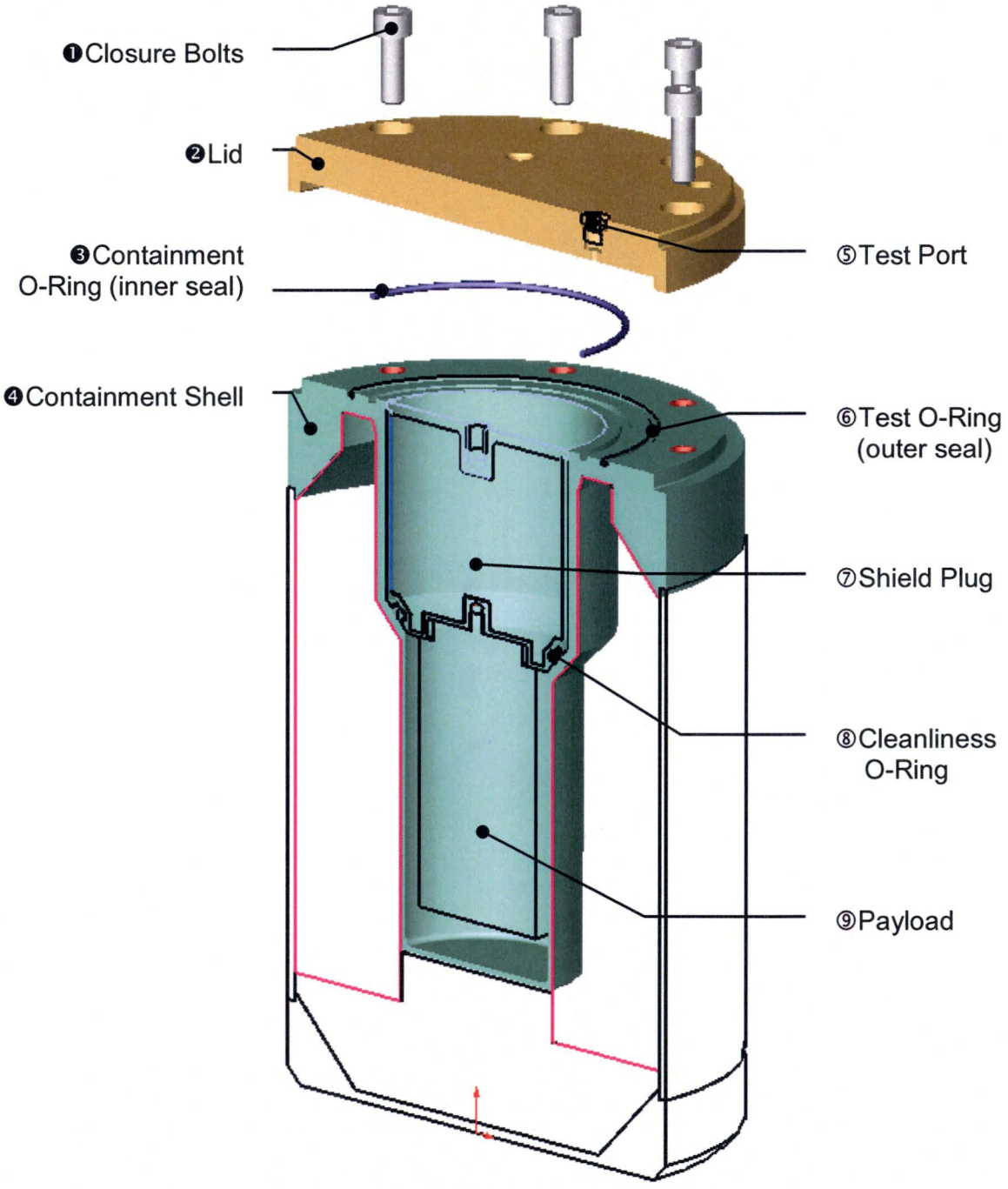

Figure 4-1 – Containment System Overview
(Filled numbers represent containment features)

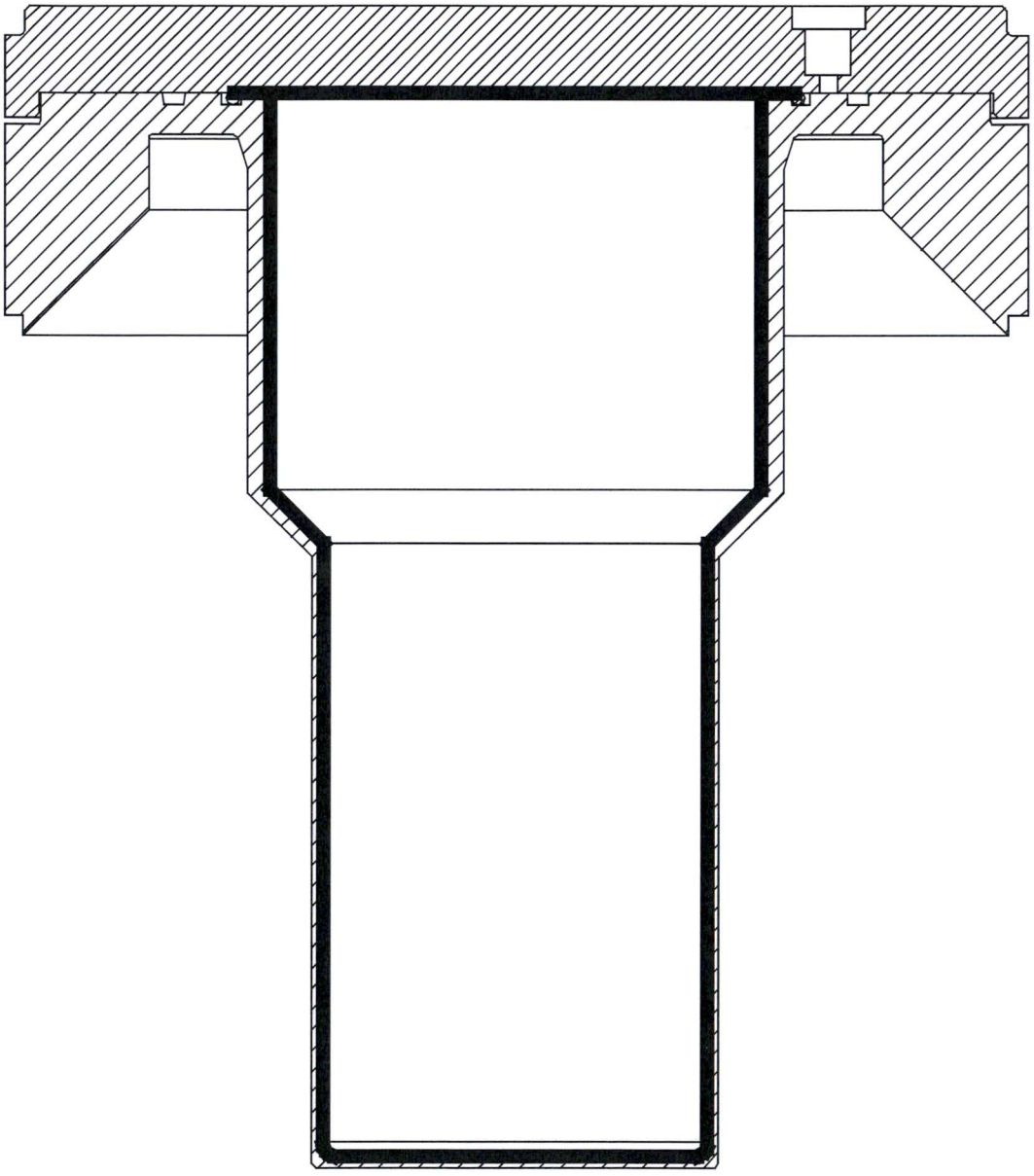

Figure 4-2 – Package Containment Boundary

4.2 Containment under Normal Conditions of Transport

4.2.1 NCT Pressurization of the Containment Vessel

The package maximum normal operating pressure (MNOP) is 7 bar, based on the definition of a Type B(U) packaging. Section 3.3.2 further discusses the NCT pressurization.

4.2.2 NCT Containment Criterion

The package is designed to a "leak-tight" containment criterion per ANSI N14.5 [4.3], therefore the containment criterion is 10^{-7} ref-cm^3/s.

4.2.3 Compliance with NCT Containment Criterion

Compliance with the NCT containment criterion is demonstrated by analysis. The structural evaluation in Section 2.6 shows that there would be no loss or dispersal of radioactive contents, and that the containment boundary, seal region, and closure bolts do not undergo any inelastic deformation when subjected to the conditions of §71.71. The thermal evaluation in Section 3.3.1 shows that the seals, bolts and containment system materials of construction do not exceed their temperature limits when subjected to the conditions of §71.71.

4.3 Containment under Hypothetical Accident Conditions

4.3.1 HAC Pressurization of the Containment Vessel

The containment evaluation for HAC is performed assuming that the maximum package pressure is 13.0 bar.

4.3.2 HAC Containment Criterion

The package is designed to a "leak-tight" containment criterion per ANSI N14.5 [4.3], therefore the containment criterion is 10^{-7} ref-cm^3/s.

4.3.3 Compliance with HAC Containment Criterion

Compliance with the HAC containment criterion is demonstrated by analysis. The structural evaluation in Section 2.7 shows that there would be no loss or dispersal of radioactive contents, and that the containment boundary, seal region, and closure bolts do not undergo any inelastic deformation when subjected to the conditions of §71.73. The thermal evaluation in Section 3.4.3 shows that the seals, bolts and containment system materials of construction do not exceed their temperature limits when subjected to the conditions of §71.73.

Although the confirmatory test program is not the basis for package acceptance, the test sequence did include a post-drop, post-fire pressure test. The damaged package passed a 10^{-3} ref-cm^3/s pressure-rise test. Calibrated temperature-indicating strips showed that the seal

temperatures remain below the seal material limits. The complete test report is included in Section 2.12.4.

4.4 Leak Rate Tests for Type B Packages

4.4.1 Fabrication Leak Rate Test

The packaging is leak rate tested during fabrication to 10^{-7} ref-cm^3/s to demonstrate that each packaging, as fabricated, provides the required level of containment. The fabrication leak rate test is further described in Section 8.1.4.

4.4.2 Maintenance Leak Rate Test

The packages are leak rate tested after maintenance to 10^{-7} ref-cm^3/s to confirm that maintenance, repair, or replacement of components has not degraded the containment system performance. The maintenance leak rate testing and the replacement or repair activities that require a maintenance leak rate test are further described in Section 8.2.2.

4.4.3 Periodic Leak Rate Test

The packages are leak rate tested annually to 10^{-7} ref-cm^3/s to confirm that the containment capabilities have not deteriorated over an extended period of use. The periodic leak rate testing is further described in Section 8.2.2.

4.4.4 Pre-shipment Leak Rate Test.

Each packaging is leak rate tested prior to shipment to 10^{-3} ref-cm^3/s to confirm that the containment system is properly assembled for shipment. The pre-shipment leak rate test is performed using the gas-pressure-rise method in ANSI N14.5, Section A.5.2, following the steps outlined in Section 7.1.3.

4.5 Appendix

[4.1] Parker Hannifin Corporation, *Parker O Ring Handbook*, ORD 5700/USA, 2001.

[4.2] Bronowski, D. R., *Performance Testing of Elastomeric Seal Materials Under Low- and High-Temperature Conditions: Final Report*, SAND94-2207, Sandia National Laboratories, June 2000.

[4.3] ANSI N14.5, *American National Standard for Radioactive Materials - Leakage Test on Packages for Shipment*, American National Standards Institute, Inc., 1997.

5 SHIELDING EVALUATION

5.1 Description of Shielding Design

The MIDUS package is designed to meet the regulatory requirements of 10 CFR 71 for a non-fissile, non-exclusive-use packaging. This chapter provides the description of the package shielding design and the shielding evaluation (§71.31(a)(1), §71.31(a)(2), and §71.35(a)). Chapter 1 provides the general package description (§71.3). The shielding evaluation presented in the body of this chapter is for the liquid payload (i.e., Content #01) described in Section 1.2.2.1. For clarity, the body of this chapter is not revised for additional contents. Instead, the shielding evaluation of each additional payload is presented in SAR addenda, starting in Chapter 9.

The package is designed, fabricated, assembled, tested, maintained, and used in accordance with the codes and standards described in Chapters 1, 7, and 8 to assure radiological safety (§71.31(c)).

The package is designed, constructed, and prepared for shipment so that, under the NCT tests specified in §71.71, there will be no loss or dispersal of radioactive contents as demonstrated to a sensitivity of 10^{-6} A_2 per hour, no significant increase in external surface radiation levels, and no substantial reduction in the effectiveness of the packaging (§71.43(f)).

Sections 5.1.2 and 5.4.4 show that, under the NCT tests specified in §71.71, the external radiation levels meet the requirements of §71.47(a) for non-exclusive-use (§71.43(f)), and that, under the HAC tests specified in §71.73, the external radiation level does not exceed 1000 mrem/hr at one meter from the surface of the package (§71.51(a)(2)).

5.1.1 Design Features

Figure 5-1 shows the shielding features of the cask assembly. The major subassemblies are the payload, cask body assembly, cask closure lid assembly, and shield lid assembly. The cask is constructed of steel and depleted uranium (DU), with thick radial and axial DU shields in the cask body, a DU shield plug, and an additional DU shield lid atop the cask closure lid. This special shield lid is designed to mitigate the potential effects of post-accident dose rate increases that could occur if the liquid payload were to seep into the capillary spaces surrounding the shield plug.

5.1.1.1 Payload Shielding Design Features

The product is loaded into the package using remote operations in a hot cell. The product is first transferred into a steel product bottle. This bottle has a metal-to-metal seal that is designed to isolate the payload and withstand the pressure buildup during shipping. Although this seal is vital for operational reasons, specifically contamination control, it is not credited as a containment seal in the safety analysis.

While still in the hot cell, the product bottle is placed into a secondary steel container, and a lid with an elastomeric O-ring seal is inserted using remote equipment. The lid is called the "snap ring" because it snaps onto the product bottle, facilitating handling in the hot cell. The secondary seal in the snap ring provides another contamination barrier for operations, but it is not credited for package containment. The top of the snap ring has a threaded stud that screws into the bottom of the shield plug as a handling aid in the hot cell.

The product bottle, secondary container, and snap ring are provided by the user and are not a part of the package design. It is anticipated that the user may occasionally require design changes to these components for production purposes; therefore, neither of the components are credited for their radiation attenuation or containment capacities. The product bottle and secondary container are always present, though, and they will provide additional photon attenuation beyond the results predicted by the safety analysis.

Although no credit is taken for attenuation by the payload materials of construction, the shielding analyses include cases to evaluate the *geometric* effects of the payload internals. The final shielding results show the worst-case situation considering the possible source fluid geometry with and without the presence of the payload internals.

The package has a third seal in the payload area. The "cleanliness seal" is an elastomeric O-ring seal between the shield plug and cask inner shell. This seal provides a housekeeping function for operations, and it provides the necessary compliance to press the shield plug against the closure lid, thereby minimizing the potential volume for flooding in the post-HAC condition.

These three seals are not credited as package containment seals, but credit is taken for their presence and effectiveness to confine the product within the boundary of the cask cavity under NCT. Since there are three independent seals, it is reasonable to assume that the payload will not enter the spaces around and above the shield plug under NCT tests.

For conservatism, it is assumed that all three of these seals fail during HAC tests, allowing the product to fill the capillary spaces around and above the shield plug. In this event, dose rates on the package top end are mitigated by an additional top DU shield lid, as discussed in Section 5.1.1.3 below.

5.1.1.2 Cask Shielding Features

The cask includes the cask body, shield plug, and closure lid assemblies. The body is constructed from two depleted uranium parts: a radial shield and a bottom axial shield. These DU components are sheathed in stainless steel by steel inner and outer shells. The shield plug is a cylinder of DU that is also sheathed by stainless steel. The closure lid is stainless steel.

Tolerances in the cask are controlled to minimize radiation streaming, allow ease of fabrication and use, and enhance the package's structural response to drop events. Section 5.3.1 summarizes the key gap sizes assumed for the shielding models.

Table 5-1 shows the key shielding parameters for the cask.

5.1.1.3 Shield Lid Assembly Shielding Features

In order to mitigate the radiological consequences of the HAC free drop, the package has a shield lid that bolts to the closure lid. The shield lid provides additional attenuation for the scenario in which the product is postulated to escape the seals on the two inner payload containers, breach the cleanliness seal, and collect in the annular space around the shield plug and in the gap between the shield plug and closure lid. In this unlikely accident scenario, some of the product seeps past much of the DU shielding in the shield plug and cask body, potentially resulting in high top axial dose rates. Without additional shielding outside the cask closure lid, HAC exposure rates in the top axial direction could exceed regulatory limits; therefore, additional shielding is necessary. The shield lid addresses the industry lesson learned from a routine ^{192}Ir shipment event in January, 2002 [5.1].

The shield lid is designed to bolt onto the closure lid, rather than being fixed to the overpack lid assembly, to avoid the separation that could potentially occur following an end drop.

Table 5-2 shows the key shielding parameters for the shield lid.

5.1.2 Summary of Maximum Radiation Levels

Table 5-3 shows the package maximum NCT dose rates for non-exclusive use. On the package surface, the dose rates comply with the regulatory limits in 10 CFR 71.47 with a large margin (factors of 3.6 to 53). At 1 meter, the dose rates comply, and the margins are even larger (factors of 6.3 to 40).

Table 5-4 shows the package maximum HAC dose rates. At 1 meter, the dose rates comply, and the margins range from 19% to a factor of 28.

The NCT results consistently show the largest margin on the package top end, followed by the package bottom and side surfaces. The HAC results differ because the some of the source is assumed to flow around the shield plug, changing the configuration of the source and shield. The HAC bottom end results show the largest margin, followed by the top and side locations.

Table 5-1 – Key Cask Body Shielding Parameters[1,2]

Parameter	Part	Value
DU Density	Radial shield, Axial Shield, Shield plug core	≥ 18.65 g/cm^3
DU radial thickness	Radial shield	≥ 6.21 cm
DU axial thickness (downward)	Bottom shield	≥ 6.44 cm
DU axial thickness (upward)	Shield plug DU (total height)	≥ 9.07 cm

Notes:

1. The dimensional values presented above are the lower-bound values (modeled in the shielding analyses) for the overall DU thickness on the cask side, bottom and top. Detailed DU shielding component dimensions, including nominal dimensions, tolerances, and the values modeled in the shielding analyses, are presented in Table 5-6 and in Drawing TYC01-1606 (in Section 1.3.2). Other, non-DU cask system components, for which nominal dimensions were modeled, are also described in Table 5-6 and in the Section 1.3.2 drawings.
2. The densities and compositions of the materials modeled in the shielding analyses are given in Table 5-9. The DU density presented above (which was modeled in the shielding analyses) is a conservative, lower-bound value

Table 5-2 – Key Shield Lid Shielding Parameters

Parameter	Part	Value
DU Density	Shield lid core	≥ 18.65 g/cm^3
DU axial thickness	Shield lid core	≥ 1.67 cm

Notes:

1. The shield lid component dimensions and materials are described in more detailed in Table 5-6, Table 5-9 and Drawing TYC01-1602.

Table 5-3 – Summary Table of External NCT Radiation Levels

Normal Conditions of Transport	Package Surface mSv/h (mrem/h)			1 Meter from Package Surface mSv/h (mrem/h)		
Location	Top	Side	Bottom	Top	Side	Bottom
Radiation	0.038 (3.8)	0.55 (55)	0.53 (53)	0.0025 (0.25)	0.016 (1.6)	0.011 (1.1)
10 CFR 71.47(a) Limit	2 (200)	2 (200)	2 (200)	0.1 (10)	0.1 (10)	0.1 (10)

Table 5-4 – Summary Table of External HAC Radiation Levels

Hypothetical Accident Conditions	1 Meter from Package Surface mSv/h (mrem/h)		
Location	Top	Side	Bottom
Radiation	5.7 (570)	8.1 (810)	0.36 (36)
10 CFR 71.51(a)(2) Limit	10 (1000)	10 (1000)	10 (1000)

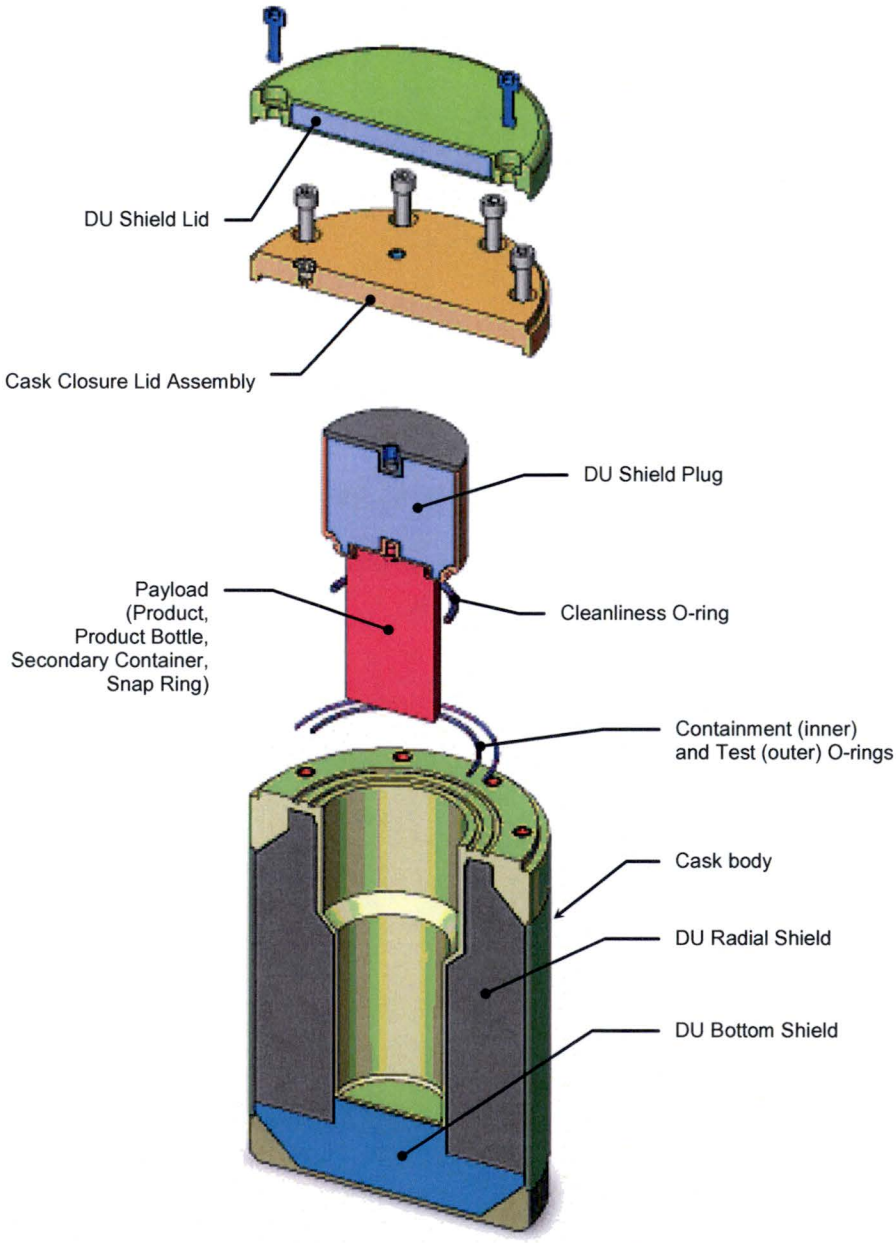

Figure 5-1 – MIDUS Cask Shielding Features

5.2 Source Specification

The shielding safety evaluations are performed assuming a bounding product activity of 4,500 Ci of ^{99}Mo in liquid form. For lower activity specifications (refer to Section 1.2.2), the shielding results would be reduced by a corresponding factor. The payload is a medical-grade solution that does not vary in composition, other than the concentration.

5.2.1 Gamma Source

The nuclide ^{99}Mo emits beta particles, electrons, and photons with a half life of 66.02 hours [5.2]. It decays to ^{99}Tc (13%) and ^{99m}Tc (87%), where ^{99m}Tc is a metastable state of ^{99}Tc. With a 6.007 hour half life, ^{99m}Tc decays 100% to ^{99}Tc. Because of its short half life, ^{99m}Tc is included in the source term calculations as a contributor. Since ^{99}Tc has an extremely long half life (214,000 years), it can be neglected as a significant source term contributor and no further decay daughters are considered.

The betas and electrons can be neglected as shielding source terms because they are 100% absorbed in the packaging materials and thus will not contribute to the exterior package dose rates.

The photon source term used for the shielding analyses is conservatively based on a bounding activity of 4,500 Ci of ^{99}Mo plus the maximum amount of the ^{99m}Tc daughter (Section 1.2.2.1 specifies a maximum payload of 4,400 Ci). Since the ^{99}Mo manufacturing timeline determines the amount of daughter products in a shipment, the exact amount of initial daughter products that will accompany the ^{99}Mo in each shipment may vary. For conservatism, the source term is developed assuming that the ^{99}Mo processing time is infinite, and, thus, that the ^{99m}Tc is in full transient equilibrium with the ^{99}Mo. The amount of ^{99m}Tc assumed for developing the source term is therefore 4,500 Ci · 0.87 = 3,915 Ci.

The photon sources in Table 5-5 were calculated for discrete energy lines using Table of Isotope data [5.3] for ^{99}Mo and ^{99m}Tc, and the total activities for ^{99}Mo and ^{99m}Tc.

5.2.2 Neutron Source

Not applicable.

Table 5-5 – Photon Source

Sorted by Energy		
MeV	**photons/s**	**MeV/s**
1.056197	1.80E+09	1.90E+09
1.017000	1.02E+09	1.03E+09
1.001340	9.16E+09	9.17E+09
0.986440	2.50E+09	2.46E+09
0.960750	1.58E+11	1.51E+11
0.861200	1.17E+10	1.00E+10
0.822970	2.22E+11	1.83E+11
0.777921	7.09E+12	5.52E+12
0.761774	6.66E+08	5.07E+08
0.739500	2.02E+13	1.49E+13
0.689600	6.99E+08	4.82E+08
0.621771	4.30E+10	2.67E+10
0.620030	3.83E+09	2.37E+09
0.599600	3.50E+09	2.10E+09
0.581300	1.67E+09	9.68E+08
0.580505	5.33E+09	3.09E+09
0.537790	5.49E+09	2.95E+09
0.528700	9.49E+10	5.02E+10
0.490530	1.83E+09	8.98E+08
0.469630	4.50E+09	2.11E+09
0.457600	1.35E+10	6.17E+09
0.455840	2.16E+09	9.87E+08
0.411491	2.43E+10	1.00E+10
0.410274	3.16E+09	1.30E+09
0.391700	5.33E+09	2.09E+09
0.380130	1.73E+10	6.58E+09
0.366421	1.98E+12	7.27E+11
0.322410	1.41E+08	4.53E+07
0.249030	6.49E+09	1.62E+09
0.242290	4.16E+09	1.01E+09
0.232720	1.23E+07	2.87E+06
0.181063	9.97E+12	1.81E+12
0.162370	1.98E+10	3.22E+09
0.158782	3.15E+10	5.00E+09
0.142628	2.71E+10	3.86E+09
0.140511	2.78E+14	3.90E+13
0.089400	5.00E+09	4.47E+08
0.040585	1.75E+12	7.10E+10

Sorted by Power		
MeV	**photons/s**	**MeV/s**
0.140511	2.78E+14	3.90E+13
0.739500	2.02E+13	1.49E+13
0.777921	7.09E+12	5.52E+12
0.181063	9.97E+12	1.81E+12
0.366421	1.98E+12	7.27E+11
0.822970	2.22E+11	1.83E+11
0.960750	1.58E+11	1.51E+11
0.040585	1.75E+12	7.10E+10
0.528700	9.49E+10	5.02E+10
0.621771	4.30E+10	2.67E+10
0.861200	1.17E+10	1.00E+10
0.411491	2.43E+10	1.00E+10
1.001340	9.16E+09	9.17E+09
0.380130	1.73E+10	6.58E+09
0.457600	1.35E+10	6.17E+09
0.158782	3.15E+10	5.00E+09
0.142628	2.71E+10	3.86E+09
0.162370	1.98E+10	3.22E+09
0.580505	5.33E+09	3.09E+09
0.537790	5.49E+09	2.95E+09
0.986440	2.50E+09	2.46E+09
0.620030	3.83E+09	2.37E+09
0.469630	4.50E+09	2.11E+09
0.599600	3.50E+09	2.10E+09
0.391700	5.33E+09	2.09E+09
1.056197	1.80E+09	1.90E+09
0.249030	6.49E+09	1.62E+09
0.410274	3.16E+09	1.30E+09
1.017000	1.02E+09	1.03E+09
0.242290	4.16E+09	1.01E+09
0.455840	2.16E+09	9.87E+08
0.581300	1.67E+09	9.68E+08
0.490530	1.83E+09	8.98E+08
0.761774	6.66E+08	5.07E+08
0.689600	6.99E+08	4.82E+08
0.089400	5.00E+09	4.47E+08
0.322410	1.41E+08	4.53E+07
0.232720	1.23E+07	2.87E+06

5.3 Shielding Model

5.3.1 Configuration of Source and Shielding

5.3.1.1 NCT Shielding Models

Figure 5-2 shows an overview of the baseline NCT shielding model, including the significant shielding features discussed above. NCT tests do not significantly affect the nominal package configuration from the shielding standpoint. Table 5-6 shows the key package component dimensions, and the corresponding dimensions used in the baseline NCT shielding model. Because of modeling simplifications, the model dimensions in Table 5-6 differ from the actual package dimensions.

The modeling approach is to represent the significant shielding components, specifically the DU, at the least material condition (LMC), accounting for manufacturing tolerances. Other package components are modeled at nominal thicknesses. The package is precision-machined; therefore, the tolerances are relatively small, and manufacturing tolerances on the steel components do not significantly impact the package shielding performance. Many overpack features are neglected, such as the joining flanges, resulting in extra conservatism in the models.

Gaps that are perpendicular to the radiation paths are neglected to simplify the MCNP models. In these cases, the gaps are neglected and overall model dimensions are compressed by a corresponding amount. Gaps that are collinear with the radiation paths, e.g., around the shield plug area, are modeled at the largest credible gap size. Figure 5-3, Figure 5-4, and Figure 5-5 show the key gap sizes assumed in the shielding models.

Several MCNP models are required because the product can be positioned at varying locations depending on the package orientation. The models cover upright, inverted, and horizontal package orientations. They also cover the range of possible product locations with and without confinement by the payload internals, because the confinement of fluid to the product bottle influences the geometric relation between source and shields. However, no credit is taken for mass attenuation by the payload internals.

Figure 5-2 is a scale illustration of the normal, upright orientation model. The figure identifies the different materials of construction as different shades, and the MCNP particle splitting surfaces as lines that subdivide the DU regions. The source fluid is modeled as a disk with an 85 mm diameter and a volume of 75 ml (4,500 Ci divided by the maximum specific activity of 60 Ci/ml). This model does not includes confinement by the product bottle or the secondary container. This case is conservative since it artificially places more source closer to the bottom end of the package and closer to the corners, thus challenging the streaming path between the radial and bottom DU pieces in the cask body. Additional cases are performed, as described below, to investigate the geometric effects of the presence of the payload internals.

Two inverted cases are run as shown in Figure 5-6. The cases represent different assumptions about the fluid displacement by the snap ring assembly of the internal product bottle shown in Figure 1-1. The dimensions of the payload internals are subject to change within the restrictions

of Section 1.2.2.1, therefore the fraction of the upper section of the cask interior cavity (illustrated in Figure 5-6) that is occupied by snap ring steel may vary. To account for this uncertainty, two extreme cases are evaluated. One case (shown on the left in Figure 5-6) assumes that the snap ring completely fills the upper cavity section, preventing any source fluid from entering the region in the event of an inverted cask. It should be noted that, although source fluid is excluded from the upper cavity zone for this first case, no steel is modeled within that zone (i.e., no credit is taken for the snap ring steel), with the exception of the small threaded hole in the bottom of the shield lid, which is modeled as being filled with the steel of the product bottle pintle. The second case (shown on the right in Figure 5-6) assumes a negligible snap ring steel volume, and models the upper cavity section as being completely filled with source fluid (while maintaining the total fluid volume of 75 ml). A third case, similar to the second case shown on the right in Figure 5-6, that models source fluid (as opposed to steel) in the small threaded hole in the bottom of the shield lid is also analyzed. As shown in Figure 5-6, the second assumption allows some of the source fluid to move into the upper section of the cask cavity, closer to the top end of the cask, but reduces the amount of fluid in the upper corner of the main cask cavity, near the streaming path between the shield plug and the cask flange.

Additional cases are performed, as described below, to investigate the geometric effects of the presence of the payload internals.

Figure 5-7 shows the horizontal case model geometry. 75 ml of fluid is modeled in a puddle along the length of the cask payload cavity. Due to the azimuthally asymmetric shape of the source region, MCNP point detectors are specified along the plane of symmetry.

Cases were run with a spherical source located near the top or bottom of the cavity. The purpose of these cases is to evaluate the geometric impact of the payload internals, which will confine the payload fluid under typical operations. The sphere is modeled with a volume of 75 ml, and its location for the top end case is chosen to closely represent the location the fluid would occupy in the neck of the product bottle in the inverted orientation. The bottom end sphere case elevates the centroid of the source region and reduces its diameter as would the presence of the payload internals.

5.3.1.2 HAC Shielding Models

The post-HAC test package configuration changes in four ways that affect the shielding models. First, the product is postulated to escape the product bottle and secondary container, and flow via capillary action around the shield plug and into the gap under the cask lid. Second, the configuration of the source and shield in the damaged package is slightly different due to the foam crush. The outside of the package does not deform significantly from a shielding standpoint, but the inside-out crush behavior means that the source will be located closer to the 1-meter package distance than in the nominal geometry models. Third, it is assumed that the shield plug is radially offset to the maximum extent possible, increasing the potential gap. Fourth, the mass of the foam is reduced due to charring and off-gassing that occur as a result of the HAC fire event. This effect is conservatively treated by assuming 100% foam loss for the purpose of the shielding models.

If the product were to leak into the thin spaces around the shield plug, four distinct regions could become flooded with a significant amount of radioactive fluid: the annular region surrounding the shield plug, the disk-shaped region above the shield plug, the threaded hole on top of the shield plug, and the small free volume of the containment O-ring groove that is not occupied by the O-ring. Each of these regions has a maximum potential source term that is proportional to its volume. The volumes and related source term fractions are summarized in Table 5-7.

The function of the cleanliness O-ring is to assure that the shield plug is in contact with the closure lid, thus minimizing the potential volume in which liquid could collect during the HAC. The disk volume presented in Table 5-7, is based on the specified surface flatness of the top of shield plug top surface and the closure lid bottom surface, and the cleanliness O-ring provides the compliance necessary to ensure that no additional gap is present. No credit is taken for the cleanliness O-ring as a seal, only that it be present and provide the compliance necessary to ensure contact. Functional testing during manufacturing (Section 8.1.5.2), maintenance (Section 8.2.5.3), and operation (Section 7.1.2, step 0) assure that the cleanliness O-ring is correctly installed and that it will perform this function. Furthermore, the cleanliness O-ring is replaced every shipment, therefore it is not susceptible to compression set.

During the HAC drop, the cask body deforms the overpack inner shell upward, downward, or to the side, depending on the drop orientation. The package's gross outer dimensions are essentially unchanged, location of the cask body (within the overpack) shifts so that it is closer to the package side, top or bottom surface (as a result of a side, top, or end drop, respectively). The top, bottom, and side drops produce the largest gross deformation. Oblique and corner drops produce local deformations, but do not appreciably change the relative cask-overpack geometry. The package stays intact (no foam or steel is dislodged). The only significant change to the cask configuration, between NCT and HAC conditions, occurs within the foam. Crushing of the foam results in a reduction in foam thickness, on the package side, top or bottom (as a result of a cask side, top end, or bottom end drop, respectively). The foam mass is also reduced as a result of the fire. No significant deformations or alterations occur in any other system components, other than the shifting of the cask body location (within the overpack) that occurs as a result of the foam crush.

To account for the package deformations (i.e., the reductions in foam thickness, and the resulting reduction in distance between the source region and the package outer surfaces), the defined 1-meter dose tally surfaces are moved inward, towards the shielding model source zone. The inward shift of each tally surface is equal to the amount of foam crush that occurs within the corresponding overpack zone (i.e., side, top or bottom). The HAC shielding models also replace all foam material with void, to conservatively bound the effects of any degree of foam mass reduction (from the fire). The above approach yields accurate calculated dose rates, as both the thickness of the steel and DU shielding components, and the distance between the source zone and the dose tally surface, are accurately modeled.

Table 5-8 shows the reduction in foam thickness for the top end, side and bottom end overpack regions, for the HAC configuration versus the NCT configuration. Table 5-8 lists the foam thickness reductions modeled in the HAC shielding analyses, and compares them to the final

foam crush depths calculated by the structural evaluation presented in Section 2.7. The hot condition drop governs for all three cases. The HAC foam thickness reductions assumed in the shielding analyses, which were estimated based on preliminary structural analysis results, are roughly equal to or greater than the final reported structural results listed in the right column of Table 5-8. Modeling a larger amount of foam crush is conservative, and the 2 mm difference between the top end crush depths is not significant. The effect of moving the 1-meter top detector 2 mm closer to the source zone would be negligible, especially considering the large HAC dose rate margin calculated for the cask top end.

5.3.2 Material Properties

The shielding evaluations were performed using the material densities shown in Table 5-9. These properties are valid for the purpose of shielding evaluations under the NCT and HAC package conditions. The DU was modeled with the specified 2% Mo alloy, at the 18.65 g/cc minimum density specified in Drawing TYC01-1606. All steel components are modeled at the standard, nominal stainless steel density of 8.027 g/cm^3. The O-rings were modeled as water for convenience. The foam was modeled at a 12 lb/ft^3 density (0.193 g/cm^3), conservatively lighter than the specified density.

The radioactive ^{99}Mo will not precipitate under the MIDUS service conditions. Under very cold conditions, the product will freeze before it precipitates because the solubility is approximately 1600 times higher than the maximum allowable payload concentration. If precipitation were to occur, it would be a concern because it could produce a higher specific activity than is assumed for the calculations. Such an increase could potentially invalidate the conclusions of this calculation package for the HAC shielding cases if precipitation were possible.

Table 5-6 – Summary of Key Component Dimensions

Feature	Nominal Design (cm)	Corresponding NCT Shielding Model Dimensions (cm)	Notes
Cask Cavity	ø8.5 x 13.4	ø8.50 x 13.4	Identical.
Shield Plug	ø10.8 x 9.8	ø10.8 x 9.77	Modeled shorter because of neglected gaps (perpendicular to primary radiation path).
Shield Plug DU	ø10.15 x 9.1	10.12 x 9.07	DU modeled at least material condition (LMC).
Cask Assembly	ø22.5 x 32.4	ø22.5 x 32.37	Modeled shorter because of neglected gaps (perpendicular to primary radiation path).
Cask Body Radial DU Shield	ø21.63 outside ø11.98 inside ø9.13 inside	ø21.61, ø12.05, ø9.20	DU modeled at least material condition (LMC).
Cask Body Bottom DU Shield	ø21.63 x 6.5	ø21.61, 6.44	DU modeled at least material condition (LMC).
Cask Lid	ø22.5 x 1.9	ø22.5, 1.9	1.9 cm is the thickness of lid not counting the shear ring on the edge.
Shield Lid	ø22.5 x 2.3	ø22.5, 2.27	2.3 cm is the thickness of lid not counting the shear ring on the edge.
Shield Lid DU	ø21.4, 1.7	ø21.2, 1.67	DU modeled at least material condition (LMC).
Overpack Cavity	ø23 x 35.2	ø23 x 34.94	Modeled shorter because of neglected gaps (perpendicular to primary radiation path).
Overpack	ø45.7 x 55.1	ø45.7 x 54.64	Modeled shorter because of neglected gaps (perpendicular to primary radiation path).
1m Surface	ø245.7 x 255.1	ø245.7, 254.64	Modeled shorter because of neglected gaps (perpendicular to primary radiation path).

Table 5-7 – Summary of Post-HAC Source Region Volumes

Region	Effective Source Volume [ml]	Percentage of 75 ml Source Volume
Annulus	15.38	20.5%
Disk	3.97	5.3%
Thimble	1.56	2.1%
Ring	0.553	0.7%

Table 5-8 – Post-HAC Reductions in Foam Thickness

Drop Orientation[1]	Shielding Model[2]	Structural Evaluation[3]
Top End Drop	5.4 cm	5.6 cm
Side Drop	5.85 cm	5.8 cm
Bottom End Drop	5.4 cm	4.5 cm

Note:

1. The values presented for the top end, side and bottom end drops refer to the resulting reduction in thickness of the top, side and bottom foam regions, respectively. The reductions in foam region thickness listed above are the only significant difference between the NCT and HAC cask system shielding configurations.
2. These are the foam thickness reduction values assumed in the shielding analyses. The treatment of this foam crush by the shielding analyses is discussed in Section 5.3.1.2.
3. These are the foam thickness reductions calculated by the final structural evaluations presented in Section 2 of this SAR.

Table 5-9 – Shielding Material Properties

Element	Water 1.00 g/cm^3	Steel[1] 8.027 g/cm^3	Depleted U[2] 18.65 g/cm^3	Foam[3] 0.193 g/cm^3	Air 0.0013 g/cm^3
O	11.20%	--	--	21.82%	23.45%
H	88.80%	--	--	6.36%	--
Cr	--	19.00%	--	--	--
Mn	--	2.00%	--	--	--
Fe	--	69.75%	--	--	--
Ni	--	9.25%	--	--	--
U	--	--	98.00%	--	--
Mo	--	--	2.00%	--	--
C	--	--	--	63.64%	--
N	--	--	--	7.27%	76.55%
K	--	--	--	0.91%	--
	100.00%	100.00%	100.00%	100.00%	100.00%

Notes:

1. This is the standard, nominal density for stainless steel.
2. This is the minimum density specified in the TYC01-1606 drawing. The nominal density for depleted uranium (w/ 2% Mo) is 18.9 g/cm^3.
3. This is a lower-bound value, based on the foam density range of 12.3- to 14.9 specified in Drawing TYC01-1608.

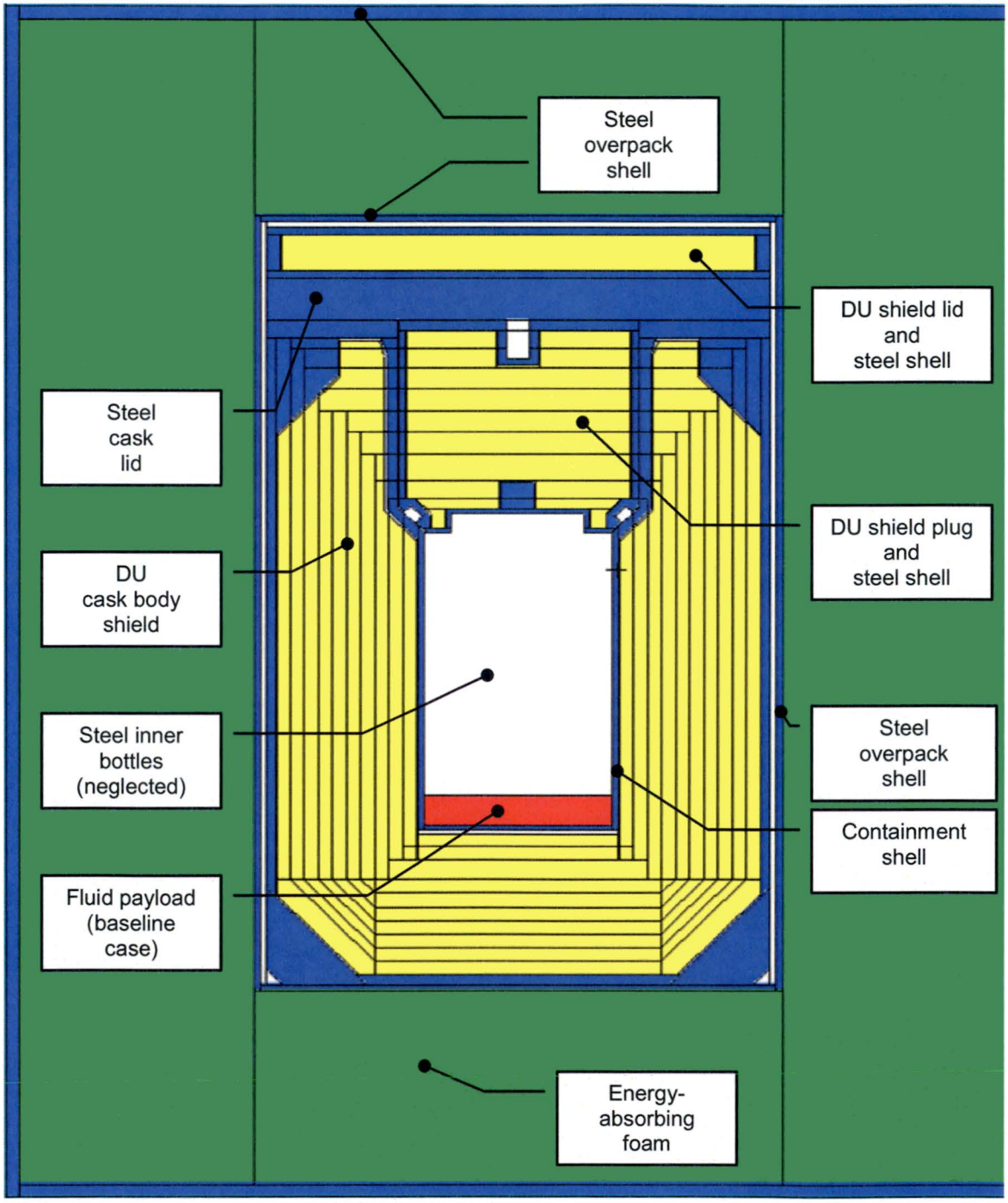

Figure 5-2 – MIDUS Package Shielding Model Overview (NCT Baseline Case)

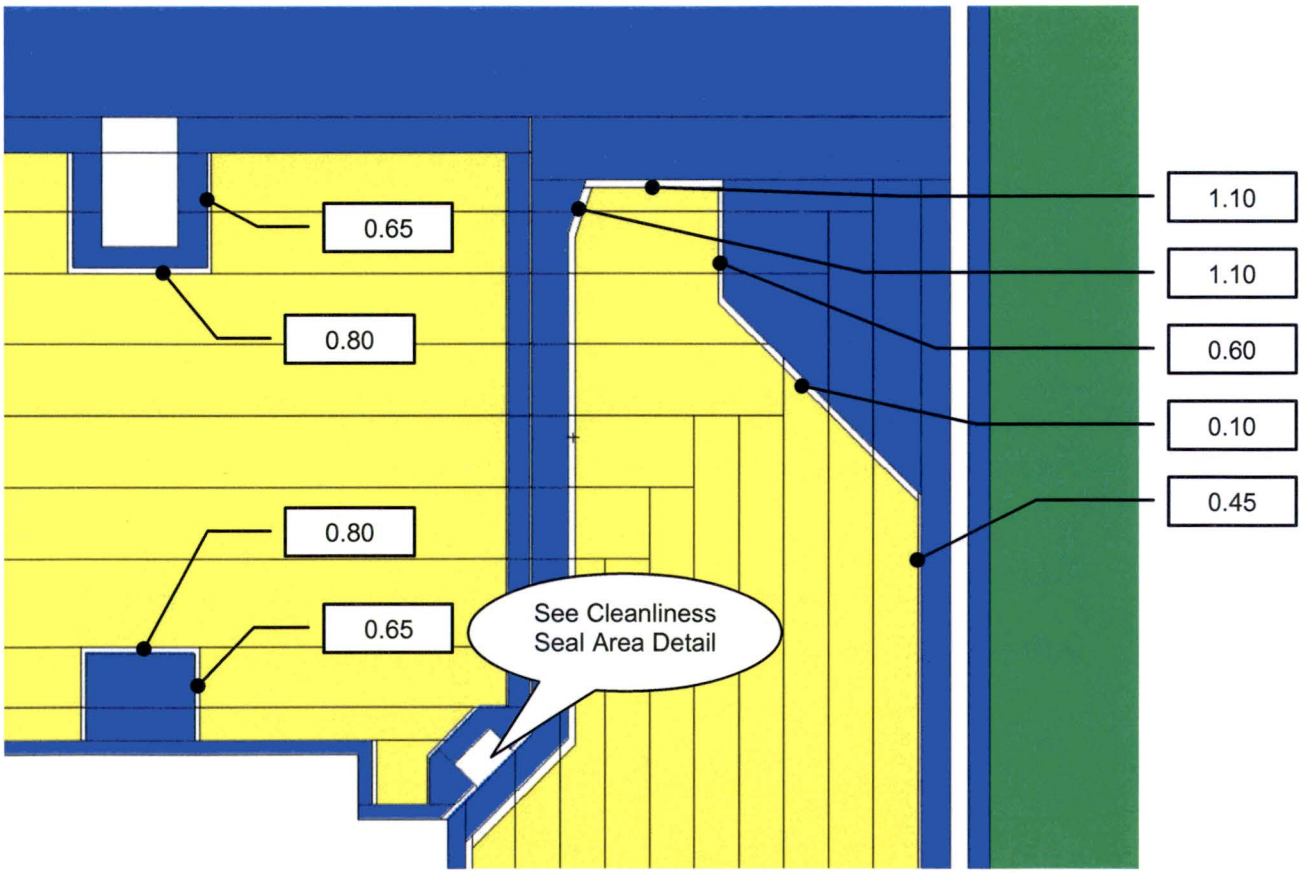

Figure 5-3 – Cask Body Top End Gaps (mm)
All Models - NCT & HAC

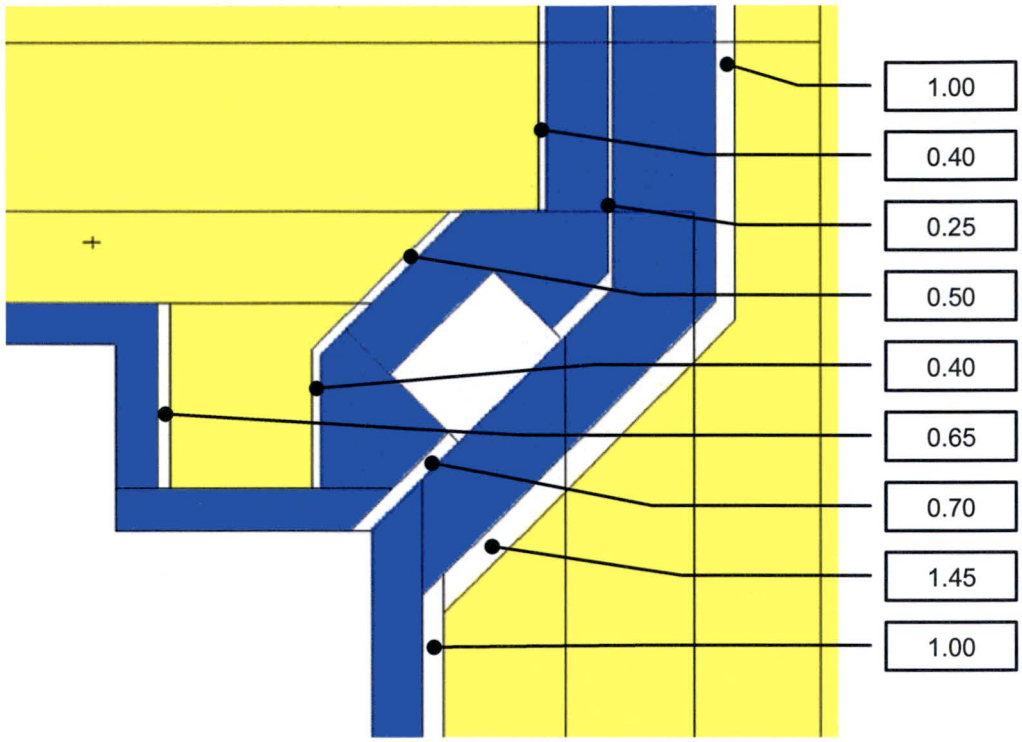

Figure 5-4 – Cleanliness Seal Area Gaps (mm) - NCT & HAC

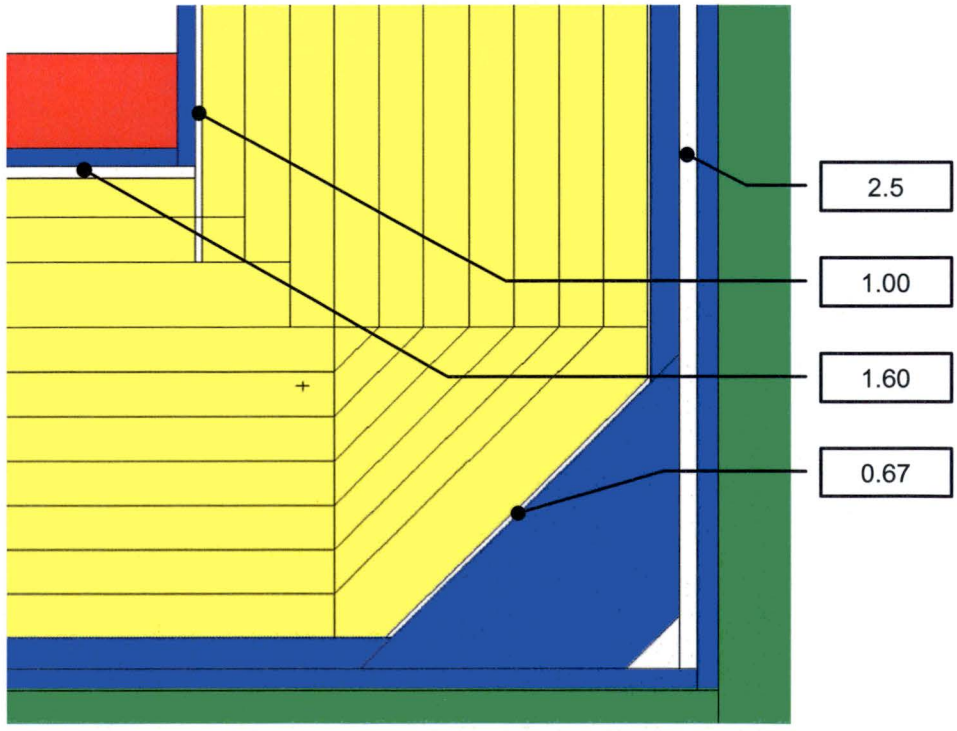

**Figure 5-5 – Cask Body Bottom End Gaps (mm)
NCT & HAC**

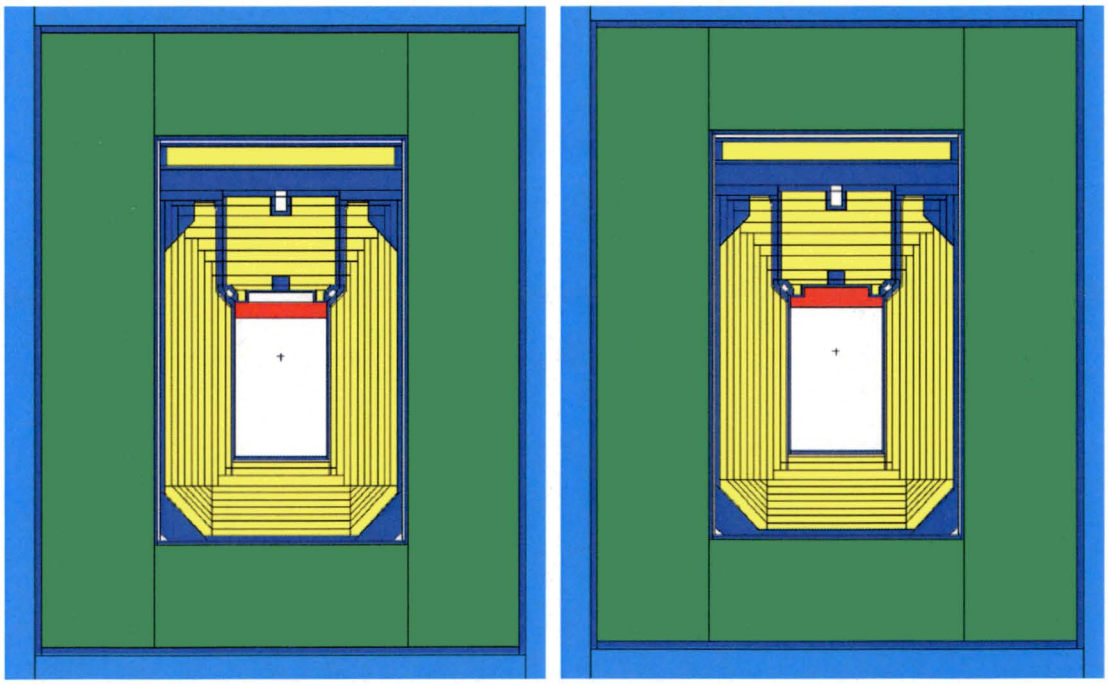

Figure 5-6 – Inverted NCT Model Geometries (Different Snap Ring Assumptions)

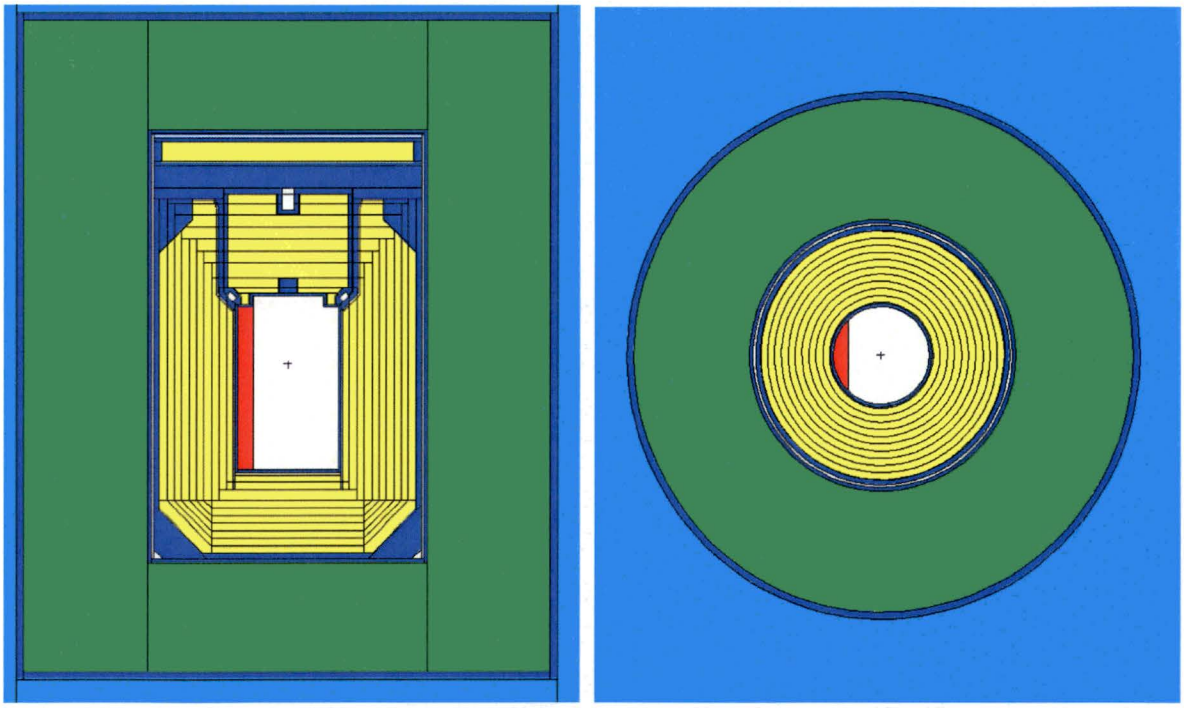

Figure 5-7 – Horizontal NCT Model Geometry

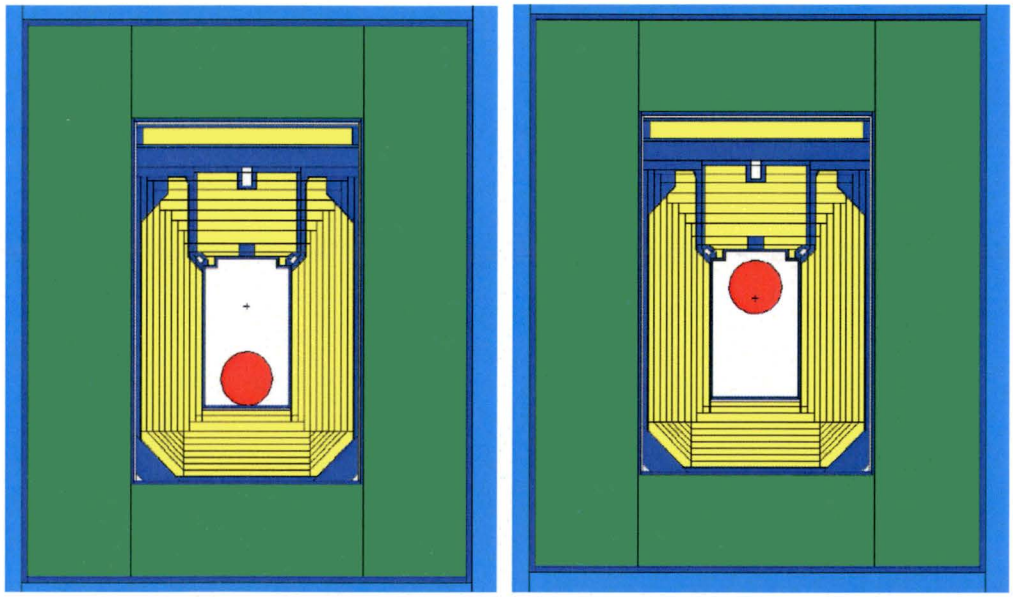

Figure 5-8 – Spherical Source Cases NCT Model Geometry

5.4 Shielding Evaluation

5.4.1 Methods

MCNP5 is a general-purpose Monte Carlo N-Particle code that can be used for neutron, photon, electron, or coupled neutron/photon/electron transport [5.4]. Specific areas of application include, but are not limited to, radiation protection and dosimetry, radiation shielding, radiography, medical physics, nuclear criticality safety, detector design and analysis, nuclear oil-well logging, accelerator target design, fission and fusion reactor design, decontamination, and decommissioning. The code treats an arbitrary three-dimensional configuration of materials in geometric cells bounded by first- and second-degree surfaces and fourth-degree elliptical tori.

Pointwise cross-section data are used, although group-wise data also are available. MCNP's neutron capabilities are not used for this application because the payload does not produce neutrons. For photons, the code accounts for incoherent and coherent scattering, the possibility of fluorescent emission after photoelectric absorption, absorption in pair production with local emission of annihilation radiation, and bremsstrahlung. A continuous-slowing-down model is used for electron transport that includes positrons, k x-rays, and bremsstrahlung, but does not include external or self-induced fields.

Calculations are performed using the MCPLIB04 cross-section data library for photon transport. This library is derived from the ENDF/B-VI.8 data. Cross-section data are given for incident photon energies from 1 keV to 100 GeV. Since the payload does not produce neutrons, a coupled cross-section library is not needed.

MCNP5 includes a powerful general source, criticality source, and surface source; both geometry and output tally plotters; a rich collection of variance reduction techniques; a flexible tally structure; and an extensive collection of cross-section data. Distributed volumetric sources are used for the MIDUS package models.

MCNP5 contains numerous flexible tallies: surface current & flux, volume flux (track length), point or ring detectors, particle heating, fission heating, pulse height tally for energy or charge deposition, mesh tallies, and radiography tallies. Surface crossing tallies and point detectors are used in the package models.

5.4.2 Input and Output Data

The shielding models are constructed in R-Z symmetric geometry. The photon sources are modeled as volumetric homogeneous regions with source particles started uniformly throughout. Source biasing and geometry splitting are used to improve the convergence rate of the problem. The number of histories executed in a typical run is on the order of 70 million. The variance reduction techniques applied in the models are conservative and the computer runs are well-converged, as shown by the MCNP figure of merit stability. Tally relative errors are generally less than 1%. Due to the size of the MCNP input and output files, they have not been reproduced in this report.

5.4.3 Flux-to-Dose-Rate Conversion

MCNP results are converted from particles/cm^2-sec to dose rate units using the ANSI/ANS 6.1.1-1977 flux-to-dose conversion factors shown in Table 5-10 [5.5].

5.4.4 External Radiation Levels

5.4.4.1 NCT Radiation Levels

Figure 5-9 summarizes the NCT radiation levels along the package surface. The maximum dose rate is 1.6 mrem/hr, occurring at the package side. For clarity, the top, side, and bottom results are combined into a single plot. The effectiveness of the top end DU shield lid can be seen in the asymmetry of the plot. The left hand side of the "W" shape is suppressed due to the extra shielding provided by the shield lid. The middle and right portions of the "W" correspond to the expected peak at the package midplane and bottom centerline. Sections 5.4.4.1.1 through 5.4.4.1.3 discuss the calculated profiles along the individual sides of the package in more detail.

Figure 5-13 summarizes the NCT radiation levels 1 meter from the package surface. The maximum dose rate is 55 mrem/hr, occurring at the package side. Again, the top, side, and bottom results are combined into a single plot. Because the bottom and radial shields are similar, the contact dose rate is almost the same at the package bottom on centerline. The effectiveness of the top end DU shield lid can again be seen in the asymmetry of the plot. Since these data are for the 1-meter package surface, the effect is less pronounced than the surface results. The modest streaming through the shield plug steel area is also apparent in Figure 5-13, where the middle peak is skewed upwards on it's left side. Sections 5.4.4.1.4 through 5.4.4.1.6 discuss the calculated profiles along the individual sides of the package in more detal.

5.4.4.1.1 Package Top 1-Meter NCT Profile

Figure 5-10 shows the worst-case MCNP results for the 1-meter surface above the top end of the package. Due to the top DU shield lid, all dose rates at the top end of the package are very low, on the order of a factor of 40 below the regulatory limit of 10 mrem/hr. The results show that the highest dose rates at the top end occur when the package is in the inverted position. This places the product closest to the top end, and most directly challenges the streaming paths around the cask shield plug. The highest peak dose rates were produced by the top spherical source case shown on the right in Figure 5-8, which is the source of the dose rate profile shown in Figure 5-10. The peak dose rates are relatively flat out to the package radius, then rise monotonically out to the 1-meter distance in the radial direction, indicating that the shield plug has a "shadowing" effect and that the streaming paths around the shield plug are not the dominating factor.

The dose rate plot in Figure 5-10 shows a rise with increasing radial distance from the package. Since the DU shield lid suppresses the top-end photon flux in the upward direction, the dose rates above the package are suppressed, resulting in the shape of Figure 5-10. Due to spatial attenuation, the dose rates eventually drop off in the radial direction. Since the dose rates along the side 1 meter profile are all within the allowable limits as shown in Figure 5-11, it can be

concluded that the dose rates along the top 1-meter plane are also below the limits. Note that the dose rates at the rightmost point in Figure 5-10 match the corresponding rightmost point in Figure 5-11.

The maximum dose rate on the package top 1-meter surface is 0.245 mrem/hr (T.I. = 0.25).

5.4.4.1.2 Package Side 1-Meter NCT Profile

Figure 5-11 shows the worst-case MCNP results for the 1-meter surface on the side of the package. All dose rates are low, on the order of a factor of 6 below the regulatory limit of 10 mrem/hr. The highest peak dose rate on the side occurs when the package is in the inverted position (specifically, for the top spherical source model illustrated on the right in Figure 5-8). The top spherical source configuration is the basis for the axial dose rate profile shown in Figure 5-11. The dose rate profile is slightly peaked toward the top of the package due to the contribution from the top-end streaming.

The maximum dose rate on the package side 1-meter surface is 1.58 mrem/hr (T.I. = 1.6).

5.4.4.1.3 Package Bottom 1-Meter NCT Profile

Figure 5-12 shows the worst-case MCNP results for the 1-meter surface below the bottom end of the package. All dose rates are low, on the order of a factor of 8 below the regulatory limit of 10 mrem/hr. The results show that the highest dose rates at the bottom end occur when the package is in the upright, vertical position. Specifically, the peak dose rates occur for the "lower sphere" source distribution shown on the left in Figure 5-8.

The maximum dose rate on the package top 1-meter surface is 1.14 mrem/hr (T.I. = 1.1).

5.4.4.1.4 Package Top Surface NCT Profile

Figure 5-14 shows the worst-case MCNP results for the package top surface. Due to the top DU shield lid, all dose rates at the top end of the package are very low, on the order of a factor of 50 below the regulatory limit of 200 mrem/hr. The very large margin is due to the presence of the shield lid, which is designed to mitigate the higher top-end dose rates in the post-HAC condition.

The results show that several competing effects occur depending on the assumed source configuration. The highest peak dose rate at the top end occurs when the package is in the inverted position (specifically, for the top sphere source case illustrated on the right in Figure 5-8, which is the basis for the entire inverted-case dose rate profile shown in Figure 5-14). This places the product closest to the top end, and most directly challenges the streaming paths around the cask shield plug. The highest dose was noted for the inverted package, i.e., the top sphere source case, in which the peak dose rate occurs out at the radial edge of the package top surface. The peak occurs near the edge because the DU in the shield plug shadows much of the cask top surface. The most significant streaming for this case is through the chamfer in the radial DU shield and the streaming gaps near the shield plug chamfer.

A slightly smaller peak occurs at about a 6 cm radius when the cask is in the upright orientation (for the bottom sphere source case illustrated on the left in Figure 5-8, which is the basis for the entire upright-case dose rate profile shown in Figure 5-14). This peak is about 8% lower than the inverted case. It occurs because of streaming through the shield plug steel when the source is more collimated due to its location in the bottom of the cavity in the upright orientation.

The maximum dose rate on the package top 1-meter surface is 3.77 mrem/hr.

5.4.4.1.5 Package Side Surface NCT Profile

Figure 5-15 shows the worst-case MCNP results for the package side surface. The peak dose rate at the package side surface is low, on the order of a factor of 30% of the regulatory limit of 200 mrem/hr. The highest peak dose rate on the side surface occurs when the package is in the inverted position (specifically, for the top sphere source case illustrated on the right in Figure 5-8, which is the basis for the entire axial dose rate profile shown in Figure 5-15). This places the product at the top of the cavity where the streaming paths around the shield plug are challenged most significantly.

The maximum dose rate on the package top 1-meter surface is 54.6 mrem/hr.

5.4.4.1.6 Package Bottom Surface NCT Profile

Figure 5-16 shows the worst-case MCNP results for the package bottom surface. The peak dose rate at the bottom end of the package is low, on the order of 25% of the regulatory limit of 200 mrem/hr. The dose rates fall off monotonically with increasing radius. The highest peak dose rate was produced by the baseline upright cask orientation case illustrated in Figure 5-2. The peak dose rates occur at the centerline of the package. The nominal source geometry in Figure 5-2 showed a slightly higher dose rate than the upright spherical case shown in the left in Figure 5-8, because the disk-shaped source challenged the DU gap to a greater extent than the smaller radius of the spherical source.

The maximum dose rate on the package top 1-meter surface is 53.2 mrem/hr.

5.4.4.1.7 NCT Conclusions

The package dose rate margins range from 70% under the regulatory allowable to a factor of 50 on the surface. At 1 meter, the margins range from factors of 6 to 40.

The package orientation affects the package dose rates. Different orientations produce maximum dose rates on the different respective package locations (top, side, and bottom). No credit is taken for attenuation in the materials of construction of the payload internals, but the studies show that the geometrical restriction of the internals increases the dose rates slightly over the baseline models for most locations of interest.

5.4.4.2 Post-HAC Radiation Levels

The results from each of the four post-HAC case runs are shown in Figure 5-17 for the 1-meter side, 1-meter top, and 1-meter bottom surfaces, respectively. The results are superimposed graphically to obtain a better understanding of the relative contributions from each of the HAC source regions.

5.4.4.2.1 1-Meter Side HAC Profile

The results show a peak side dose of 906 mrem/hr. The annulus source is the largest contributor, accounting for over one-half of the peak. The annulus source's spatial distribution favors the upper end of the package (to the right in the plot) due to the orientation of the DU in relation to the annulus. The next largest source contribution comes from the disk source, at about one-third of the total. The O-ring, thimble, and payload cavity sources are minimal contributors at the package side.

The dose rate contribution from the shield plug annulus model was conservatively doubled for the side results to account for any potential eccentric positioning of the shield plug. This assumes the shield plug could be displaced such that it was in contact with the containment cavity wall, increasing the thickness of the fluid layer to as much as double the nominal value. The cleanliness O-ring should keep the plug centered; therefore this approach introduces a considerable conservatism. If the shield plug is in its nominal position following the HAC, the peak side dose rate would be about 240 mrem/hr lower than reported.

The contribution from the product remaining in the cask cavity (approximately 2/3) was conservatively accounted for by taking 100% of the contribution from a spherical source of 75 ml centered in the payload cavity.

5.4.4.2.2 1-Meter Top HAC Profile

The results show a peak top dose of 606 mrem/hr. The annulus and disk sources are the largest contributors, each accounting for about 40% of the peak. The O-ring and thimble sources are more significant contributors at the top, providing in combination most of the remaining peak dose.

The contribution from the shield plug annulus was taken at 100% of the MCNP output values since eccentric positioning of the plug would not appreciably affect top-end dose rates.

The contribution from the product remaining in the cask cavity (approximately 2/3) was conservatively accounted for by taking 100% of the contribution from a spherical source of 75 ml centered in the payload cavity.

5.4.4.2.3 1-Meter Bottom HAC Results

The results show a peak bottom dose of only 38.7 mrem/hr. The annulus and disk sources source are the largest contributors, together accounting for about 80% of the peak.

The contribution from the shield plug annulus was taken at 100% of the MCNP output values since eccentric positioning of the plug would not appreciably affect bottom-end dose rates.

The contribution from the product remaining in the cask cavity (approximately 2/3) was conservatively accounted for by taking 100% of the contribution from a spherical source of 75 ml centered in the payload cavity.

5.4.4.2.4 HAC Conclusions

The package margins range from 9% under the regulatory allowable to a factor of 30.

The annulus and disk contributions dominate the top and bottom cases. Due to the offset assumption, the annulus source dominates the side dose.

Table 5-10 – Photon Dose Rate Response Functions

E, MeV	Factor (mrem/hr) / γ/cm^2-sec
0.015	1.95E-03
0.025	8.01E-04
0.045	3.17E-04
0.08	2.61E-04
0.15	3.79E-04
0.3	7.59E-04
0.5	1.15E-03
0.65	1.44E-03
0.75	1.60E-03
0.9	1.83E-03
1.25	2.32E-03
1.75	2.93E-03
2.5	3.72E-03
3.5	4.63E-03
4.5	5.42E-03
5.5	6.19E-03
6.5	6.93E-03
7.5	7.66E-03
9	8.77E-03
12	1.10E-02

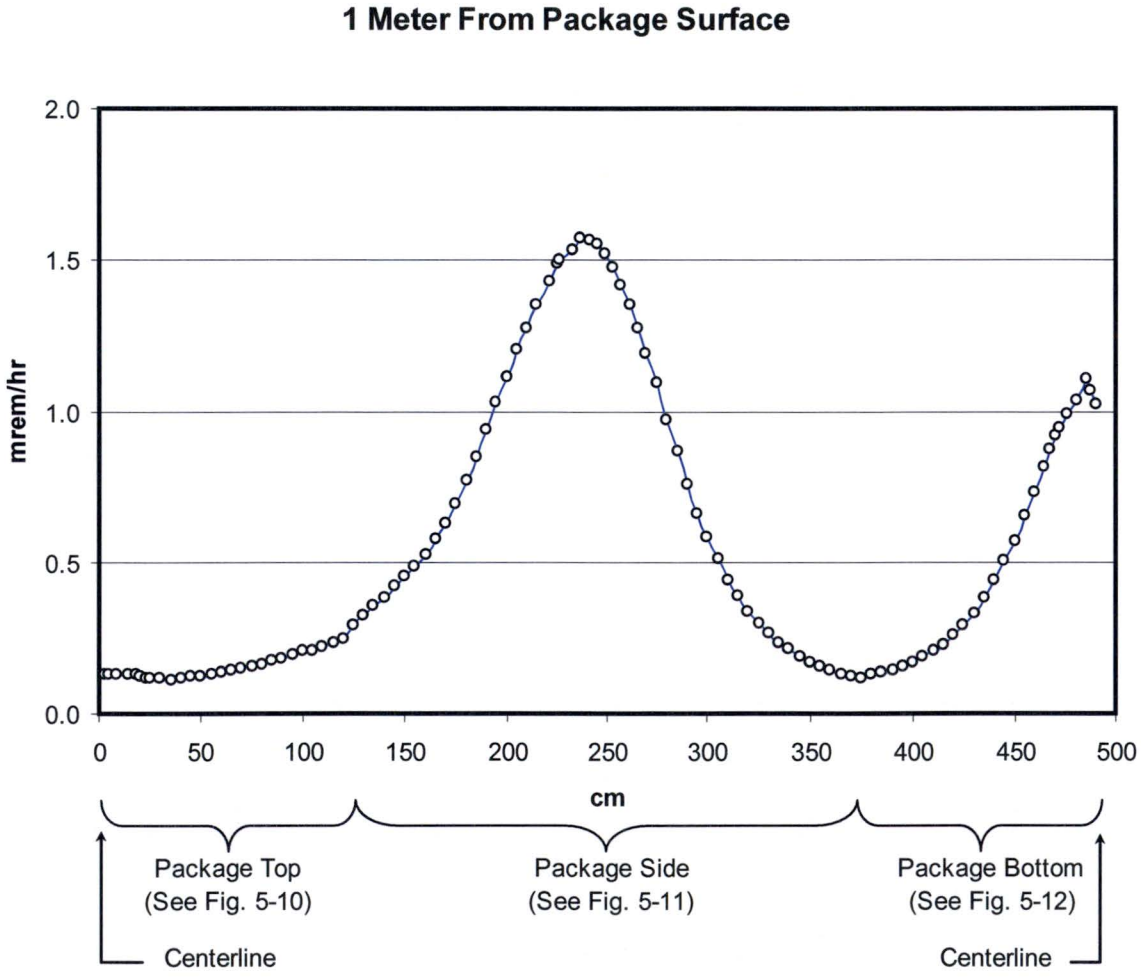

Figure 5-9 – Summary Profile for 1-Meter NCT Dose Rates

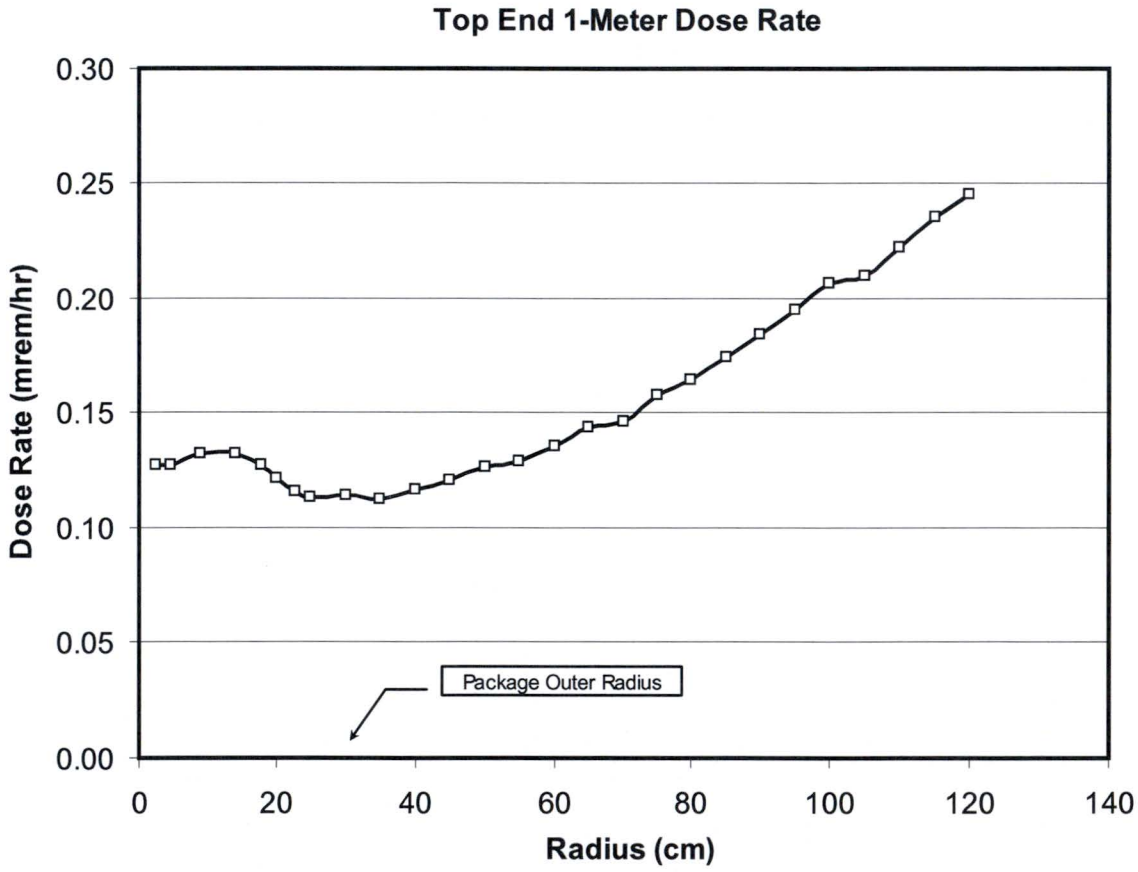

Figure 5-10 – Top-End 1-Meter Dose Rate Profile

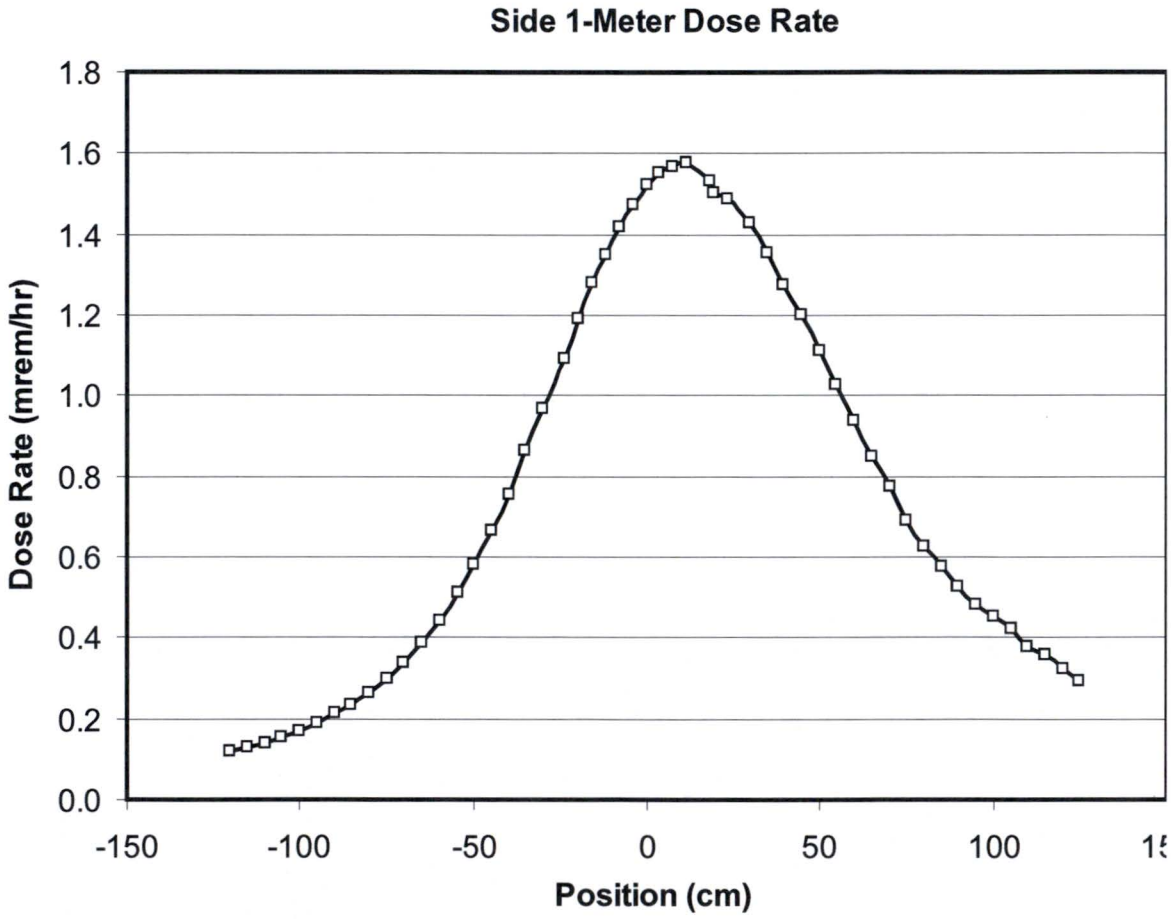

Figure 5-11 – Side 1-Meter Dose Rate Profile

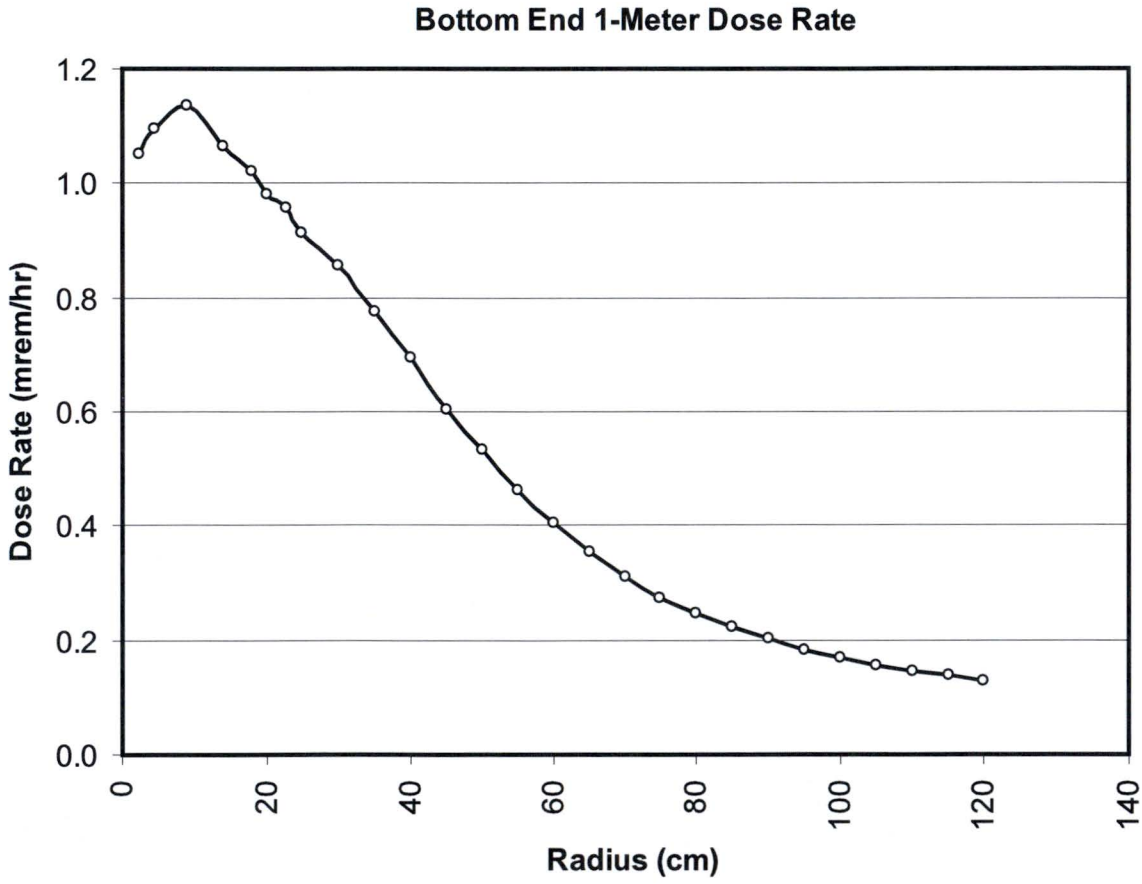

Figure 5-12 – Bottom-End 1-Meter Dose Rate Profile

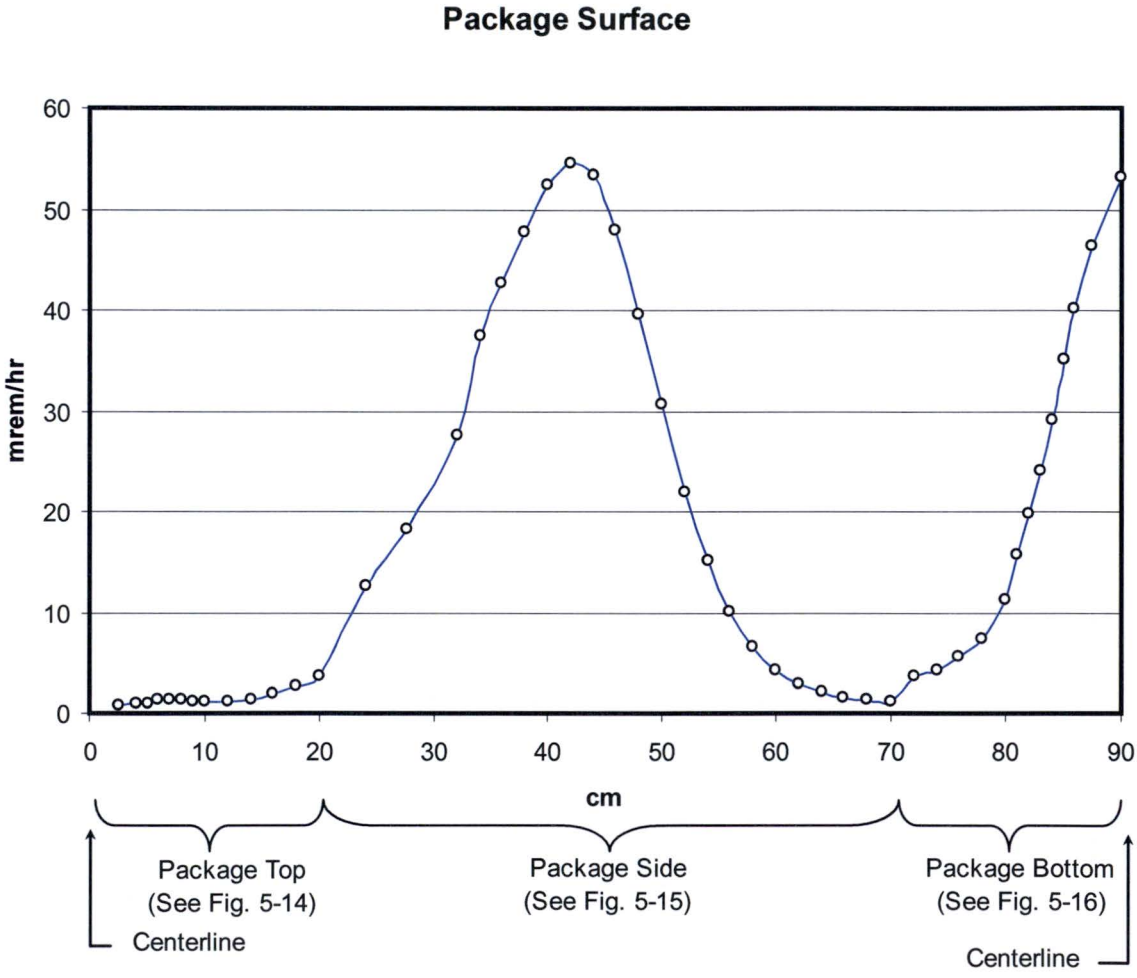

Figure 5-13 – Summary Profile for Package Surface NCT Dose Rates

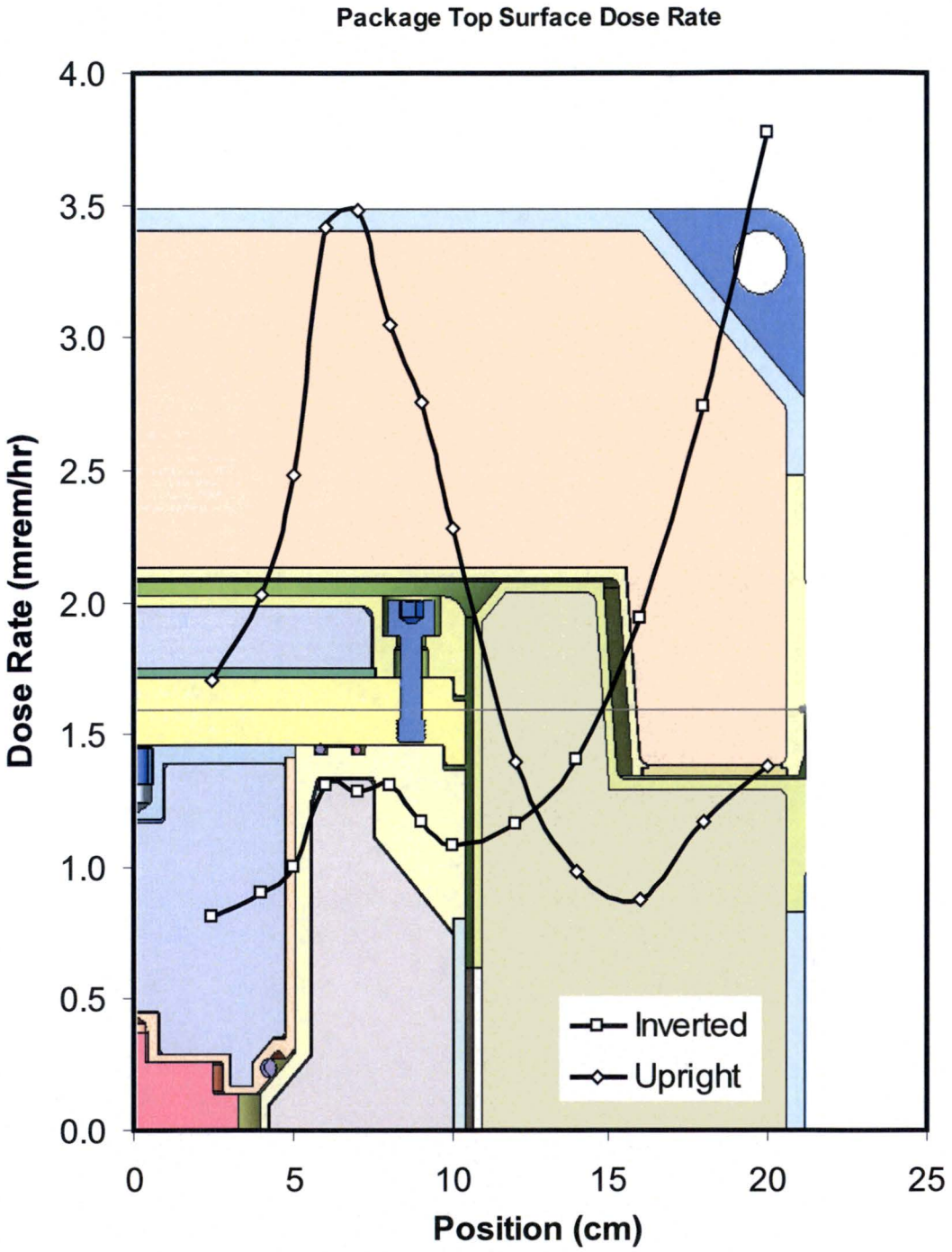

Figure 5-14 – Top-End-Surface Dose Rate Profile

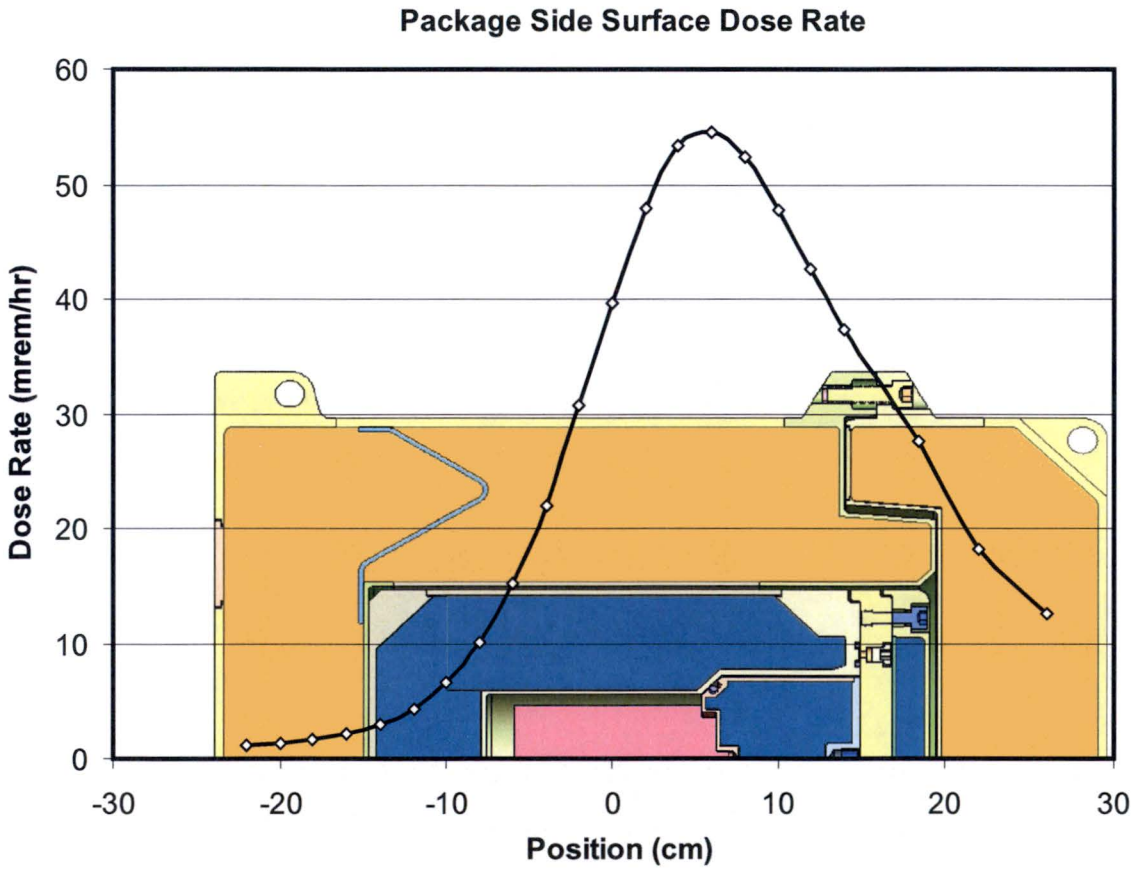

Figure 5-15 – Side-Surface Dose Rate Profile

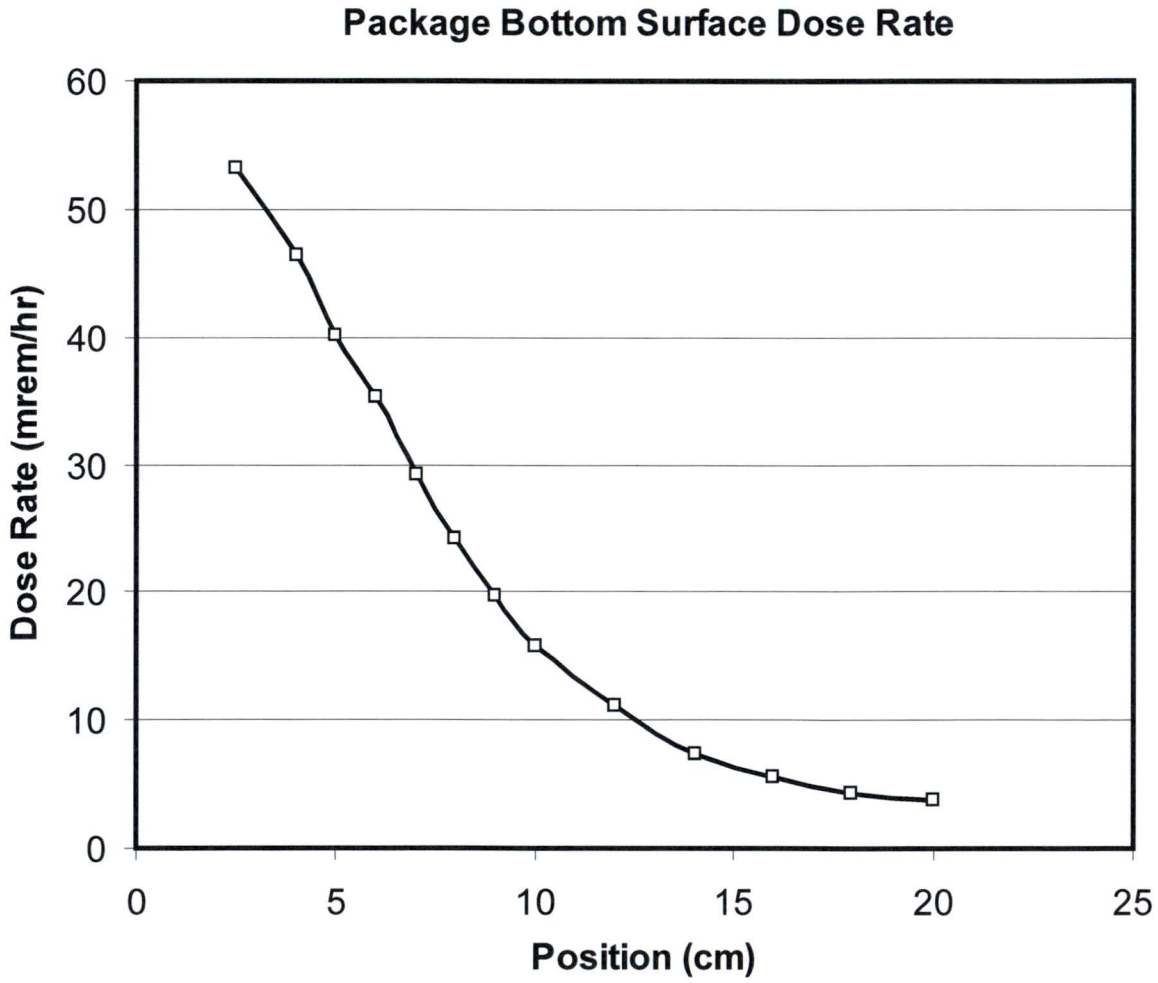

Figure 5-16 – Bottom-Surface Dose Rate Profile

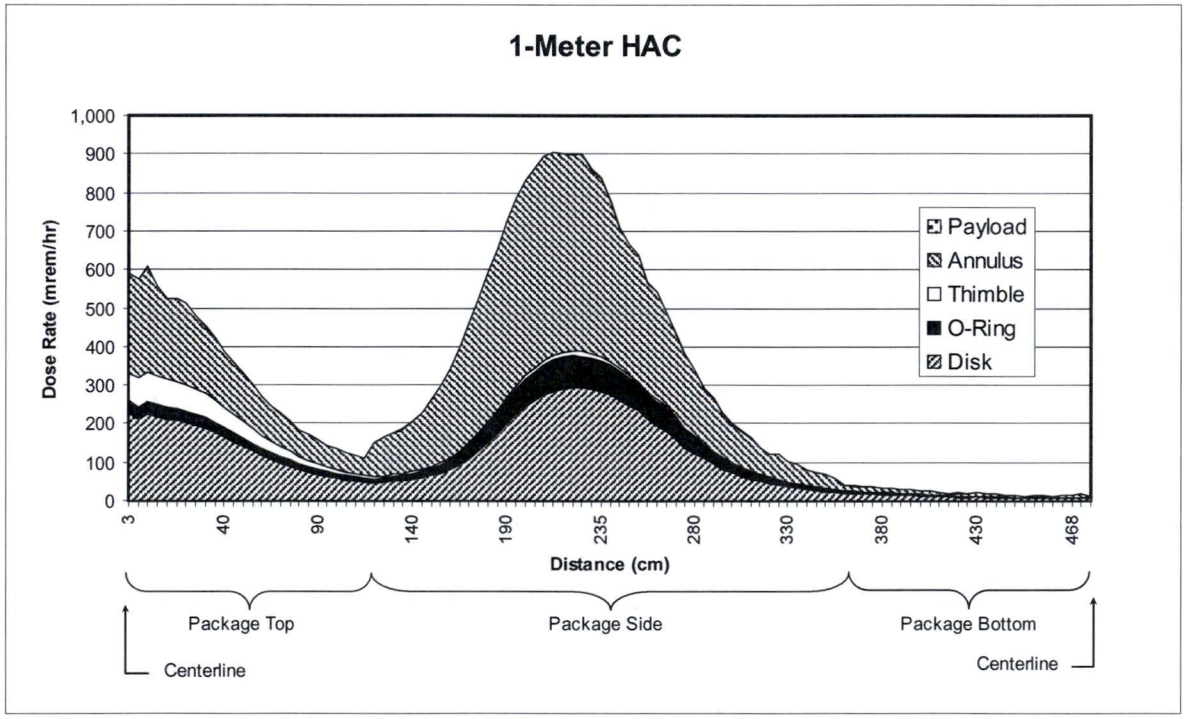

Figure 5-17 – 1-Meter HAC Results

5.5 Appendix

5.5.1 References

[5.1] *Federal Register*/Vol. 68, No. 75/Friday, April 18, 2003/Notices.

[5.2] Lederer, C., Shirley, V. Ed., *Table of Isotopes*, 7th Edition, John Wiley & Sons, New York, 1978.

[5.3] Ernest O. Lawrence Berkeley National Laboratory, *WWW Table of Radioactive Isotopes*, The Berkeley Laboratory Isotopes Project, http://ie.lbl.gov/education/isotopes.htm (accessed January 18, 2006).

[5.4] *MCNP — A General Monte Carlo N-Particle Transport Code, Version 5*, LA-UR-03-1987, Los Alamos National Laboratory, Los Alamos, New Mexico, April 2003.

[5.5] American National Standard ANSI/ANS-6.1.1-1977, *Neutron and Gamma-Ray Flux-to-Dose-Rate Factors*.

6 CRITICALITY EVALUATION

Not applicable.

7 PACKAGE OPERATIONS

This chapter describes the operations used to load the MIDUS package and prepare it for transport (Section 7.1), unload the package (Section 7.2), and prepare the empty package for transport (Section 7.3). It presents the fundamental operating steps in the order in which they are performed. The operating steps are intended to ensure that the package is properly prepared for transport, consistent with the package evaluation in Chapters 2 through 6, and to ensure that occupational exposure rates are as low as reasonably achievable (ALARA).

The package shall be operated in accordance with detailed written procedures that are based on, and consistent with, the operations described in this section. To provide a comprehensive description of the package operations, this chapter describes a particular sequence for steps and makes reference to specific facility areas. The specific sequence and locations in the detailed written operating procedures may be tailored to meet facility requirements.

7.1 Package Loading

This section describes loading-related preparations, tests, and inspections for the package. These include the inspections made before loading the package to determine that it is not damaged and that radiation and surface contamination levels are within the regulatory limits.

7.1.1 Preparation for Loading

Special Equipment Required: *Radioactive contamination detector, radiation survey meter*

Special Controls or Precautions: *The contents are highly radioactive. To avoid injury in the unlikely event that a loaded cask is received for preparation, DO NOT REMOVE THE SHIELD PLUG UNTIL A RADIATION SURVEY IS PERFORMED.*

1. Visually inspect the package for cleanliness and swipe for radioactive contamination in accordance with facility procedures. Clean or decontaminate the package as necessary. If decontamination is necessary, determine the cause and take precautionary measures before opening the package for preparation.

2. Remove any tie-downs and transfer the package to the assembly area.

3. Remove the overpack closure bolts and lift the overpack lid.

4. Perform a radiation survey to confirm that the package is empty. If radiation levels indicate that the package may have an active payload, discontinue operations, determine the cause, and take corrective actions.

5. Visually inspect the accessible interior surfaces of the package to assure cleanliness. Swipe the accessible interior surfaces of the package for surface contamination in accordance with

facility procedures. Clean or decontaminate the interior surfaces if necessary. If decontamination is necessary, determine the cause and take precautionary measures before proceeding further.

6. Remove the shield lid.

7. Using the two closure lid lifting points, remove the cask from the overpack.

8. Remove the cask closure bolts and the closure lid.

9. Remove the test port from the closure lid.

10. Using the shield plug lifting point, remove the shield plug and any other items from the payload cavity.

11. Visually inspect the cavity and shield plug for cleanliness and damage. If necessary, clean with a soft, clean cloth and demineralized water. Repair damaged items per Section 8.2.3.

12. Visually inspect the following for damage that may have occurred during shipping and handling:

    - Overpack lid and base
    - Closure lid and cask body
    - Overpack and cask closure bolts
    - Closure lid test port plug
    - Overpack base, cask body, and closure lid threaded inserts
    - Closure lid test port plug drilled and tapped holes

    Repair or replace damaged items per Section 8.2.3.

13. Remove the leak test, containment, and cleanliness seals.

14. Gently wipe away any debris from the O-ring grooves and sealing surfaces with a soft, clean cloth and demineralized water. Visually inspect the following surfaces for scratches, blemishes, adhered particles, debris, etc.:

    - The sealing surfaces on the bottom of the closure lid
    - The O-ring grooves on the cask flange
    - The O-ring groove on the shield plug
    - The cleanliness O-ring sealing surface on the beveled surface of the containment shell
    - The closure lid test port plug seal surface

    Repair any damage to the sealing surfaces per Section 8.2.3.

15. Discard the cleanliness seal and obtain a new one.

16. Gently wipe away the lubricant and any debris from the O-rings with a soft, clean cloth and demineralized water. Visually inspect the O-rings for pliability, nicks, scratches, cuts, and debris. Replace any damaged O-rings as necessary. Apply a thin film of approved lubricant and install all three of the O-rings. Assure that the following conditions are met:

    - If the containment O-ring has not been leak tested within 12 months prior to the shipment, then perform a helium leak test as described in Section 8.1.4, and return to this step. Performance of the helium leak test does not relieve the need to perform the pre-shipment leak rate test in Section 7.1.3, step 1.
    - If the containment O-ring must be replaced, then perform a helium leak test using the package and replacement O-ring as described in Section 8.1.4, and return to this step. Performance of the helium leak test does not relieve the need to perform the pre-shipment leak rate test in Section 7.1.3, step 1.

7.1.2 Loading of Contents

Special Equipment Required: *Calibrated torque wrench*

Special Controls or Precautions: *Because the contents are highly radioactive, some loading operations are performed in a hot cell in accordance with facility procedures. DO NOT REMOVE THE SHIELD PLUG OUTSIDE THE HOT CELL AFTER THE CASK IS LOADED.*

1. Confirm that the intended payload, including the product, product container(s), and optional dunnage, meets the contents specification in the Certificate of Compliance.

2. Optional step: Before performing step 6, place any optional dunnage into the cask cavity, as required by facility procedures.

3. Move the cask to the hot cell.

4. Put the product into the product container(s).

5. Place the product container(s) and any other associated payload internals into the cask, or attach them to the shield plug, in accordance with facility procedures.

6. Carefully lower the shield plug (and payload, if applicable) into the cask body.

7. Remove the cask from the hot cell.

8. Visually or mechanically inspect the top of the shield plug to confirm that it is slightly higher than the cask flange, Figure 7-1. If the top of the shield plug is lower than the cask flange, return the cask to the hot cell, remove the shield plug, assure that the new cleanliness O-ring has been installed, and re-perform this step.

9. Place the closure lid onto the cask body with alignment marks aligned.

10. Visually inspect the leak test port to assure that it is not blocked by an O-ring. If any O-ring material is visible, remove the cask lid, inspect the O-ring(s) for damage, reinstall the O-ring(s) and cask lid, and re-perform this step.

Figure 7-1 - Shield Plug Fit-Up

- If the containment O-ring must be replaced, then perform a helium leak test using the package and replacement O-ring as described in Section 8.1.4, and return to this step. Performance of the helium leak test does not relieve the need to perform the pre-shipment leak rate test in Section 7.1.3, step 1.

11. Coat the cask closure bolts with anti-seize coating as needed and reinstall to a torque of 10 ± 0.5 N-m.

12. Transfer the cask to the leak test area.

7.1.3 Preparation for Transport

Special Equipment Required: *Calibrated pressure-rise leak-detection system, radioactive contamination detector, radiation survey meter, thermometer or other temperature measurement device*

Special Controls or Precautions: *In Step 2 below, if the contents must be removed for any purpose, DO NOT REMOVE THE SHIELD PLUG OUTSIDE THE HOT CELL.*

1. Perform a pre-shipment leak rate test per Section 7.4.
2. If the leak rate is unacceptable:
   - Recheck all the connections and seals of the test equipment.
   - If the test equipment is functioning properly, disconnect it from the cask.
   - Remove the cask closure bolts and remove the closure lid.

- Inspect, clean, and replace the containment or test O-ring(s) as necessary using the appropriate steps from Section 7.1.1 and 7.1.2, or return the cask to the hot cell and transfer the payload to another cask unit.
- Repeat Step 1 of this section.

3. Disconnect the leak test equipment and reinstall the test port.
4. Transfer the cask to the assembly area and lower it into the overpack base.
5. Place the shield lid on top of the closure lid and tighten the shield lid attachment bolts.
6. Place the overpack lid onto the base, assuring that the alignment marks are aligned.
7. Apply anti-seize coating as needed to the overpack closure bolts and install the bolts.
8. Perform a contamination survey of the external surfaces of the package to determine if the contamination levels are as low as reasonably achievable. If the non-fixed surface contamination exceeds local requirements, then decontaminate the external surfaces using distilled water or a mild decontamination agent.[2]
9. Perform a radiation survey of the package. If the external radiation levels exceed 200 mrem/h, return the cask to the hot cell, investigate the cause of the high radiation levels, and begin again at Section 7.1.3, Step 1 or earlier. Because of the radiolytic gas generation, it is not acceptable to allow the payload to decay until the external radiation reaches acceptable levels.
10. Check the temperature on the outside surface of the package. If the temperature exceeds 50°C, investigate the cause of the high temperature, and take corrective action. If necessary, return the cask to the hot cell and begin again at Section 7.1.2.
11. Install the tamper-indicating seal.
12. Optional step: Attach the package to the shipping pallet using the package's lower lugs.

    Note: The lower lugs may be used for attachment to a shipping pallet, or they may be used directly for securing the package in combination with the four upper lugs. It is not necessary to render the lower lugs inoperable for use as lifting or tie-down devices.
13. Transfer the package and its shipping pallet, to the transport conveyance and connect the tie-downs in accordance with the specifications in Section 1.3.2, Drawing No. TYC01-1609.
14. Review the package loading/closure documentation for completeness.
15. Visually inspect the package nameplate to assure that it is not obstructed from view or degraded and that the information is clear and legible. If it is not, clear the obstruction as necessary to make the information legible.
16. Before releasing the package for shipment, assure that the procedures for opening and unloading the package (per Section 7.2) have been forwarded to the Consignee receiving the package. If they have not, then forward them before releasing the package for shipment.

[2] Requirements for swiping and acceptance criteria are based on 49 CFR 173.443, or other applicable regulation.

17. Release the package to the Carrier for shipment to the Consignee.

7.2 Package Unloading

This section describes the package unloading operations, including the inspections, tests, and preparations of the package for unloading.

7.2.1 Receipt of Package from Carrier

Special Equipment Required: *Radioactive contamination detector, radiation survey meter*

Special Controls or Precautions: *None*

1. Before handling the package, the Consignee must have and understand the procedures for opening and unloading the package.

2. Perform a radiation survey of the package. If the external radiation levels exceed 200 mrem/h, then take the following steps:
   a) Notify the Consignor immediately.
   b) Investigate the cause of the high radiation levels before proceeding.
   c) Take extra precautions as necessary when proceeding with the remaining unloading steps.

3. Perform a contamination survey of the external surfaces of the package to determine if contamination has occurred during transit. If contamination levels exceed shipping release levels[3], then take the following steps.
   a) Notify the Consignor.
   b) Investigate the cause of the contamination.
   c) Decontaminate using distilled water or a mild decontamination agent.
   d) Take extra precautions as necessary before opening the package for unloading.

4. Assure that the tamper-indicating seal is intact. If it is NOT intact, investigate the cause and take actions per facility procedures.

5. Remove the tie-downs.

6. Transfer the package to the assembly area.

[3] Requirements for swiping and acceptance criteria are based on 49 CFR 173.443, or other applicable regulation.

7.2.2 Removal of Contents

Special Equipment Required: *Radioactive contamination detector, radiation survey meter*

Special Controls or Precautions: *Because the contents are highly radioactive, some loading operations are performed in a hot cell in accordance with facility procedures. DO NOT REMOVE THE SHIELD PLUG OF A LOADED CASK OUTSIDE THE HOT CELL. To avoid injury, CHECK THE EMPTY CASK FOR RADIATION AND CONTAMINATION PRIOR TO REMOVING THE SHIELD PLUG FOR INSPECTION AND PREPARATION FOR RETURN SHIPMENT (Step 8).*

1. Remove the overpack closure bolts and the overpack lid.
2. Remove the shield lid.
3. Lift the cask from the overpack base and transfer it to the hot cell using the two closure lid lifting points.
4. Remove the cask closure bolts and the closure lid.
5. Lift the shield plug (and payload, if applicable) from the cask body. If the payload internals are not mechanically attached to the bottom of the shield plug or if they do not lift out with the shield plug, then remove them from the cask cavity.
6. Process the payload in the hot cell in accordance with the Consignee's facility procedures.
7. Return the cask body, dunnage (if present), shield plug, closure lid, closure bolts, and shield lid to the assembly area. Process the payload internals in accordance with facility procedures.
8. Perform radiation and contamination surveys in accordance with facility procedures before proceeding to Section 7.3. Decontaminate as necessary in order to continue work.

7.3 Preparation of Empty Package for Transport

Special Equipment Required: *Radioactive contamination detector, radiation survey meter*

Special Controls or Precautions: *None*

1. Visually inspect the following components for damage that may have occurred during shipping and handling:
   - Overpack lid and base
   - Shield lid, closure lid, cask body, and shield plug
   - Overpack and cask closure bolts
   - Closure lid test port plug
   - Overpack base, cask body, closure lid, and shield plug threaded inserts

- Closure lid test port plug and shield plug payload container drilled and tapped holes

Notify the Consignor of any damage. Prepare damaged items for return shipment as instructed by the Consignor.

2. Visually inspect the containment, leak test, and cleanliness O-rings for scratches, blemishes, adhered particles, debris, etc. As needed, remove the O-ring(s) and gently wipe away any debris with a soft, clean cloth and clean, demineralized water. Notify the Consignor if any damaged or missing O-rings must be replaced. Prepare any damaged items for return shipment as instructed by the Consignor.

3. Perform a contamination survey of the internal surfaces of the package (cask cavity, cask flange, and underside of the closure lid) and any empty payload internals to be shipped. If the non-fixed surface contamination exceeds local requirements for empty package shipment, then decontaminate using distilled water or a mild decontamination agent.[4]

4. Carefully lower the shield plug into the cask body. Optionally, the empty product container(s) may be loaded if desired.

5. Install the closure lid onto the cask body with the alignment marks aligned.

6. Apply anti-seize coating as needed to the cask closure bolts and reinstall them.

7. Place the cask into the overpack base.

8. Install the shield lid onto the cask closure lid.

9. Install the overpack lid onto the overpack base with the alignment marks aligned.

10. Apply anti-seize coating as needed to the overpack closure bolts and install them.

11. Optional step: Attach the package to the shipping pallet using the package's lower lugs.

    Note: The lower lugs may be used for attachment to a shipping pallet, or they may be used directly for securing the empty package. It is not necessary to render the lower lugs inoperable for use as lifting or tie-down devices.

12. Assure that the package and shipping pallet are assembled correctly and are in unimpaired physical condition.

13. Transfer the package and its shipping pallet to the transport container/conveyance and connect its associated tie-downs.

[4] Internal contamination cannot exceed 100 times the limits in 49 CFR 173.443(a), or other applicable regulation.

14. Perform a contamination survey of the external surfaces of the package to determine if the surface contamination levels are as low as reasonably achievable. If the non-fixed surface contamination exceeds local requirements, then decontaminate using distilled water or a mild decontamination agent.[5]

15. Perform a radiation survey to confirm that the package is empty and meets the requirements for shipment of empty packagings.[6]

16. Release the package to the Carrier for the return shipment.

7.4 Other Operations

The package containment seal is a reusable, elastomeric O-ring, which is tested before each loaded shipment. This section provides the requirements for package pre-shipment leak rate testing. More sensitive leak testing procedures are necessary for certain maintenance activities as described in Section 8.2.

Chapter 4 discusses the basis for the pre-shipment leak test criterion of 10^{-3} ref-cm^3/s. The package is designed for performing the pre-shipment leak test using the gas pressure rise method described in Section A.5.2 of ANSI N14.5 [7.1].

The pre-shipment leak test shall be performed in accordance with written test procedures that are based on and consistent with the following specifications.

7.4.1 Pre-Shipment Leak Detection Equipment

Type .....Pressure-rise
Accuracy .....Pressure measurements shall be accurate to within 1% or less of the full scale of the measuring device
Range .....1.5 to 4 times the specified test pressure
Sensitivity .....Sufficient to detect a leak rate of 1 x 10^{-3} ref-cm^3/s

7.4.2 Pre-Shipment Leak Testing Procedure

1. The test shall be performed on the loaded package at room temperature and atmospheric conditions. Corrections shall be made for temperature effects if necessary.

2. Connect the test apparatus to the package test port as shown in Figure 7-2.

3. Determine the test volume as follows. Open all three valves and record the atmospheric pressure and temperature. With valve A closed, valve B open, and valve C closed, evacuate

[5] Requirements for swiping and acceptance criteria are based on 49 CFR 173.443, or other applicable regulation.

[6] Requirements for external radiation acceptance criteria are 0.5 mrem/hr based on 49 CFR 71.421(a)(2), as referenced in 49 CFR 71.428, or other applicable regulation.

the test space. Close the isolation valve B, allow the pressure reading to stabilize, and record pressure P_1. Open valve C to add the calibrated volume (V_c), allow the pressure to stabilize, and record the final pressure P_2. Calculate the test volume using the following equation.

$$V_{test} = V_c\left(\frac{P_{atm} - P_1}{P_1 - P_2}\right)$$

4. Calculate the test duration using the following equation derived from ANSI N14.5, equations B.14 and B.17. This test duration assures the required minimum test sensitivity to meet the requirements of Section 7.4.1.

$$t = 2000 \cdot V_{test} \frac{T_s}{T_{amb}} \frac{\Delta P}{P_s}$$

Where t = test time [seconds]
V_{test} = test volume [cm^3], (Step 3)
T_s = standard temperature, 298K
T_{amb} = ambient test temperature, K
ΔP = sensitivity of pressure measurement, atm
P_s = standard pressure, 1 atm abs

5. Perform a go-no-go leakage rate test as follows. With valve A closed, valve B open, and valve C closed, evacuate the test space (between the test and containment O-rings), close the isolation valve B, and allow the system to stabilize. This step may be repeated as necessary to allow for off-gassing or other effects that may result in false test results. Measure the change in pressure for the minimum time specified in Step 4. The test passes if there is no indicated leakage (at the pressure measurement sensitivity, ΔP).
6. If, after repeated attempts, the O-ring seal does not pass the test, the package may not be shipped until the steps indicated in Section 7.1.3, Step 2 are performed and an acceptable test is performed.

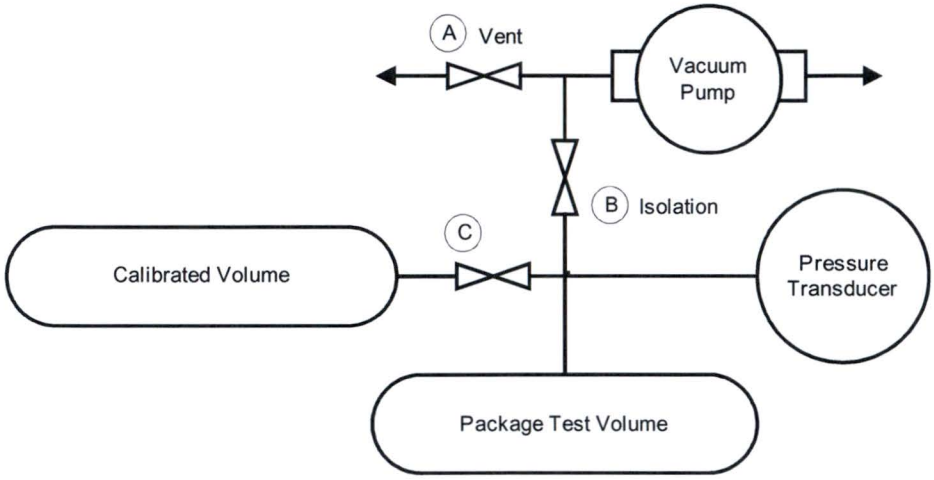

Figure 7-2 – Pre-Shipment Leak Rate Test Configuration (Typical)

7.5 Appendix

7.5.1 References

[7.1] ANSI N14.5, American National Standard for Radioactive Materials – *Leakage Tests on Packages for Shipment*, American National Standards Institute, 1997.

8 ACCEPTANCE TESTS AND MAINTENANCE PROGRAM

This chapter presents the acceptance tests and maintenance program for the MIDUS Package. These activities assure that the packaging meets the requirements of 10 CFR 71, Subpart G.

8.1 Acceptance Tests

This section describes the tests to be performed before the first use of each packaging. The acceptance tests confirm that each packaging is fabricated in accordance with the general arrangement drawings in the Certificate of Compliance.

8.1.1 Visual Inspections and Measurements

Packaging components shall receive visual and mechanical inspections to verify that the package has been fabricated and assembled in accordance with the general arrangement drawings in Section 1.3.2. The dimensions, tolerances, and surface finishes shown on the drawings shall be verified by measurement on each package. Nonconforming components shall be reworked or replaced.

8.1.2 Weld Examinations

All package welds shall be examined to the requirements in drawings TYC01-1602 and TYC01-1603 (included in Section 1.3.2). Nonconforming components shall be reworked or rejected.

All brazed joints shall be visually examined on all accessible surfaces to determine whether there has been adequate flow of brazing metal between the thermal spider and overpack shells. Nonconforming components shall be reworked or rejected.

8.1.3 Structural and Pressure Tests

A pressure test shall be performed on each package to verify the capability of the containment system to maintain its structural integrity at the test pressure. The test will be performed per ASME BPVC, Subsection WB [8.1], to a pressure of 1050 kPa (150% of the package MNOP). The acceptance criteria is no unacceptable leakage, in accordance with WB-6224. Nonconforming packages shall be reworked or rejected.

8.1.4 Leakage Tests

The package containment boundary, defined in Section 4.1, shall be leak rate tested in accordance with Section 8 of ANSI N14.5 [8.2] to an acceptance criterion of 1×10^{-7} ref-cm^3/s. Leak rate testing shall be performed using the Evacuated Envelope-Gas Detector method of ANSI N14.5, Section A.5.4, using a suitable helium leak detector with a sensitivity of at least 5×10^{-8} ref-cm^3/s.

Packages not meeting the acceptance criteria shall be reworked or rejected.

8.1.5 Component and Material Tests

8.1.5.1 Package Weight

The packaging shall be weighed to determine that it does not exceed 329 kg, such that the total weight of the package including the payload does not exceed the maximum specified weight of 330 kg. Nonconforming packages shall be reworked or rejected.

8.1.5.2 Shield Plug Fit Up

The shield plug shall be visually or mechanically inspected to assure proper fit up. Without the cleanliness O-ring in place, the inspection shall determine that the top of the shield plug is below the plane of the cask flange. With the cleanliness O-ring in place, the inspection shall determine that the top of the shield plug is above the plane of the cask flange. Assemblies not meeting the acceptance criteria shall be reworked or rejected.

8.1.5.3 Overpack Foam

Each batch of overpack foam shall be tested for the following attributes:

- Average density
- Static crush strength
- Flame retardancy
- Intumescence

Foam not meeting the acceptance criteria in drawings TYC01-1607 and TYC-1608 (included in Section 1.3.2) shall be rejected.

8.1.5.4 Depleted Uranium

The density of depleted uranium (DU) components shall be determined by measuring their weight and volume. The chemical composition of each DU heat will be analyzed to assure that the alloy meets the specifications. Finished DU components shall be visually examined to verify that their surfaces are free of voids, cracks, or porosity. DU components not meeting the acceptance criteria in drawing TYC01-1606 (included in Section 1.3.2) shall be rejected.

8.1.6 Shielding Tests

Section 8.1.5 discusses the material tests for the DU parts.

8.1.7 Thermal Tests

Section 8.1.5 discusses the material tests for the overpack foam. The material tests provide assurance that the material will perform under NCT and HAC conditions. Section 8.1.2

describes the examination of the overpack thermal spider brazing. The function of the thermal shunt is to balance the heat rejection (i.e., provide a similar heat transfer path as provided by the overpack flange). Because of the package's low heat load (less than 18 watts peak) and the large design margins on allowable material temperatures (Table 3-1, Table 3-2), no additional thermal test are necessary.

8.1.8 Miscellaneous Tests

Not applicable.

8.2 Maintenance Program

Table 8-1 summarizes the MIDUS maintenance program. The program includes periodic inspections, tests, and maintenance activities designed to ensure continued performance of the packaging. This section describes the periodic testing, inspection, and replacement schedules, as well as the criteria for replacement and repair of components and subsystems on an as-needed basis.

8.2.1 Structural and Pressure Tests

There are no routine structural or pressure tests required for the package. This includes the replacement of cask closure bolts or cask bolting flange threaded inserts as exempted by ASME BPVC, Section III, Division 3, Subsection WB, Paragraph WB-6111. Replacement requirements for threaded components or inserts are presented in Section 8.2.3.

8.2.2 Leakage Test

The package containment boundary, defined in Section 4.1, shall be leak rate tested in accordance with Section 8 of ANSI N14.5 to an acceptance criterion of 1×10^{-7} ref-cm^3/s. Leak rate testing shall be performed using the Evacuated Envelope-Gas Detector method of ANSI N14.5, Section A.5.4, using a suitable helium leak detector with a sensitivity of at least 5×10^{-8} ref-cm^3/s.

Section A.3.2 in ANSI N14.5 says that care should be taken to ensure that the test procedure adequately tests the seal of interest (e.g., the containment seal). The package leak rate testing procedure requires removal of the cleanliness seal because it could cause a false pass. It is acceptable to simultaneously test the concentric test and containment O-rings for this package because both O-rings are backed by helium during the test. A leak in either O-ring would result in a test failure.

Leak rate testing shall be performed periodically, not to exceed 12 months prior to package use, and after the following maintenance activities:

- Replacement of the containment seal
- Repair of the containment seal sealing surface, including the O-ring gland surface, or the cask closure lid sealing surface
- Repair or replacement of the shield plug or closure lid

The periodic and maintenance leak rate testing shall be performed in accordance with the following procedure:

1. Prepare the cask body and closure lid. Install the containment and test seals. Prepare the shield plug WITHOUT the cleanliness O-ring. Remove the closure lid test port.
2. Prepare the helium fill device. Fill the device with helium of 99% or greater purity until it's volume, V_{He}, is 405 ml or greater ($\geq$ 50% of the cask cavity volume).

3. Place the helium fill device into the cask cavity and install the shield plug and cask lid.
4. Install the cask closure bolts to a torque of 10 ± 0.5 N-m.
5. Place the cask into the glove box enclosure, connect the helium leak detector to the test port, and seal the enclosure.
6. Evacuate the glove box to a vacuum of 5 kPa or lower, then backfill to atmospheric pressure using helium of 99% or greater purity.
7. Using the test port connection, evacuate the space between the containment and test O-rings to 100 Pa or less and hold for ten minutes. If the pressure cannot be maintained for ten minutes, then open the glove box, inspect and clean the O-rings and sealing surfaces, check the instrumentation connections, and restart the test.
8. Actuate the helium fill device, releasing helium into the cask cavity.
9. Using the test port connection, sample the gas from between the containment and test O-rings using a helium leak detector. Since both the glove box and cask cavities are filled with helium, this test will indicate the combined leak rate through both the test and containment O-rings. The acceptance criterion is a equivalent leakage rate of $\leq 1 \times 10^{-7}$ ref-cm^3/s, taking into account V_{He}, the partial volume of helium in the cask cavity. If the package does not pass, then open the glove box, inspect and clean the O-rings and sealing surfaces, check the instrumentation connections, perform any replacements or repairs as necessary, and restart the test.
10. Open the cask and check that the helium fill device actuated properly. If not, then repair the device and restart the test.
11. Note the test results and any necessary corrective actions in the package maintenance log.

Pre-shipment leak rate testing is described in the operating procedures in Section 7.1.3.

8.2.3 Component and Material Tests

The following sections describe the periodic maintenance program for package operation. Additional maintenance may be required on an as-needed basis when wear or damage is noted during routine operations. When as-needed maintenance is performed, the associated repair, replacement, and records-keeping activities shall follow the maintenance program requirements for the corresponding periodic maintenance activity.

8.2.3.1 O-ring Seals

The following O-ring seals shall be replaced annually, or as needed, with seals as specified in the general arrangement drawings in Section 1.3.2. The replacements shall be recorded in the packaging maintenance log.

- Containment O-ring
- Leak Test O-ring

- Leak Test port plug O-ring

Cleanliness O-rings are replaced with every shipment and therefore do not require annual replacement.

8.2.3.2 Sealing Surfaces

The following O-ring sealing surfaces shall be inspected annually for damage and wear. If sealing surfaces show damage or wear in excess of the surface finish requirements specified in the general arrangement drawings in Section 1.3.2, then the damage may be repaired using emery cloth or a similar polishing agent to return the surface to the specifications in the drawings. The inspection results, and any necessary repairs, shall be recorded in the packaging maintenance log. The annual sealing surface inspection shall include, as a minimum, the following surfaces:

- Containment seal groove sealing surfaces (bottom and outside diameter of groove)
- Containment seal contact surface on the cask closure lid

8.2.3.3 Fasteners

All package fasteners shall be visually inspected annually for excessive wear or damage. Fasteners which show visible signs of excessive wear or damage shall be replaced in accordance with the specifications in the general arrangement drawings in Section 1.3.2. The inspection results, and any necessary replacements, shall be recorded in the packaging maintenance log. The fasteners to be inspected include:

- Cask closure bolts
- Shield lid attachment bolts
- Test port plug
- Overpack closure bolts

Fastener holes with threaded inserts shall be visually inspected annually for excessive wear or damage. Threaded inserts which show visible signs of excessive wear or damage shall be replaced in accordance with the specifications in the general arrangement drawings in Section 1.3.2. The threaded inserts at the following locations shall be inspected:

- Cask closure bolts
- Shield lid attachment bolts
- Cask lifting attachment points
- Shield plug lift point
- Overpack closure bolts

The inspection results, and any necessary replacements, shall be recorded in the packaging maintenance log.

When inspections reveal mild damage or wear to threaded fasteners or tapped holes, repairs may be performed as follows. Barbs may be removed, taking care not to further damage the threads. Threads may be refurbished using taps and dies specifically intended for thread chasing or repair.

When inspections reveal more significant damage to threaded fasteners, or threaded inserts, they shall be replaced according to the specifications in the general arrangement drawings in Section 1.3.2 and the manufacturer's instructions. Replacements shall be noted in the package's maintenance log. The associated assemblies shall be functionally tested to confirm proper fit and function.

Tapped holes for threaded inserts may be refurbished using the manufacturer's thread repair tools. Tapped holes without threaded inserts may be refurbished using taps specifically intended for thread chasing or repair.

The overpack thermal relief plugs shall be visually inspected for damage, wear, or weathering of the nylon material, threads, and elastomeric weather seals. Damaged or missing thermal relief plugs or O-rings shall be replaced according to the specifications in the general arrangement drawings in Section 1.3.2. The inspection results, and any necessary replacements, shall be recorded in the packaging maintenance log.

The overpack locating pins shall be visually inspected annually for damage. Damaged or missing locating pins shall be repaired or replaced. The inspection results, and any necessary replacements or repairs, shall be recorded in the packaging maintenance log.

8.2.3.4 Package Visual Inspections

Chapter 7 describes the requirements for visual inspections of the packaging during each phase of operation. As permitted by §71.87(b), their physical condition may contain superficial defects such as marks and dents that do not impair the operation of the components.

Superficial polishing of package components may be performed using emery cloth or a similar fine abrasive to remove corrosion, scratches, blemishes, adhered material/particles, etc.

The following replacement and repair tasks shall be evaluated and approved by the Certificate Holder/Designer prior to implementation:

- Any change to the configuration of the package as shown in the general arrangement drawings in Section 1.3.2
- Any metal removal that reduces the thickness of a containment, structural, shielding, or thermal component below its licensed dimension including all tolerances as shown in the general arrangement drawings in Certificate of Compliance
- Any welding repair

- Any re-tapping of a hole to accommodate a larger threaded component
- Mechanical straightening the overpack lugs or opening a damaged lug eye

Each package shall be visually inspected annually, and the results shall be noted in the package's maintenance log confirming:

- General condition of packaging (significant scratches, marks, or dents)
- Identification numbers of cask body, shield plug, closure lid, shield lid, overpack base, and overpack lid for configuration control
- Legibility of the nameplate information

8.2.4 Thermal Tests

Not applicable.

8.2.5 Miscellaneous Tests

The following subsections discuss the requirements following replacement of package components. These requirements apply to newly manufactured components (spares), or substituted components from other MIDUS packages. For the purpose of configuration management, the overpack base unit is the host component because it bears the package nameplate. Other components may be substituted following these procedures.

8.2.5.1 Replacement of a Shield lid

In the event that a shield lid must be replaced, the replacement shall be noted in the package's maintenance log.

8.2.5.2 Replacement of a Closure Lid

In the event that a closure lid must be replaced, a maintenance leak rate test shall be performed in accordance with Section 8.1.4 above. The replacement shall be noted in the package's maintenance log along with the test results.

8.2.5.3 Replacement of a Shield Plug

In the event that a shield plug must be replaced, the functional fit-up tests described in 8.1.5.2 shall be performed to assure proper operation. The replacement shall be noted in the package's maintenance log along with the inspection results.

8.2.5.4 Replacement of a Cask Body

In the event that a cask body must be replaced, the steps in Sections 8.2.5.2 and 8.2.5.3 shall be performed to assure proper fit-up of the closure lid and shield plug. A maintenance leak rate test shall be performed in accordance with Section 8.1.4 above. The replacement shall be noted in the package's maintenance log along with the test and inspection results.

8.2.5.5 Replacement of an Overpack Lid

In the event that an overpack lid must be replaced, the replacement shall be noted in the package's maintenance log.

8.2.5.6 Replacement of a Cask Assembly

In the event that an entire cask assembly (cask body, shield plug, closure lid, and shield lid) must be substituted, the replacement shall be noted in the package's maintenance log. The substitute cask assembly must either be a unit currently in service, or another unit manufactured or refurbished to the requirements shown in the general arrangement drawings in Section 1.3.2.

Table 8-1 – Package Maintenance Program Summary

Item	SAR Section[2]	Inspection/Test/Maintenance[1]		
		Each Use	Replace / Repair[3]	Annual
Containment O-ring	8.2.3.1	V, LT1	LT2	R, LT2
Containment O-ring sealing surfaces	8.2.3.2	V	LT2	V
Leak Test O-ring	8.2.3.1	V		R
Leak Test O-ring sealing surfaces	8.2.3.2	V		V
Cleanliness O-ring	8.2.3.1	R		
Cleanliness O-ring sealing surfaces	--	V		V
Thermal relief plugs and hole threads	8.2.3.3			V
Thermal relief plug O-rings	8.2.3.3			V
Cask closure bolts	8.2.3.3	V		V
Threaded inserts-cask closure bolts	8.2.3.3		LT2	V
Shield lid attachment bolts	8.2.3.3	V		V
Threaded inserts-shield lid bolts	8.2.3.3			V
Tapped holes[4]	8.2.3.3			
Test port plug	8.2.3.3	V		V
Test port plug O-ring	8.2.3.1	V		V
Threaded insert-shield plug lift point	8.2.3.3			V
Threaded inserts-cask lid lift points	8.2.3.3			V
Overpack closure bolts	8.2.3.3	V		V
Threaded inserts-overpack bolts	8.2.3.3			V
Overpack locating pins	8.2.3.3			V
Nameplate	8.2.3.4			V

Notes:
1. R = Replace, V = Visual Inspection,
   LT1 = Pre-shipment leak test (Section 7.4.2),
   LT2 = maintenance/periodic leak test (Section 8.2.2).
2. Reference SAR section.
3. Tests or inspections necessary when replacement or repair as needed.
4. Tapped holes without threaded inserts: shield plug bottom, and test port

8.3 Appendix

8.3.1 References

[8.1] American Society of Mechanical Engineers (ASME) Boiler and Pressure Vessel Code (BPVC), Section III, Division 3, Subsection WB, Class TP (Type B) Containment, 2001 Edition with Addenda through July 1, 2003.

[8.2] ANSI N14.5, American National Standard for Radioactive Materials – *Leakage Tests on Packages for Shipment*, American National Standards Institute, 1997.

9 EVALUATION OF CONTENT #02

This SAR addendum describes the evaluation of the MIDUS package for Content #02.

9.1 Content #02 – General Information

Content #02 is a solid payload, or product, consisting of ^{99}Mo with its daughter products as solid metallic molybdenum. This payload is non-fissile and does not generate neutrons. The specification for Content #02 is provided on Drawing No. TYC01-1601 in Section 1.3.2 and discussed below.

The maximum product activity is 4,400 Ci of ^{99}Mo at the time of shipment. The maximum product *specific* activity is limited to 60 Ci/ml ^{99}Mo at the time of shipment. The specific activity affects the concentration of the potential radiological source terms for HAC, in the event that molybdenum powder or fines were to migrate within the containment boundary. Both the activity and specific activity specifications are the same as for Content #01.

The product is solid and does not generate gas by radiolytic decomposition.

The maximum mass of the product and payload internals shall not exceed 1.0 kg.

The contents volume is not restricted because there are no sources of radiolytic decomposition that would result in gas generation. Sections 9.2 and 9.3 further discuss package pressures.

The package materials of construction have been evaluated and are compatible with the chemical form of the product and payload internals. Section 9.2 discusses the materials evaluation in further detail.

The payload internals are provided by the user and include sealed aluminum target cans (which contain the irradiated molybdenum disks), and aluminum carriers. Figure 9-1 shows a typical configuration.

The ^{98}Mo target material is prepared in the form of high-purity metallic disks, placed in dry, thin-walled, close-fitting aluminum target cans, which are seal-welded and then leak tested prior to irradiation. After irradiation, ^{99}Mo and its daughter product ^{99m}Tc are the only significant activation sources. There are several configurations of target cans (containing various quantities of disks) and carriers to suit the requirements for particular shipments. No containment or other safety credit is taken for the target cans.

The carrier is constructed from aluminum and serves as a hot-cell handling aid during the cask loading and unloading processes, and as dunnage during shipment. There is no safety credit taken for the presence of the aluminum carriers.

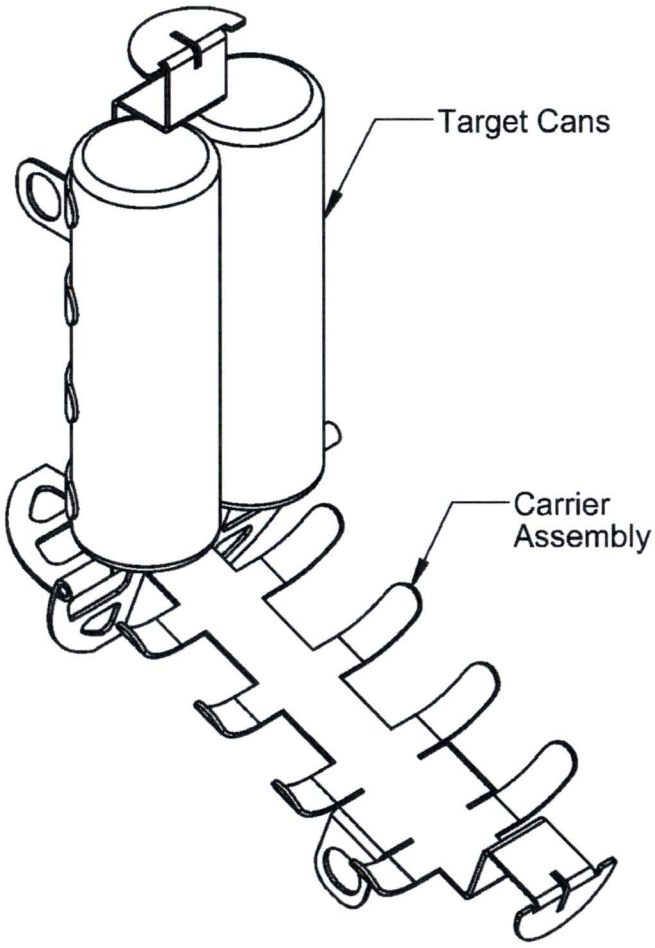

Figure 9-1 – Content #02 Payload Internals

9.2 Content #02 – Structural Evaluation

The structural evaluation in Chapter 2 bounds Content #02 based on the comparison of the structural analysis inputs for the Content #02 (i.e., mass, internal pressure, and temperature) to those used in the baseline structural analysis.

The total mass of the product and product containers for Content #02 is limited to 1.0 kg, which is less than the 1.1 kg payload mass assumed in the base structural analysis. Furthermore, the base structural analysis takes no credit for structural support provided by the product containers, and instead conservatively applies the inertia loading from the payload as pressure on the supporting cavity surfaces. Therefore, the applied loads used in the base structural analysis to account for the payload are bounding for Content #02.

As discussed in Section 9.3, the package temperatures and internal pressures for Content #02 are bounded by the baseline design. Therefore, the temperature and internal pressure loads used in the base structural analysis are bounding for content #02.

Since the inputs used in the baseline structural analysis for the contents (i.e., mass, internal pressure, and temperature) all bound those for Content #02, the stress results of the baseline structural analysis are also bounding for Content #02.

Content #02 includes metallic molybdenum and aluminum, which were not evaluated previously in Chapter 2 for compatibility with the package materials of construction. Neither the aluminum target cans nor the metallic molybdenum disks will result in significant chemical, galvanic, or other reactions with gas production or corrosion potential because of the favorable galvanic potentials and lack of aqueous environment in the containment cavity.

9.3 Content #02 – Thermal Evaluation

The thermal analysis in Chapter 3 was based on an initial thermal power resulting from 4,500 Ci of ^{99}Mo. The maximum activity of Content #02 is 4,400 Ci of ^{99}Mo. Because content #02 has a lower allowable number of Curies than was used for the analyses in Chapter 3, the package temperatures for Content #02 will be bounded by those from the baseline thermal analysis.

The package internal pressure loads for NCT and HAC are calculated in Chapter 3 for the highest bulk average temperature of the gases within the containment system for Content #01 considering gas generation due to radiolysis of the liquid payload. But radiolytic gas generation does not occur in Content #02 because the form is solid, metallic molybdenum. The package pressures for Content #02 will therefore be significantly lower than predicted in Chapter 3.

Because content #02 has a lower initial thermal power than that used in the base thermal analysis and it does not generate gas due to radiolysis, it is concluded that the package temperatures and internal pressures for Content #02 will be bounded by the baseline thermal analyses in Chapter 3.

9.4 Content #02 –Containment Evaluation

Chapter 4 describes that the package is designed to a "leak-tight" containment criterion per ANSI N14.5 [4.3], therefore the containment criterion is 10^{-7} ref-cm^3/s and is not dependent on the source specification. Content #02 is therefore bounded by the baseline design discussed in Chapter 4.

9.5 Content #02 – Shielding Evaluation

9.5.1 Source Specification

Section 5.2.1 discusses the photon source term calculations, including all significant equilibrium daughter products. Because Content #02 has the same source specification as the baseline liquid payload, the source terms are identical.

9.5.1.1 Evaluation of Metallic Form

The baseline shielding analysis described in Chapter 5 was performed for 4,500 Ci of Mo-99 (plus ^{99m}Tc in full equilibrium) in an aqueous solution that was modeled as water for shielding purposes. An MCNP model was run to determine whether Content #02 is bounded by the baseline shielding analysis. The liquid ^{99}Mo source in a representative NCT MIDUS shielding model was substituted with the solid molybdenum source in Content #02. Like the baseline Content #01, the Content #02 payload is limited to 60 Ci/ml maximum specific activity, therefore the smallest possible amount of self-shielding is present when the volume of molybdenum metal is 4,500 Ci / 60 Ci/ml = 75 ml. This corresponds to a sphere of molybdenum with a radius of 2.62 cm (Figure 9-2), the same as radius of the liquid source. No changes were made to the other model parameters, including source terms and importance biasing.

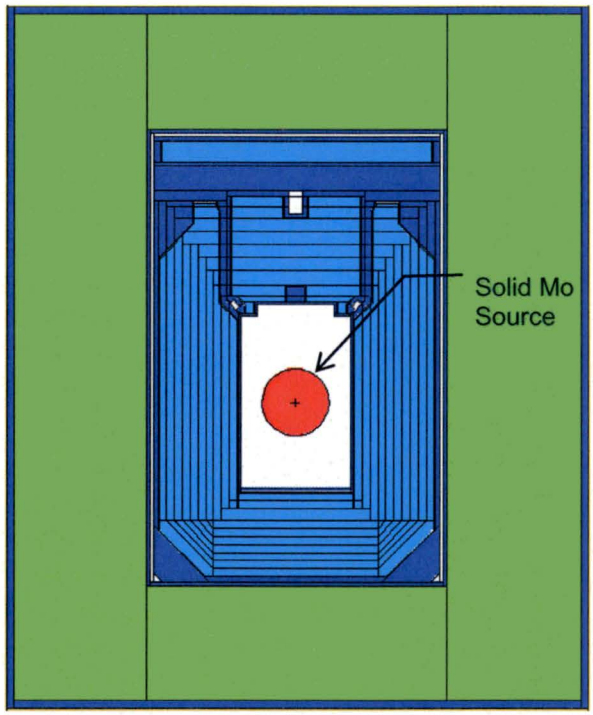

Figure 9-2 – Solid Source MCNP Model

The calculation was performed using MCNP5, v.1.51 and the MCPLIB84 cross section data library for photon transport[7]. At the two highest package exposure rate locations (the radial and bottom surfaces), the resulting photon exposure rates were less than one-half of those for the baseline liquid payload analyzed in Chapter 5.

[7] LA-UR- 00-3581, "Electron Upgrade for MCNP4B," Los Alamos National Laboratory.

Due to the increased attenuation in the metallic source region, the package dose rates for Content #02 are well bounded by the baseline evaluation in Chapter 5. There is an additional margin of conservatism since the ^{99}Mo activity specification for Content #02 is 4,400 Ci, versus the 4,500 Ci analyzed in Chapter 5.

9.5.1.2 Evaluation of Bremsstrahlung Radiation

Bremsstrahlung radiation is x-ray or gamma radiation caused by betas or electrons during the stopping process. The production of bremsstrahlung radiation is known to increase with the atomic number of the attenuating medium. Since the atomic number of molybdenum (Z=42) is greater than the constituents of the Content #01 ^{99}Mo solution (Z= 1, 7, 8, 11), there is a possibility that bremsstrahlung radiation could be a significant contributor to package dose rates for Content #2.

An MCNP model was prepared to investigate whether bremsstrahlung radiation might be a significant contributor for Content #02. The model described in Section 9.5.1.1 was modified for electron transport using the 'mode' card in MCNP. Beta and electron emission data for 4,500 Ci of ^{99}Mo plus equilibrium daughters were input as source terms. ^{99}Mo and ^{99m}Tc produce relatively low-energy beta-rays and electrons, with most of the power resulting from the ^{99}Mo beta with E_{avg} = 442.9 keV. Betas from the ^{99m}Tc and ^{99}Tc decays were neglected because of their low energies, small branching ratio (0.0037 for ^{99m}Tc) and very long half life (200,000 years for ^{99}Tc).The bremsstrahlung photon production was biased using the MCNP 'bbrem' card, and the beta/electron sources were biased by their energy levels.

The calculated bremsstrahlung exposure rate at the package radial surface was 0.03 mrem/hr, or 0.06% of the corresponding primary gamma exposure rate from the model described in Section 9.5.1.1. By comparison, 4,400 Ci is 2.2% less than 4,500 Ci, and the Content #02 package exposure rates are expected to be less 50% of the baseline liquid payload analyzed in Chapter 5. Bremsstrahlung production is therefore not a significant contributor in Content #02.

9.6 Content #02 – Criticality Evaluation

Not applicable.

9.7 Content #02 – Operating Procedures

The operating procedures for the package with content #02 are the same as described in Chapter 7.

9.8 Content #02 – Acceptance Tests and Maintenance Program

The acceptance tests and maintenance program for the package with Content #02 are the same as described in Chapter 8.